

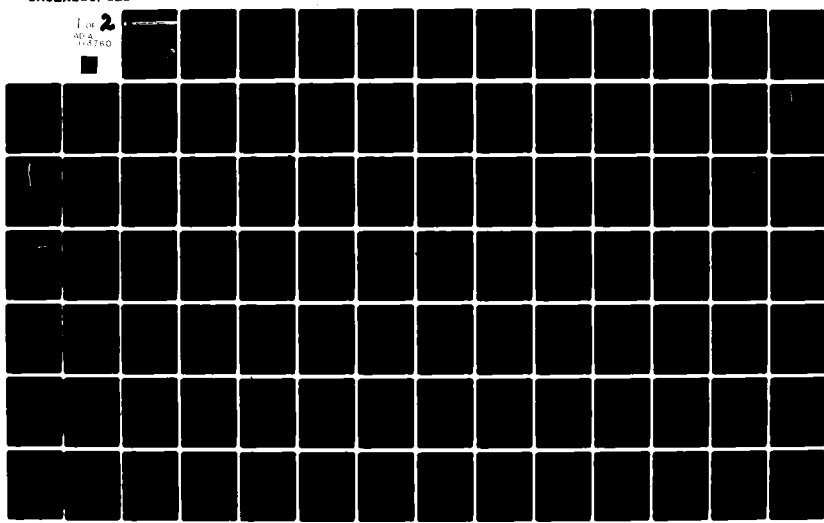
AD-A113 760

SYSTEMS CONTROL INC (VT) PALO ALTO CA
DEVELOPMENT OF A LOW-ORDER MODEL OF AN X-WING AIRCRAFT BY SYSTE—ETC(U)
FEB 82 J H VINCENT, J W BUNNELL
N00014-79-C-0578

F/6 1/3
NL

UNCLASSIFIED

1 of 2
AD-A113 760



DTIC FILE COPY

AD A113760

12

ISCT SYSTEMS CONTROL TECHNOLOGY, INC.

1601 PAGE MILL RD. P.O. BOX 10180 PALO ALTO, CALIFORNIA 94303 (415) 494-2233

FEBRUARY 1982

FINAL REPORT

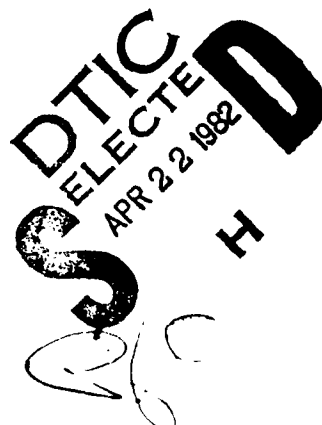
DEVELOPMENT OF A LOW-ORDER MODEL OF AN X-WING AIRCRAFT BY SYSTEM IDENTIFICATION

Project 5332

Prepared by
J.H. Vincent
J.W. Bunnell

Prepared for
OFFICE OF NAVAL RESEARCH
800 N. Quincy Street
Arlington, Virginia 22217

Under Contract No. N00014-79-C-0578



82 00 00 010

FOREWORD

This report describes the work performed by Systems Control, Inc. (Vt) for the Office of Naval Research and the David W. Taylor Naval Ship Research and Development Center. The objective of this work was the development of a low-order math model of the X-wing aircraft using system identification technology. The program manager for this work was Dr. Earl Hall, Jr.; the project manager was Mr. James Vincent; Mr. John Bunnell and Mr. James Fuller were the project engineers; programming support was provided by Mr. Robert Bullock and Ms. Susan DuHamel. Report preparation efforts were directed by Ms. Clare Walker.

Accession For	
NTIS GEN&I	<input type="checkbox"/>
DTIC TAB	<input type="checkbox"/>
Unannounced	<input type="checkbox"/>
Justification	
By <u>Pex Ltr. on file</u>	
Distribution/	
Availability Codes	
Dist	Avail and/or Special
A	



TABLE OF CONTENTS

	Page
I. INTRODUCTION.....	1
1.1 Background	1
1.2 Method of Approach	2
1.3 Report Summary	2
II. X-WING DESCRIPTION	5
2.1 Rotor Design	5
2.2 Dynamic Characteristics	8
2.3 Flight Control System	9
III. GENERATION OF SIMULATION DATA	13
3.1 Overview	13
3.2 Rexor Description	13
3.3 Test Data Generation	14
3.4 Post-Simulation Data Processing	20
3.4.1 Kinematic Consistency	20
3.4.2 Data Filtering	27
IV. IDENTIFICATION OF REDUCED-ORDER MODEL	33
4.1 Overview	33
4.2 System Identification Overview	33
4.3 X-Wing Modeling Approach	37
4.4 Identified Model Results	44
V. CONCLUSIONS AND RECOMMENDATIONS	89
5.1 Conclusions	89
5.2 Recommendations	89
REFERENCES	91

LIST OF FIGURES

	Page
2.1 General Arrangement of X-Wing Demonstrator	6
2.2 Pilot Cyclic Control, Simulation Model	11
3.1 Control Inputs	15
3.2 Response to Longitudinal Cyclic Stick	17
3.3 Response to Lateral Cyclic Stick	18
3.4 Comparison of \dot{P} with dP/dt	22
3.5 Comparison of \dot{Q} with dQ/dt	23
3.6 Comparison of \dot{R} with dR/dt	24
3.7 Comparison of Reconstructed Roll Rate with Original	25
3.8 Comparison of Reconstructed Pitch Rate with Original	26
3.9 Effect of Fourth-Order Butterworth Filter ($\omega_B = 2\Omega$) on Vertical Acceleration (Hover, Collective Input)	28
3.10 Effect of Fourth-Order Butterworth Filter ($\omega_B = 2\Omega$) on Vertical Velocity (Hover, Collective Input)	29
3.11 Effect of Fourth-Order Butterworth Filter ($\omega_B = 2\Omega$) on Yaw Acceleration (Hover, Collective Input)	30
3.12 Effect of Fourth-Order Butterworth Filter ($\omega_B = 2\Omega$) on Roll Rate (Hover, Collective Input) ..	31
3.13 Effect of Fourth-Order Butterworth Filter ($\omega_B = 2\Omega$) on Pitch Hub Moment (Hover, Collective Input)	32
4.1 Total Coupled System Model Structure	39
4.2 General Rotorcraft State Model	41
4.3 Method for Reducing Rotor/Fuselage Modes to Conventional Rigid Body, Quasi-Static Derivatives	42
4.4 Forward Acceleration (Hover)	50

LIST OF FIGURES (Continued)

4.5	Forward Acceleration (Hover, Collective Input) ..	51
4.6	Forward Acceleration (100 fps)	52
4.7	Forward Acceleration (100 fps, Collective Input)	53
4.8	Lateral Acceleration (Hover)	55
4.9	Lateral Acceleration (Hover, Collective Input) ..	56
4.10	Lateral Acceleration (100 fps)	57
4.11	Lateral Acceleration (100 fps, Tail Rotor Collective)	58
4.12	Normal Acceleration (Hover)	60
4.13	Normal Acceleration (Hover, Collective Input) ...	61
4.14	Normal Acceleration (100 fps)	62
4.15	Normal Acceleration (100 fps, Collective Input)	63
4.16	Roll Acceleration (Hover)	65
4.17	Roll Acceleration (Hover, Collective Input)	66
4.18	Roll Acceleration (100 fps)	67
4.19	Roll Acceleration (100 fps, Collective Input) ...	68
4.20	Pitch Acceleration (Hover)	70
4.21	Pitch Acceleration (Hover, Longitudinal Cyclic)	71
4.22	Pitch Acceleration (100 fps)	72
4.23	Pitch Acceleration (100 fps, Collective Input) ..	73
4.24	Yaw Acceleration (Hover)	75
4.25	Yaw Acceleration (Hover, Tail Rotor Collective)	76
4.26	Yaw Acceleration (100 fps)	77
4.27	Yaw Acceleration (100 fps, Tail Rotor Collective)	78

LIST OF FIGURES (Concluded)

4.28	Roll Hub Moment (Hover)	80
4.29	Roll Hub Moment (Hover, Collective Input)	81
4.30	Roll Hub Moment (100 fps)	82
4.31	Roll Hub Moment (100 fps, Collective Input)	83
4.32	Pitch Hub Moment (Hover)	85
4.33	Pitch Hub Moment (Hover, Longitudinal Cyclic Input)	86
4.34	Pitch Hub Moment (100 fps)	87
4.35	Pitch Hub Moment (100 fps, Collective Input)	88

LIST OF TABLES

	Page
2.1 X-Wing Geometry	7
2.2 Flight Control System Parameters	12
3.1 Test Cases	19
3.2 REXOR Output Variables	21
4.1 Role of Parameter Identification for Aircraft Design, Test, and Evaluation	34
4.2 Equations of Motion Used for X-Wing Analysis	43
4.3 X-Wing A Priori Applied Acceleration Models	45
4.4 Summary of Identified Model Equation Error Fit Statistics	47
4.5 Regression on Ax	49
4.6 Regression on Ay	54
4.7 Regression on Az	59
4.8 Regression on P	64
4.9 Regression on Q	69
4.10 Regression on R	74
4.11 Regression on L _H	79
4.12 Regression on M _H	84

NOMENCLATURE

SYMBOL	DESCRIPTION	UNITS
A_x	Forward acceleration	ft/sec ²
A_y	Lateral acceleration	ft/sec ²
A_z	Normal acceleration	ft/sec ²
A_{1B}	Cosine blowing valve area ratio	ft/sec ²
B_{1B}	Sine blowing valve area ratio	---
C	Constant	---
c.g.	Center of gravity	---
F	(1) Ratio of explained variation to the unexplained variation (adjusted for degrees of freedom)	---
	(2) (Subscript) Fuselage	---
H	(Subscript) Hub	---
H_F	Height of c.g. above fuselage ref.	ft
H_{TR}	Height of tail rotor	ft
H_{VS}	Height of vertical stabilizer	ft
K_{1P}	Cosine blowing gain	(ft) ⁻¹
K_{1R}	Sine blowing gain	(ft) ⁻¹
K_L	Roll moment feedback gain	ft/in-lb
K_M	Pitch moment feedback gain	ft/in-lb
K_p	Long. cyclic stick gain	ft/ft
K_p	Roll rate feedback gain	ft/(rad/sec)
K_q	Pitch rate feedback gain	ft/(rad/sec)
K_R	Lateral cyclic stick gain	ft/ft
L_H	Hub roll moment	in-lb

NOMENCLATURE (Continued)

SYMBOL	DESCRIPTION	UNITS
M _H	Hub pitch moment	in-lb
P	(1) Blowing pressure	lbs/ft ²
	(2) Roll rate	rad/sec
Q	Pitch rate	rad/sec
R	(1) Yaw rate	rad/sec
	(2) (Subscript) Rotor	---
R _{P0}	Collected blowing pressure ratio	---
r _R	Rotor radius	ft
t	Time sec	
u	Forward velocity	ft/sec
v	Lateral velocity	ft/sec
w	Vertical velocity	ft/sec
w _L	Roll moment filter frequency	rad/sec
w _M	Pitch moment filter frequency	rad/sec
w _P	Roll rate filter frequency	rad/sec
w _q	Pitch rate filter frequency	rad/sec
X _F	c.g. location in fuselage axes	ft
X _{CS}	Long. cyclic stick deflection	ft (in)
Y _{CS}	Lateral cyclic stick deflection	ft (in)
Z _P	Thrustor distance below fuselage ref.	ft
Δ	Variation from initial value	---

NOMENCLATURE (Concluded)

SYMBOL	DESCRIPTION	UNITS
ζ_p	Roll rate filter damping	---
ζ_q	Pitch rate filter damping	---
θ	Pitch Euler angle	radians
θ_{OTR}	Tail rotor collective	radians
τ_c	Actuator time constant	sec
ϕ	Bank Euler angle	radians
ψ_c	Rotor control input phase	radians
ψ_R	Rotor reference (blade 1) azimuth	radians
Ω_R	Rotor angular velocity	rad/sec
ω_N	Natural frequency	rad/sec

I. INTRODUCTION

1.1 BACKGROUND

The X-wing concept is a novel approach to the problem of combining VTOL and hover capability with efficient high-speed cruise operation [1]. The concept uses a rotating X-platform wing to operate like a conventional helicopter for VTOL, hover and low-to-moderate speed operation; the rotor may also be stopped when at sufficient forward speed, allowing the aircraft to cruise as a fixed-wing vehicle.

A key technology element of this concept, as developed by the Lockheed California Aircraft Company in their preliminary design study [2], is the use of a very rigid, circulation-controlled rotor. Lift and control moments are maintained in both rotary- and fixed-wing flight by ejection of low-energy air from the trailing edge of the blade.

→ The original purpose of this contract was to prepare a flight test plan for the proposed X-wing demonstrator using system identification to extract useful math models from the flight test data. Since the original statement of work was submitted, however, the scope of this study changed. An X-wing program decision has been reached not to carry the Lockheed X-wing configuration to flight test. Therefore, this task was modified to provide a demonstration of the feasibility of using system identification techniques to extract low-order math models from time history data from a detailed X-wing rotor simulation (REXOR).

The X-wing concept has been simulated by Lockheed using a general-purpose helicopter simulation program known as REXOR [3]. REXOR models the rotor in a rotating frame of reference and models each blade separately. This program has been installed by

SCI (Vt) on the CDC-7600 computer system at NASA-Ames Research Center, Moffett Field, CA, as a basis for this study.

1.2 METHOD OF APPROACH

The REXOR simulation program, as implemented on the CDC 7600 at NASA-Ames, provided the data base from which the X-wing math models were to be identified. Numerous simulation runs were made, and the data files produced were written to tape and transported to SCI (Vt) for analysis on SCI's VAX computer system. Data used represented hover and 100-foot-per-second flight conditions for collective, longitudinal and lateral cyclic, and tail rotor collective inputs. A reduced-order math model of the X-wing was then identified using SCI's Optimal Subset Regression (OSR) program. The simplified model describes the fuselage degrees of freedom and the rotor hub moments.

One of the problems anticipated in identifying a low-order model from the REXOR data is that the REXOR model includes high-frequency ($\omega_N > \Omega_R$) aeroelastic modes which are of little value to the flight controls designer. For this reason, it was expected that prefiltering the data to remove this unnecessary information would result in better identification of the simplified model, since this reduced-order model cannot account for the high-frequency effects seen in the data.

1.3 REPORT SUMMARY

The second section of this report presents a description of the X-wing configuration. The intent of this description is to provide background information for those features of the rotor design, the vehicle's dynamic characteristics, and the flight control system which have an impact on the modeling approach. Section III describes the methodology for generating simulation time history data with REXOR, the X-wing nonlinear, high-fidelity

simulation math model. Section IV describes the developed methodology for extracting reduced-order models of the X-wing configuration from REXOR simulation data. Report conclusions and recommendations are presented in Section V.

II. X-WING DESCRIPTION

This chapter presents a description of the Lockheed X-wing configuration. The intent of this description is to provide background information for those features of the rotor design, the vehicle's dynamic characteristics, and the flight control system which have an impact on the modeling approach. The X-wing configuration is shown in Figure 2.1, and its geometric parameters are listed in Table 2.1.

2.1 ROTOR DESIGN

The principal feature of the X-wing aircraft is a single, stoppable rotor on top of the fuselage, which enables the airplane to operate like a helicopter with the rotor turning, or like a fixed-wing aircraft with the rotor stopped in any X-position relative to the airplane's centerline. The only other lifting surfaces on the aircraft, as presently conceived, are on the empennage. In the helicopter mode, forward propulsion is provided by both rotor axis tilt and auxiliary engines. In the stopped-rotor mode, propulsion is provided directly by the engines. The rotor is a key advancement in the state of the art; it is a very rigid, hingeless rotor, much stiffer than the so-called "rigid" rotors used on some helicopters, and able to support the vehicle and provide maneuvering capability in stopped-rotor cruise. Even the requirement for a collective hinge has been eliminated by use of circulation control (CC) to regulate blade lift. The CC concept involves a stream of high pressure air exhausted from the trailing edge of the elliptical blade airfoil section which fixes the rear stagnation point (through the Coanda effect), and results in a net circulation about the airfoil. Hence, the common name for the system is circulation-controlled rotor (CCR). The X-wing uses the CC

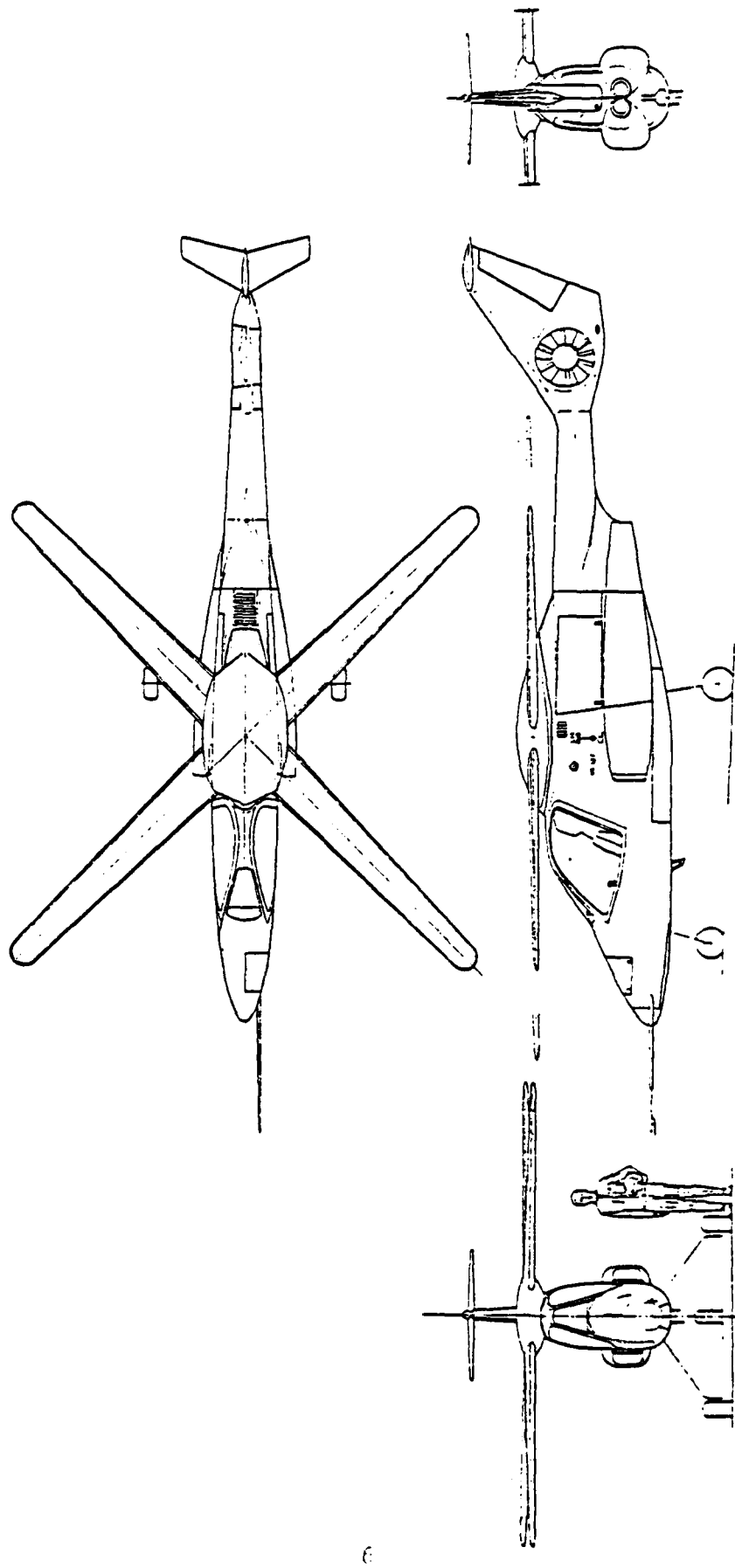


Figure 2.1 General Arrangement of X-Wing Demonstrator

Table 2.1
X-Wing Geometry

PARAMETER	DESCRIPTION	VALUE	UNITS
X_F	c.g. location (fuselage axes)	0.31	ft
H_F	Height of hub above fuselage ref.	1.13	ft
l_{TR}	Distance aft to tail rotor	14.80	ft
l_{VS}	Distance aft to vert. stabilizer	15.80	ft
l_{HS}	Distance aft to horiz. stabilizer	19.10	ft
H_{VS}	Height of vert. stabilizer	6.88	ft
H_{TR}	Height of tail rotor	3.67	ft
Z_p	Dist. of thruster below fuselage ref.	- 0.58	ft
r_R	Radius of main rotor	12.50	ft

concept in a mode wherein high advance ratio capability is achieved by using dual-slotted airfoils for useful lift production in the reverse flow regime. This mode is identified as the "reverse blowing circulation-controlled rotor (RBCCR)."

Theoretical and experimental studies, many funded by ONR and NASC, have confirmed the feasibility of the RBCCR concept. Aircraft characteristics are satisfactory in both performance and control, according to analysis and small-scale wind tunnel data [1]. Aerodynamic characteristics of the aircraft with the rotor turning and with it locked have been predicted using a number of Lockheed and government programs [2,3]. The characteristics combine those of helicopters, fixed-wing, and powered-lift aircraft, and are therefore dependent on angle of attack, blowing pressure, and rotor RPM. Analyses of thrust (lift) and moment, both critical to performance and longitudinal control, show adequate trim capability and acceptable static margin with the addition of a small (6 ft^2) horizontal tail. Of special interest are neutral point and trim shifts at transition. The ability to use the fixed-wing for both lift and pitch control introduces a "direct lift control" capability and reduces the role of the horizontal tail to that of minimizing trim drag.

2.2 DYNAMIC CHARACTERISTICS

Flight dynamics studies have been performed [3] to analyze the aircraft's dynamic modes of motion, both rigid-body and aeroelastic, in various flight conditions. The predominant dynamic effect, in the helicopter mode, is the inertial cross-coupling, which causes unacceptable handling qualities if not compensated by an automatic control system. A principal area of study in X-mode operation (rotor-stopped) is static stability and control authority. The conversion process contains its own areas of concern, particularly oscillatory loads caused by a slowly turned rotor and their effect on dynamics and handling

qualities. An RPM load-factor schedule must be defined for the conversion and reconversion maneuvers.

Each of the three major flight regimes (helicopters, X-cruise, and transition) has been analyzed using linear and nonlinear models, and no fundamental flaws in the concept have been found. The rotor aeroelastic modes are of very high frequency (100 rad/sec) due to the extreme rigidity of the rotor, and do not couple with the aircraft rigid-body modes. The eigenanalysis discussed in Ref. 3 predicts a static instability in the helicopter mode. It appears that a full-time, fail-operational augmentation system is required for stability reasons, as well as for control of rotor cross-coupling. The approximately 1.2 sec time to double pitch amplitude discussed in Ref. 3 is not acceptable under such handling qualities criteria as MIL-F-83300.

2.3 FLIGHT CONTROL SYSTEM

Control of the X-wing configuration is based on the regulation of the air pressure level in the circulation control (CC) plenums, a lift fan in the vertical tail and aerodynamic empennage controls. The CC pneumatic blowing for each blade is regulated as a function of blade position to achieve collective and cyclic control.

Two types of augmentation systems have been considered for the aircraft, referred to as low-gain and high-gain systems. Both are aircraft rate command systems, but the high-gain system features a high-gain rotor moment feedback loop within the aircraft rate loop that drives the rotor controls to produce a commanded moment and null out disturbances from turbulence or inertial cross-coupling. The X-wing aircraft, as modeled for this study, uses the high-gain control system for the pitch and roll degrees of freedom (i.e. cyclic augmentation).

The cyclic control augmentation system is shown in Figure 2.2. Rotor hub moments (M_H and L_H) are fed back at high gain to remove external aerodynamic effects on the rotor. Phasing networks were included in the initial design for the moment feedback loop, but analysis showed negligible benefit so the feedback phase angle was set to zero in the REXOR simulation. Pitch and roll rates are also fed back to augment damping. Normal acceleration (A_z) feedback was not implemented.

In the forward path, control input phasing is used to compensate for the phase shift in rotor moment with advance ratio. This phase angle must be adjusted for rotor speed, and is equal to 60° for maximum RPM. Since all runs for this study were made at 100% RPM, the phase angle was a constant. Forward loop integration is used to stabilize the aircraft, and the actuators control the area of cosine and sine blowing values, A_{1B} and B_{1B} . This gives a total blowing pressure of

$$P_B = 2116. \times R_{P0} (1. - A_{1B} \cos\psi_R - B_{1B} \sin\psi_R) \text{ psf}$$

where

R_{P0} = collective pressure ratio.

The gains and other parameters used in the cyclic control system are listed in Table 2.2.

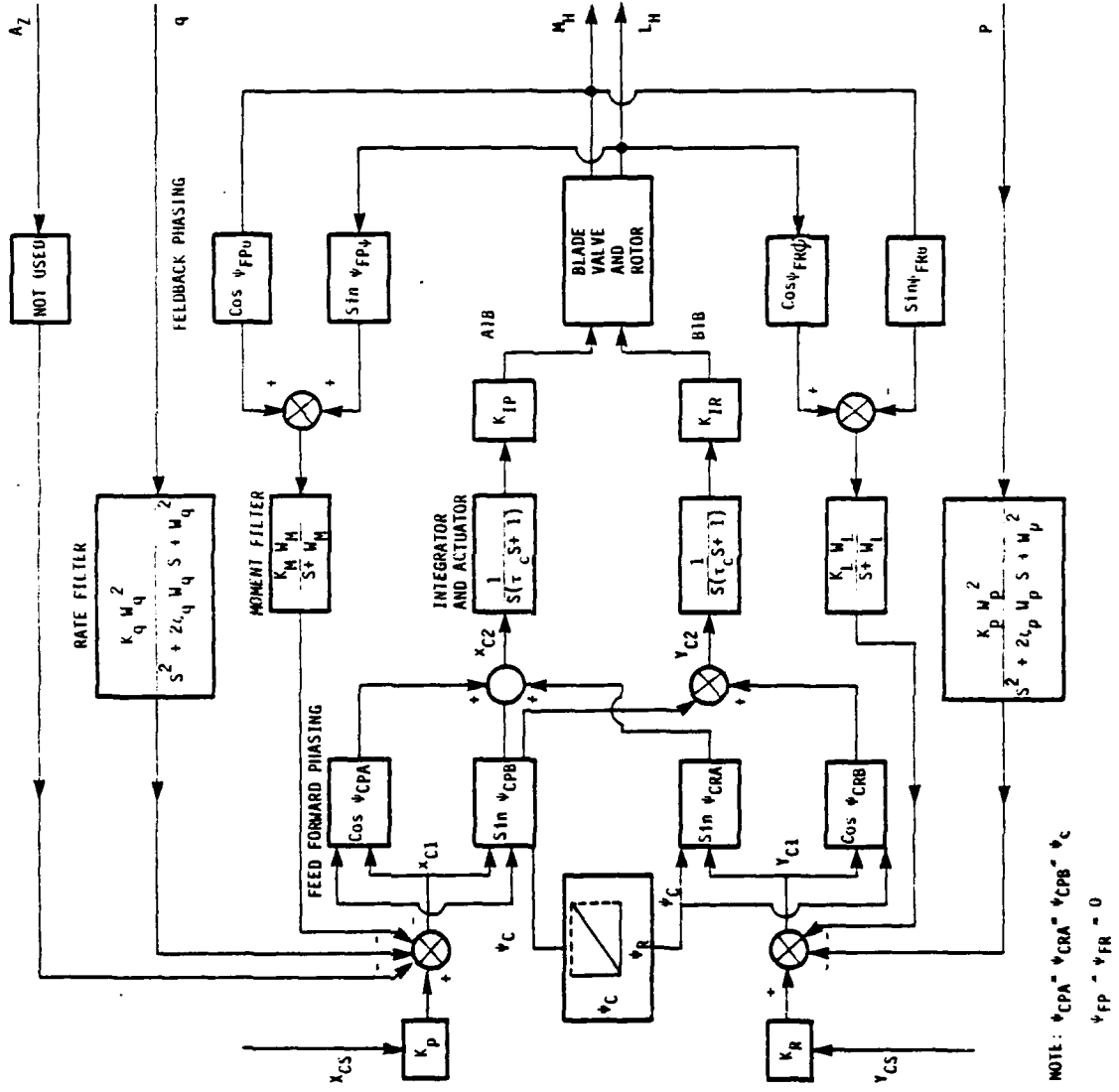


Figure 2.2 Pilot Cyclic Control, Simulation Model

Table 2.2
Flight Control System Parameters

PARAMETER	DESCRIPTION	VALUE	UNITS
K_p	Longitudinal stick gain	1.0	ft/ft
K_R	Lateral stick gain	1.0	ft/ft
K_q	Pitch rate feedback gain	2.52	ft-sec/rad
w_q	Pitch rate filter freq.	120.	rad/sec
q	Pitch rate filter damp.	0.7	---
K_p	Roll rate feedback gain	2.8	ft-sec/rad
w_p	Roll rate filter freq.	120.	rad/sec
p	Roll rate filter damp.	0.7	---
K	Pitch moment feedback gain	2.1×10^{-4}	ft/in-lb
w	Pitch moment filter freq.	120.	rad/sec
K_L	Roll moment feedback gain	3.2×10^{-4}	ft/in-lb
w_L	Roll moment filter freq.	120.	rad/sec
K_{IP}	Cosine blowing gain	0.7	(ft) ⁻¹
K_{IR}	Sine blowing gain	0.7	(ft) ⁻¹
τ_c	Actuator time constant	0.033	sec
ψ_c	Rotor control input phase	1.047	rad

III. GENERATION OF SIMULATION DATA

3.1 OVERVIEW

The first task in this study was to produce time history data representative of the X-wing design proposed by Lockheed. This was done using the REXOR simulation program developed by Lockheed. The simulation was implemented and run on the CDC 7600 computer system at NASA-Ames for this study.

3.2 REXOR DESCRIPTION

The REXOR (Revised and Extended Rotor Senior) program is a general-purpose simulation developed for analysis of rotocraft. The version of REXOR implemented at NASA-Ames has been modified to simulate the X-wing configuration designed by Lockheed, and a data deck representing the X-wing was also available at NASA-Ames. The basic REXOR program is documented in Ref. 3. No documentation exists for the X-wing version.

The standard REXOR program was written to simulate a single, two- or four-bladed, hingeless-rotor helicopter with a gyro control on the rotor. The program also has the ability to simulate conventional controls. The X-wing version contains modifications to simulate the pneumatic controls used in that design, as well as simulating the transition to fixed-wing flight.

The REXOR math model was developed to provide accurate analysis of rotor characteristics. This has been achieved using a blade-element approach, in which the blade aerodynamics and kinematics are computed as a summation of finite elements of each blade. This approach is more complex than the classical tip-path plane models commonly used, but it allows in-depth harmonic analysis of the aeroelastic rotor dynamics. However, it is also

cumbersome to operate, and is computationally expensive. As an example of this, one 2-sec simulation run by SCI (Vt) on the CDC CYBERNET system took 1030.417 sec of CPU time. Obviously, this is not an efficient program for handling-qualities and flight control design studies which require repeated runs, but do not require extreme accuracy in the modeling of high-frequency aeroelastic deflections of the rotor. By identifying a lower order model of the X-wing aircraft, a tool can be developed which would allow the flight control designer to make many runs efficiently, and produce the data needed for control system design and handling qualities analysis.

The math model used by the REXOR program also complicates the process of determining a low-order model in that it is not feasible to extract stability derivatives by the perturbation method commonly used with fixed-wing aircraft simulations. This is because the aerodynamics of the rotor cannot be determined statically from a blade-element model. An entire revolution of the rotor must be computed in order to get the averaged effects of the rotor states. For this reason, system identification is the logical way to generate reduced-order models from the REXOR math model.

3.3 TEST DATA GENERATION

The control inputs used for generating the time histories to be identified were chosen to excite any modes within the frequency range of interest for handling-qualities analysis. The inputs to all four pilot controls (main rotor collective, tail rotor collective, longitudinal cyclic stick and lateral cyclic stick) consisted of a series of four doublets. Each doublet had twice the period and half the magnitude of the previous one. These inputs are shown in Figure 3.1. Note that the tail-rotor collective input was the same as the main-rotor collective blowing input, but the time history shown was the actuator

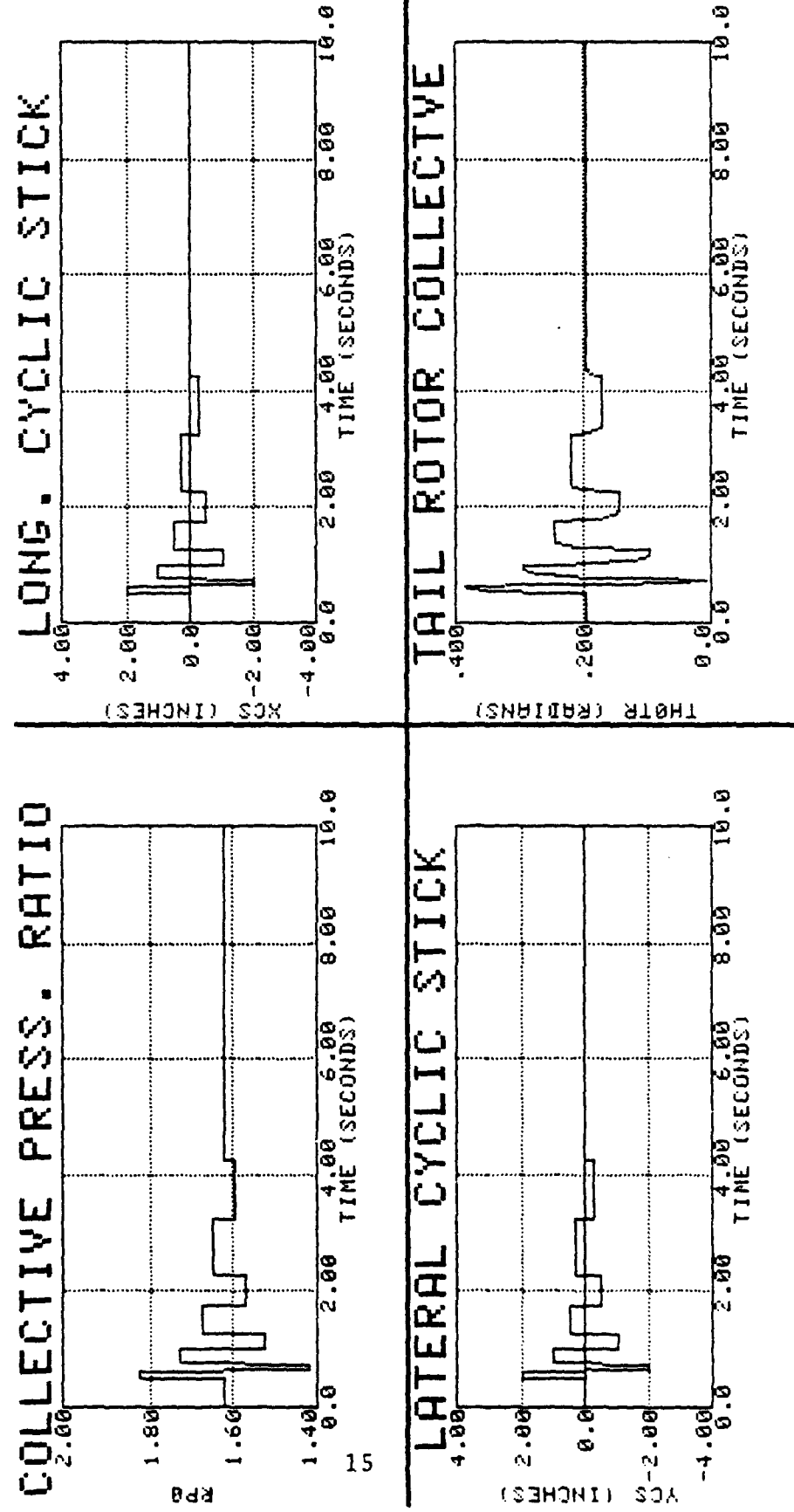


Figure 3.1 Control Inputs

output. The actuator for collective blowing was not simulated in the code.

After analyzing the generated REXOR simulation responses, it was apparent that very little pitch and roll rate response was achieved with the cyclic stick inputs. This is shown in Figures 3.2 and 3.3. The cyclic data were, however, included for system identification, since the feedbacks and an initial miss trim caused the cyclic blowing (A_{1B} and B_{1B}) to drive the simulation dynamics throughout these maneuvers.

The miss trim, primarily seen as a hub moment transient, is most likely due to an initialization problem with REXOR. When REXOR was first loaded onto the NASA-Ames CDC 7600 computer, numerous initialization problems (i.e., undefined variables) were encountered. The approach adopted at the time was initially to set all variables to zero. This across-the-board initialization of all variables to zero could cause problems with the hub moment feedback filter. The filter was probably initialized correctly in the trim mode, but then the filter output could have been zeroed after switching the simulation to the run mode. From the standpoint of identifying unaugmented airframe math models, which is the objective of this study, this miss trim situation provides acceptable, albeit unnatural, control excitation. In conclusion, better documentation for the X-wing version of REXOR would have helped this problem.

The test cases used for this study included two flight conditions: hover and 100-feet-per-second forward velocity. Both cases were run with the aircraft in the helicopter mode of flight. For each flight condition, four runs were made, one for each control input. Each of the runs made had a duration of 10 seconds. These test cases are summarized in Table 3.1.

For the identification processing, the four runs for each flight condition were concatenated. This allows simultaneous identification of the effects of all four control inputs.

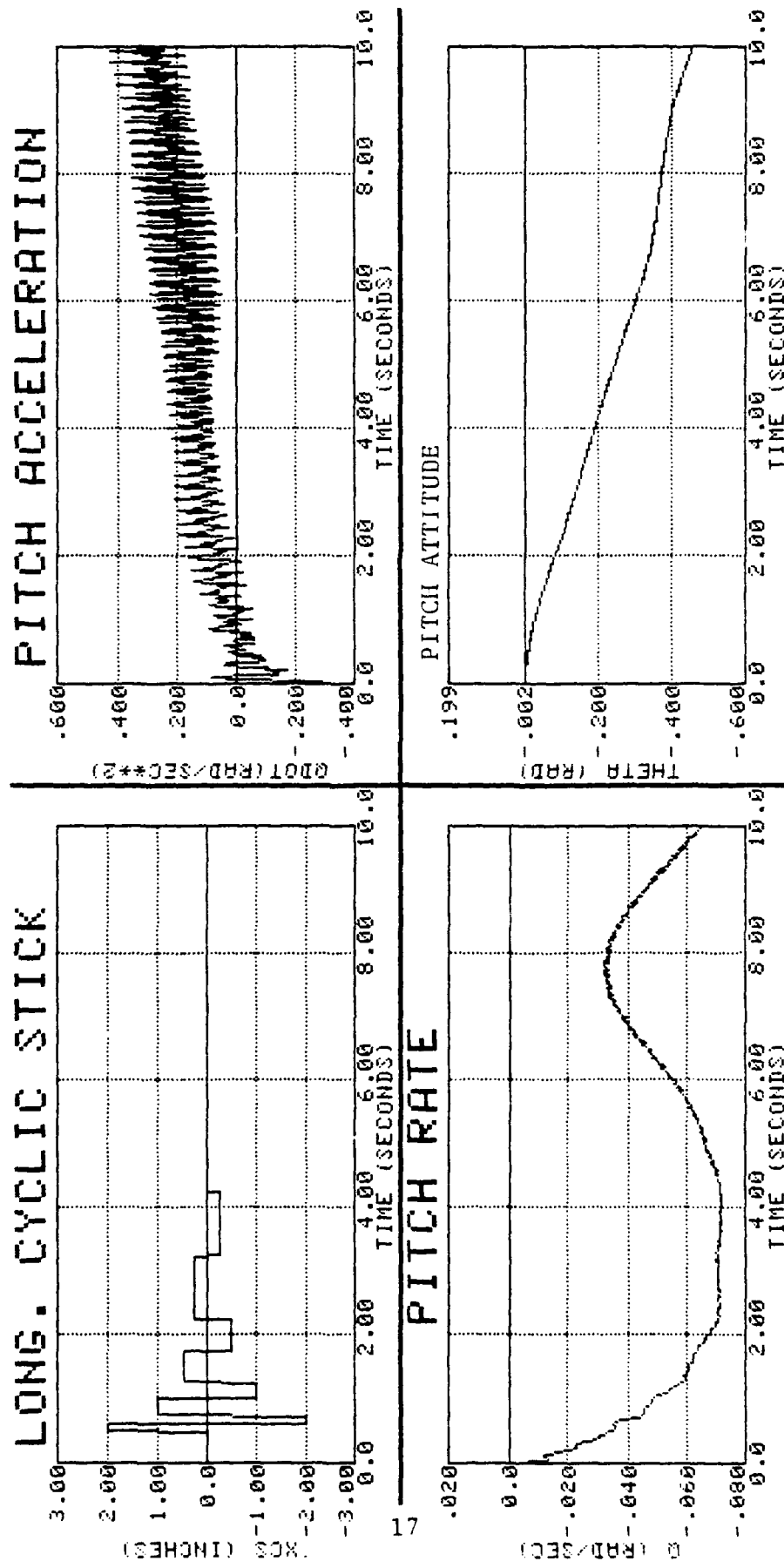


Figure 3.2 Response to Longitudinal Cyclic Stick

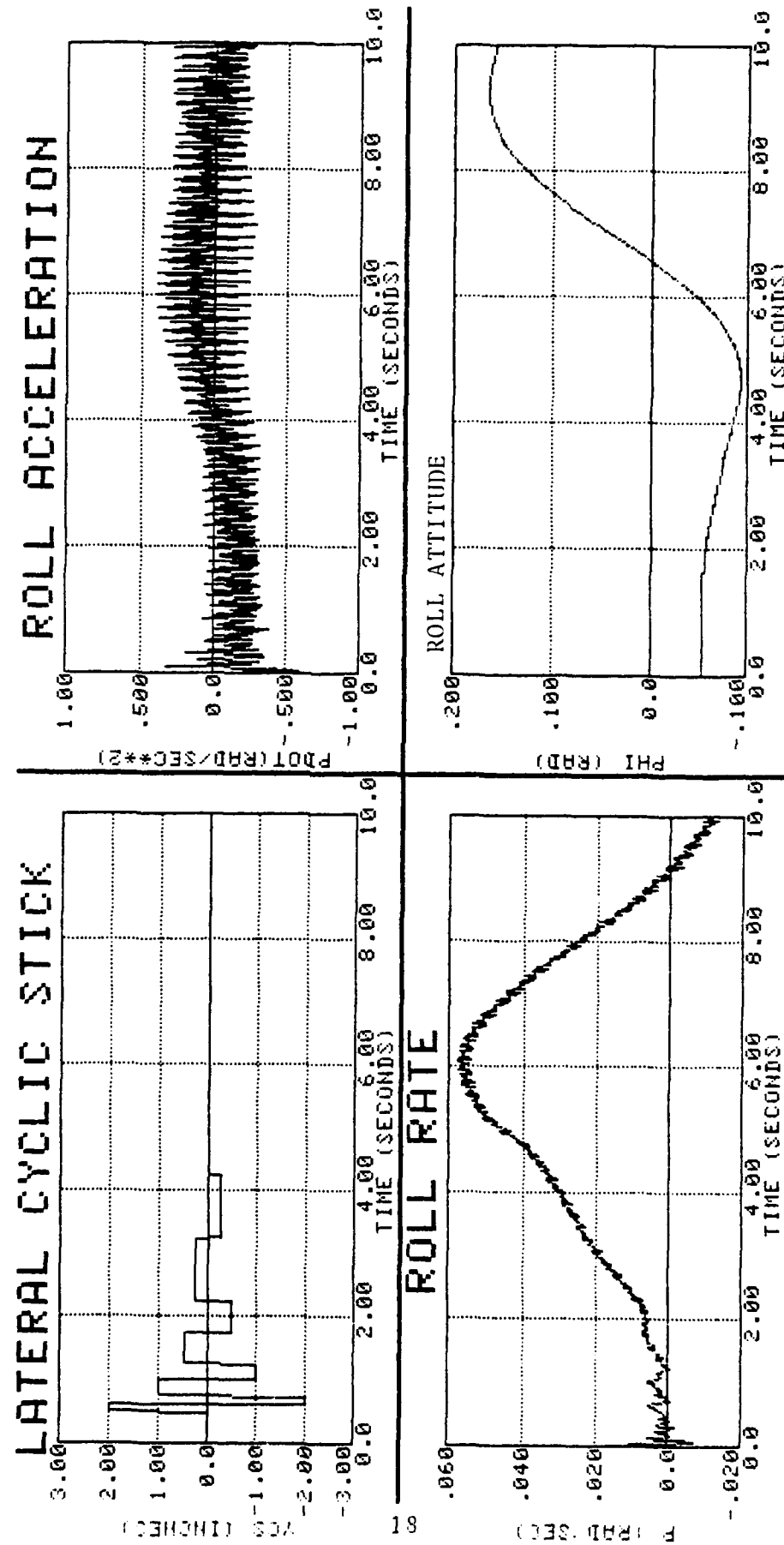


Figure 3.3 Response to Lateral Cyclic Stick

Table 3.1
Test Cases

RUN I.D.	FLIGHT CONDITION	CONTROL INPUT
1004.02	Hover	Collective blowing
1014.01	Hover	Longitudinal stick
1024.01	Hover	Lateral stick
1034.01	Hover	Tail rotor collective
1104.02	$V_T = 100$ FPS	Collective blowing
1114.01	$V_T = 100$ FPS	Longitudinal stick
1124.01	$V_T = 100$ FPS	Lateral stick
1134.01	$V_T = 100$ FPS	Tail rotor collective

Prior to making production data runs with REXOR, the output subroutine was modified to store the data required for the identification process. The variables which were output and stored are listed in Table 3.2.

3.4 POST-SIMULATION DATA PROCESSING

Before using the REXOR simulation data with the identification program, it was checked for consistency between redundant variables (i.e., does $dQ/dt = Q$). The REXOR simulation data were also filtered to remove multiple-per-rev dynamics associated with the structural degrees of freedom.

3.4.1 Kinematic Consistency

Examination of the REXOR output data showed a discrepancy between the time histories of the pitch and roll rates and their derivatives. Figures 3.4 through 3.6 show the comparison between the angular accelerations output by REXOR (PDOT, QDOT, and RDOT) and the numerical derivatives of the angular velocities (dP/dT , dQ/dT , and dR/dT).

Further examination of the data showed that the angular velocities P and Q were consistent with the Euler angle rates, $\dot{\phi}$ and $\dot{\theta}$. This was shown to be the case by comparing time histories of P and Q with reconstructed time histories calculated from $\dot{\phi}$ and $\dot{\theta}$. These comparisons are shown in Figure 3.7 and 3.8.

Since P and Q were consistent with $\dot{\phi}$ and $\dot{\theta}$, but not with P and Q , the numerical derivatives of P and Q were used for the system identification. The numerical derivative of R was also used, although it was virtually identical to the \dot{R} output by REXOR.

Table 3.2
REXOR Output Variables

CHANNEL	FORTRAN NAME	VARIABLE	UNITS	CHANNEL	FORTRAN NAME	VARIABLE	UNITS
1	STIME	t	sec	21	AUXE(4)	θ_{1B}	non-dim
2	UFD	\dot{u}_f	ft/sec ²	22	PSIR	R	rad
3	VFD	\dot{v}_f	ft/sec ²	23	(XCS-XCST)*12.	x_{cs}	inches
4	WFD	\dot{w}_f	ft/sec ²	24	(YCS-YCST)*12.	y_{cs}	inches
5	PRO	\dot{p}	rad/sec ²	25	RPO	r_{po}	non-dim
6	QRD	\dot{q}	rad/sec ²	26	THOTR	OTR	rad
7	RRD	\dot{r}	rad/sec ²	27	REFSIG	.1 sin θ_R	non-dim
8	PHID	$\dot{\phi}$	rad/sec	28	XCI	x_{ci}	inches
9	THETD	$\dot{\theta}$	rad/sec	29	YCI	y_{ci}	inches
10	AUXE(1)	A_{1B}	non-dim	30	V(2,1,1)*12.	A_{21}	inches
11	AUXE(2)	B_{1B}	non-dim	31	V(2,2,1)*12.	A_{21}	in/sec
12	UF	u_f	ft/sec	32	V(2,3,1)*12.	A_{21}	in/sec ²
13	VF	v_f	ft/sec	33	V(2,1,2)*12.	A_{22}	inches
14	WF	w_f	ft/sec	34	V(2,2,2)*12.	A_{22}	in/sec
15	PR	P	rad/sec	35	V(2,3,2)*12.	A_{22}	in/sec ²
16	QR	Q	rad/sec	36	V(2,1,3)*12.	A_{23}	inches
17	RR	R	rad/sec	37	V(2,2,3)*12.	A_{23}	in/sec
18	PHI	ϕ	rad	38	V(2,3,3)*12.	A_{23}	in/sec ²
19	THETA	θ	rad	39	FF(5)-FF(1)*ZCELL	M_H	ft-lbs
20	AUXE(3)	A_{1B}	non-dim	40	FF(4)+FF(2)*ZCELL	L_H	ft-lbs

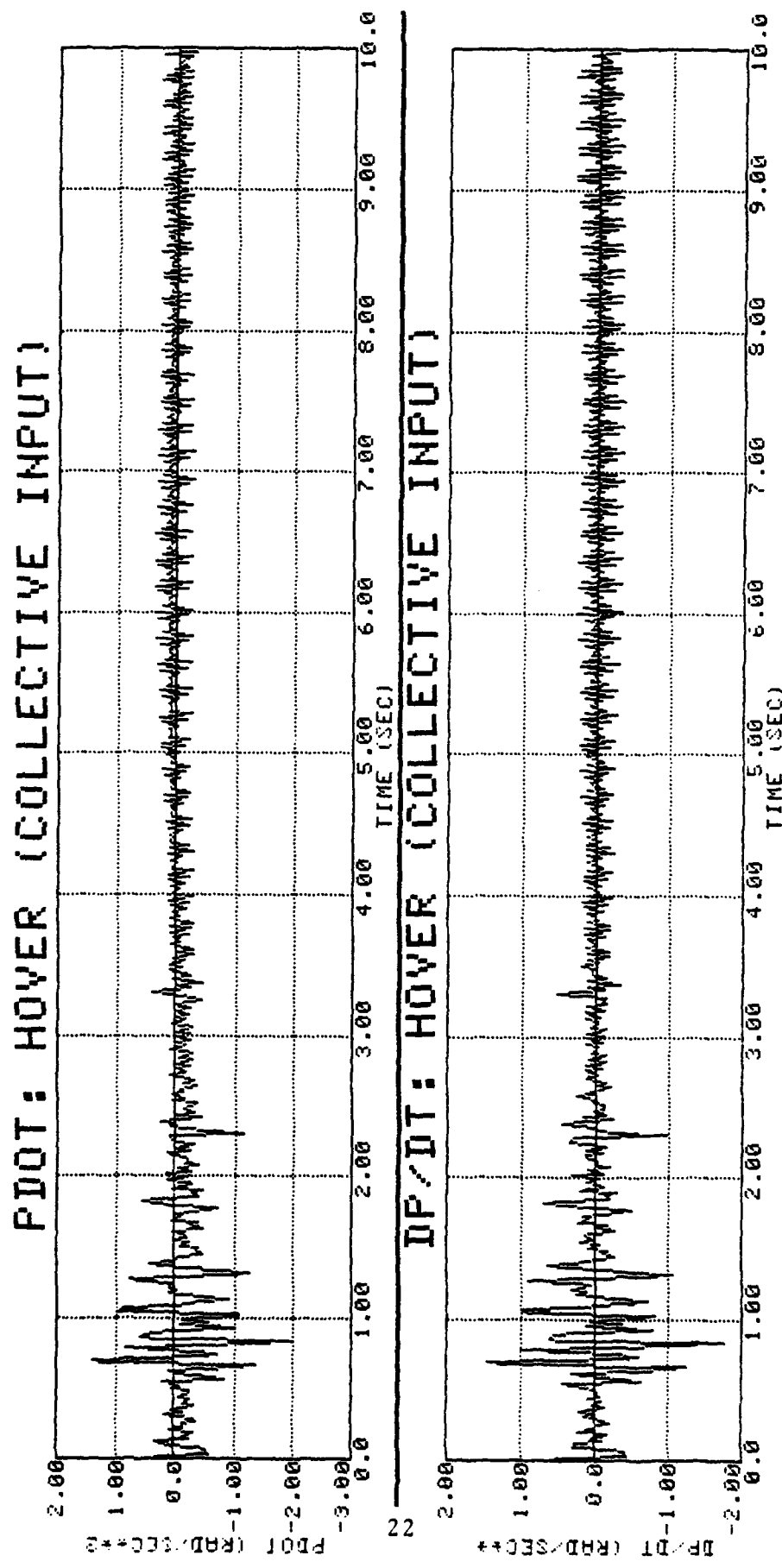


Figure 3.4 Comparison of \dot{P} with dP/dt

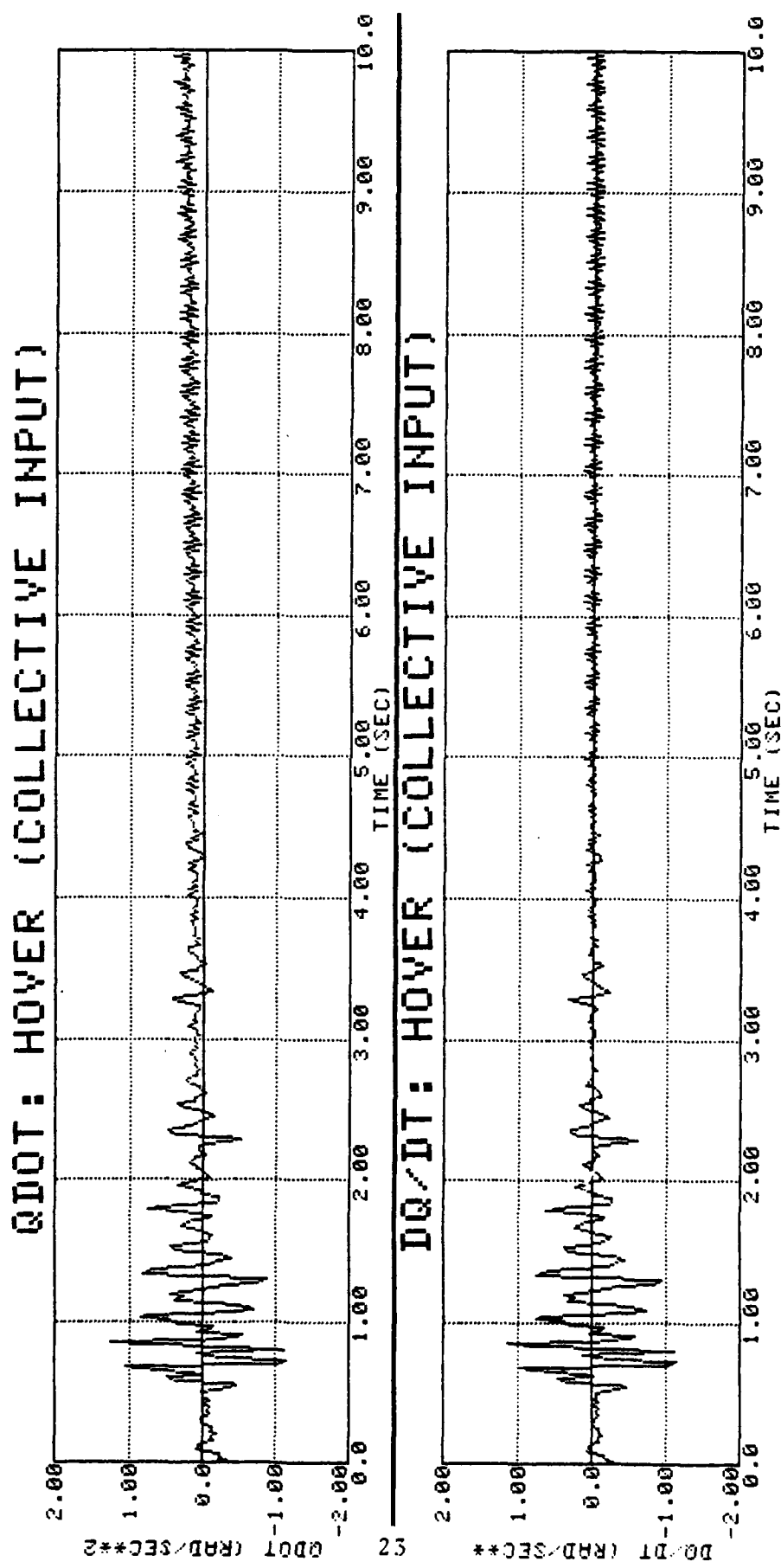
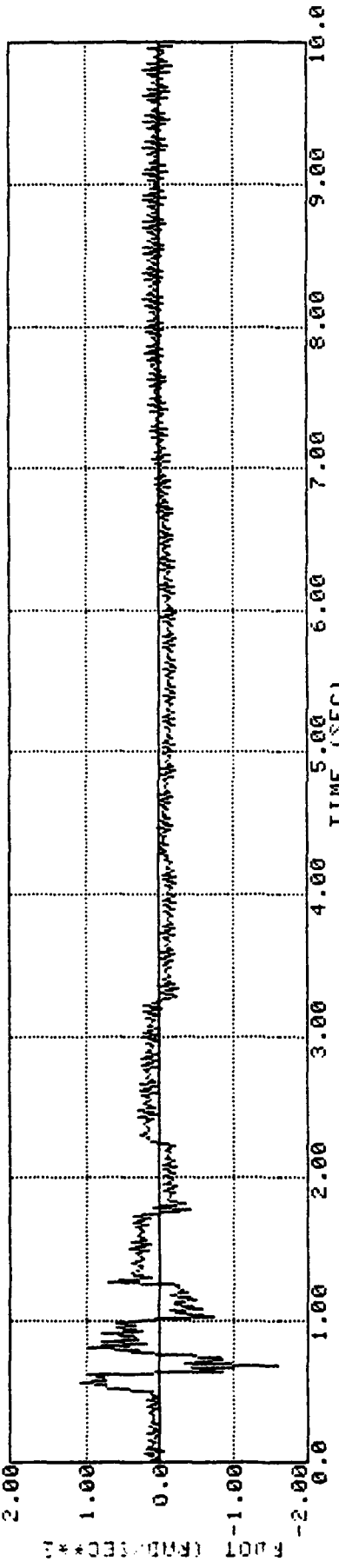


Figure 3.5 Comparison of \dot{Q} with dQ/dt

R DOT: HOVER (COLLECTIVE INPUT)



DR./DT: HOVER (COLLECTIVE INPUT)

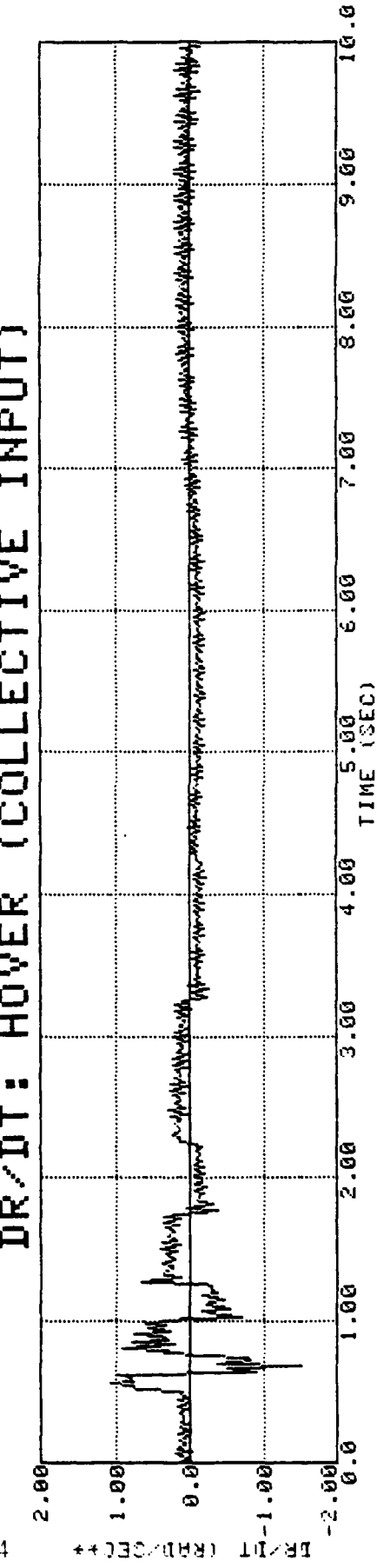
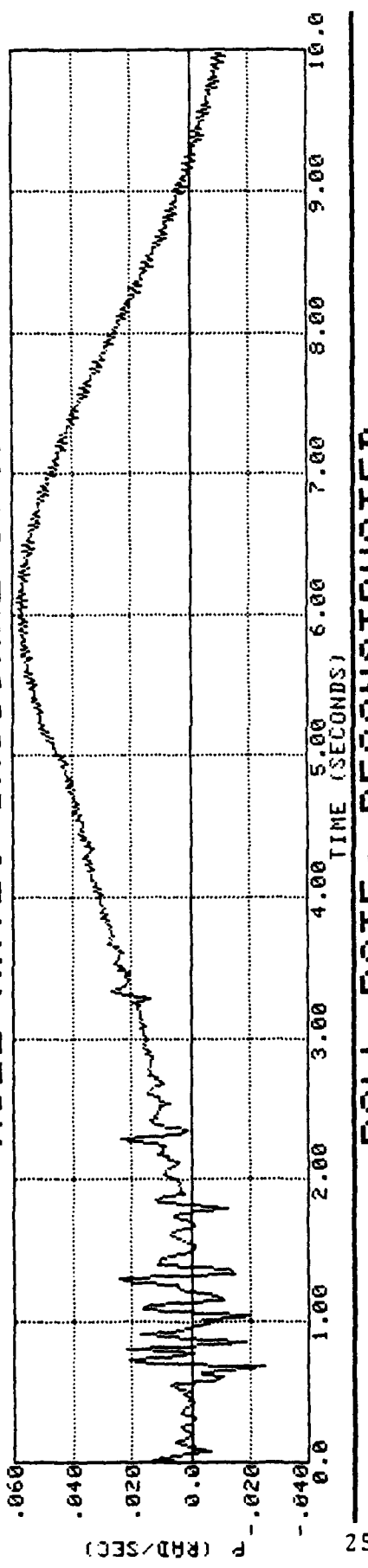


Figure 3.6 Comparison of \dot{R} with dR/dt

ROLL RATE: ORIGINAL DATA



ROLL RATE: RECONSTRUCTED

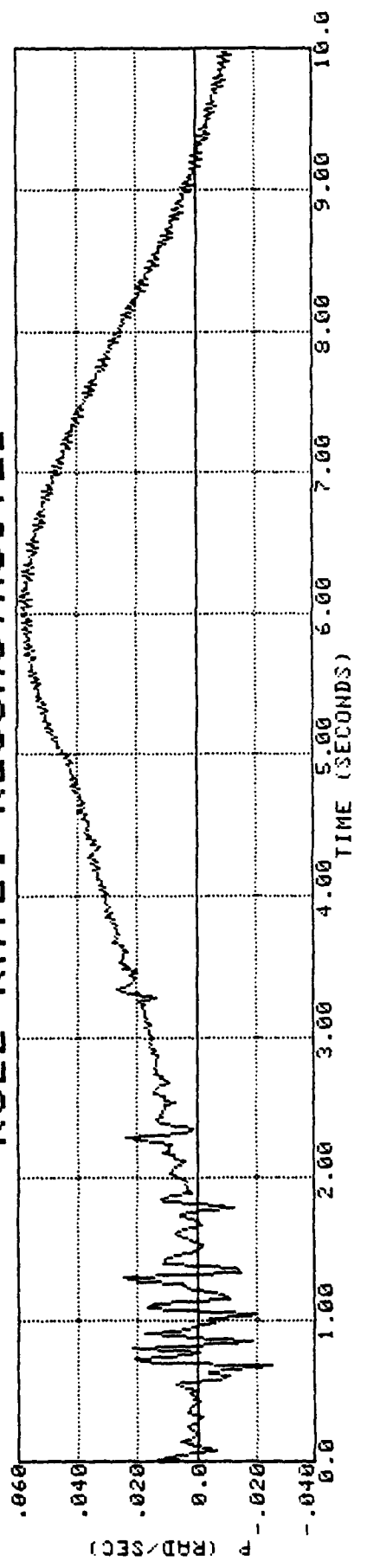


Figure 3.7 Comparison of Reconstructed Roll Rate with Original

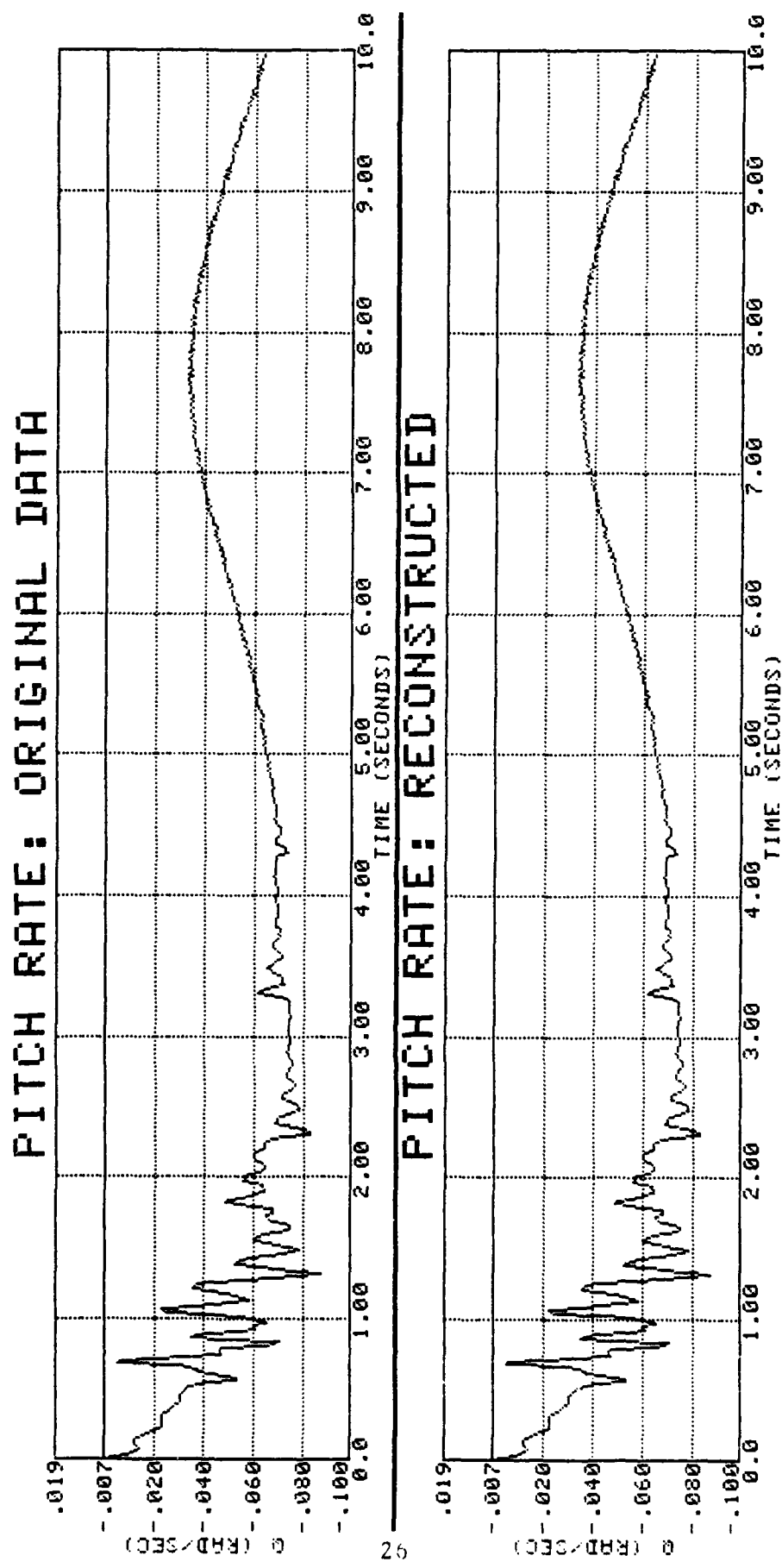


Figure 3.8 Comparison of Reconstructed Pitch Rate with Original

3.4.2 Data Filtering

The REXOR time history data contain high-frequency oscillatory components, with a frequency of four per revolution, excited by the rotation of the four blades. This frequency, $4 \times \Omega_R$, is equal to 26.94 Hz. This is a much higher frequency than any to which the pilot could respond. It could therefore be classified as a vibration rather than a response. For this reason, it was decided to filter out these higher frequencies.

To achieve this filtering, a digital implementation of a fourth-order Butterworth filter, with a cutoff frequency of 13.47 Hz ($2 \times \Omega_R$) was used. By passing the data through the filter twice, once forward and once backward, it was possible to achieve virtually zero phase shift throughout the pass band. This also effectively doubled the order of the filter, thus producing a steep cutoff above the filter frequency. Samples of the filtered REXOR data for the hover flight condition, main rotor collective blowing input, are shown in Figures 3.9 through 3.13.

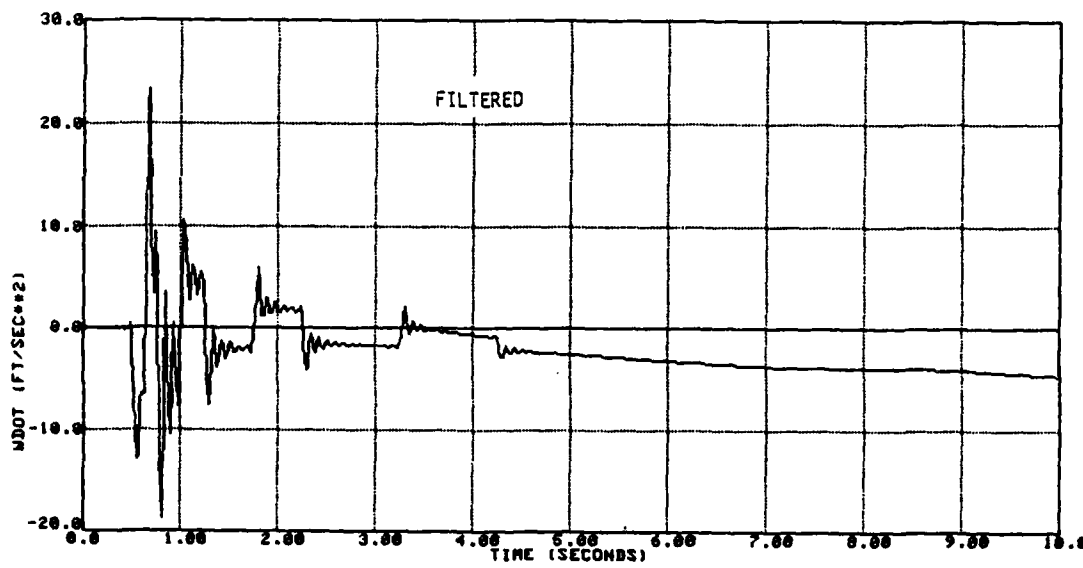
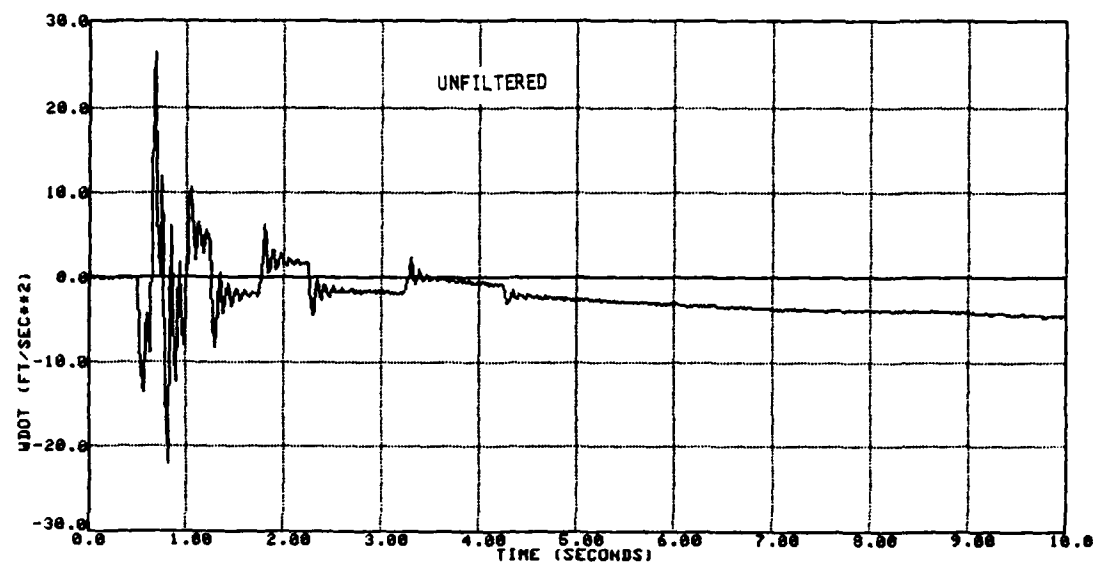


Figure 3.9 Effect of Fourth-Order Butterworth Filter ($\omega_B = 2\Omega$) on Vertical Acceleration (Hover, Collective Input)

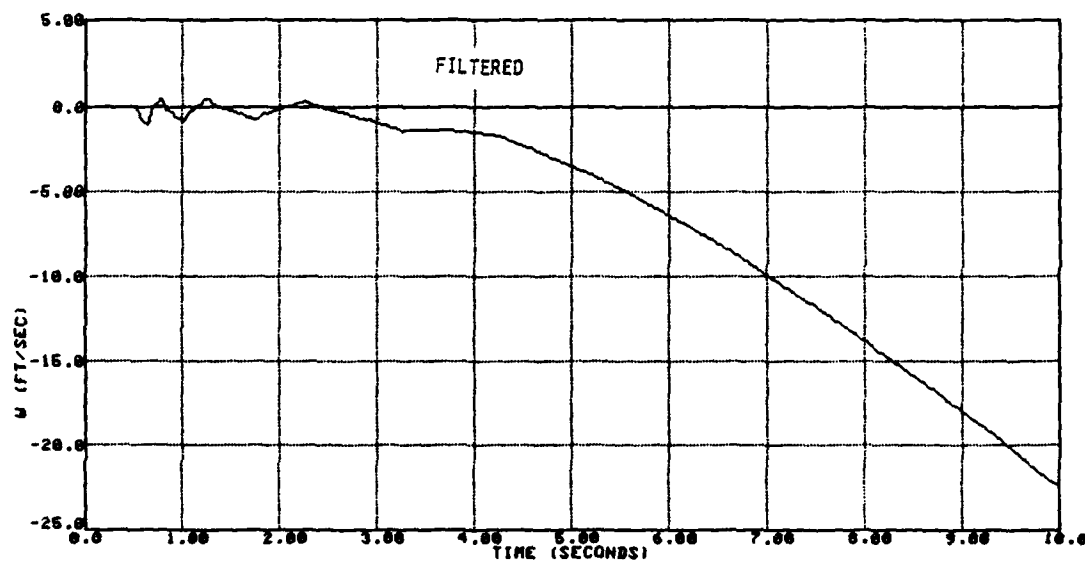
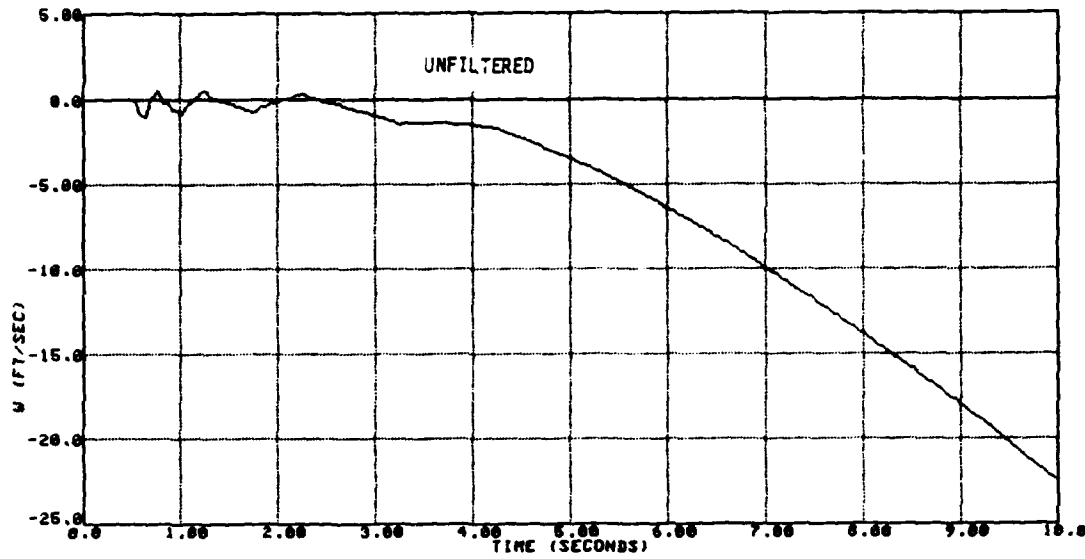


Figure 3.10 Effect of Fourth-Order Butterworth Filter ($\omega_B = 2\Omega$)
on Vertical Velocity (Hover, Collective Input)

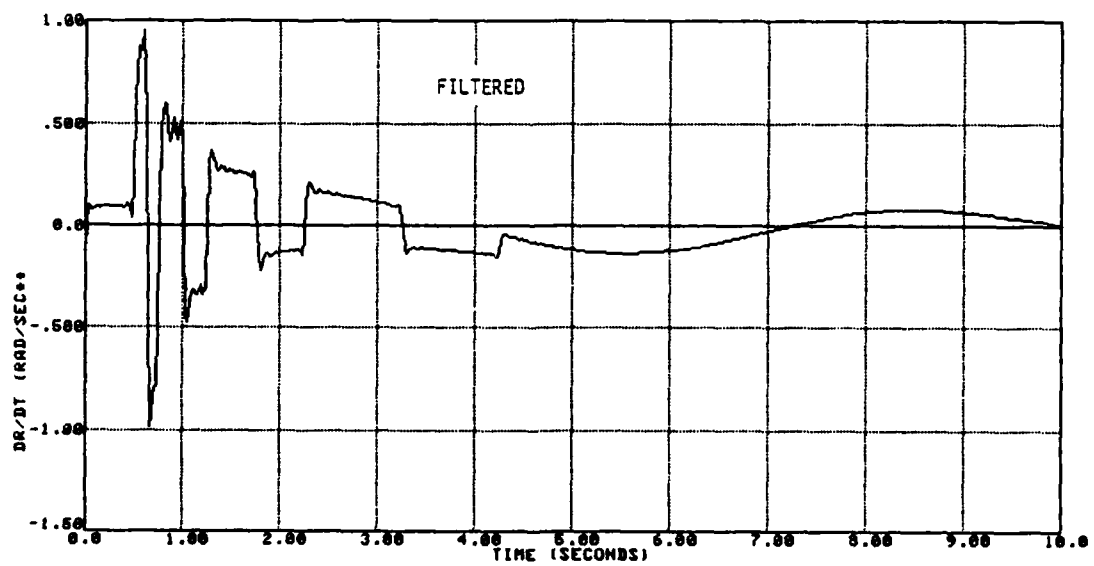
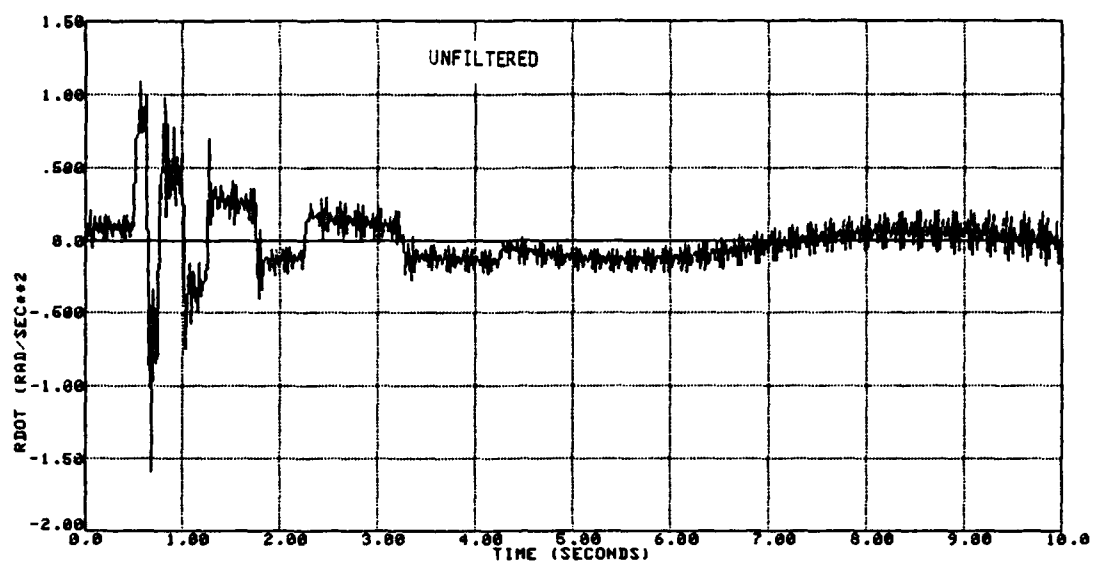


Figure 3.11 Effect of Fourth-Order Butterworth Filter ($\omega_B = 2\Omega$) on Yaw Acceleration (Hover, Collective Input)

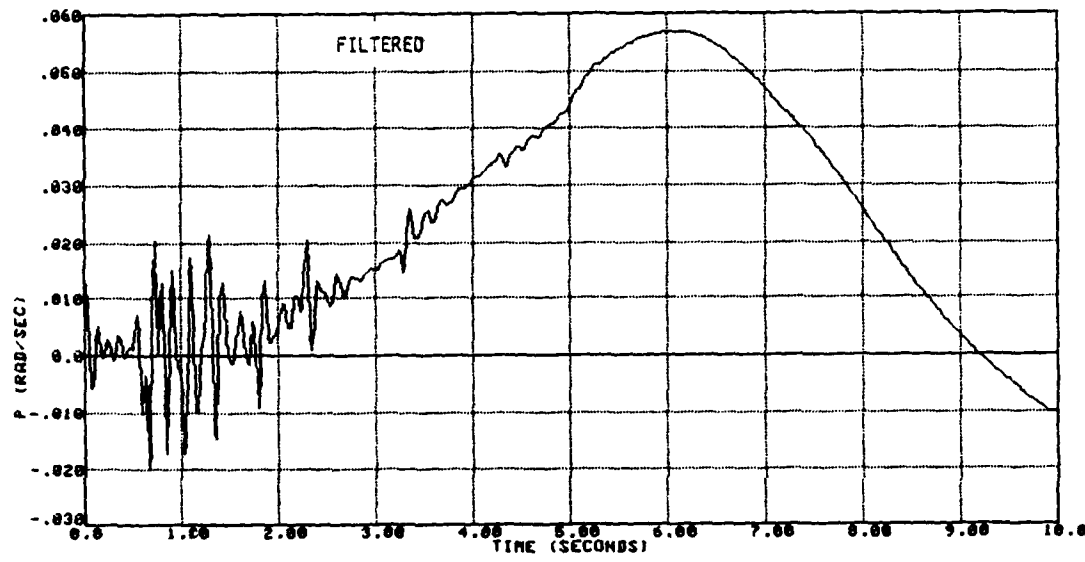
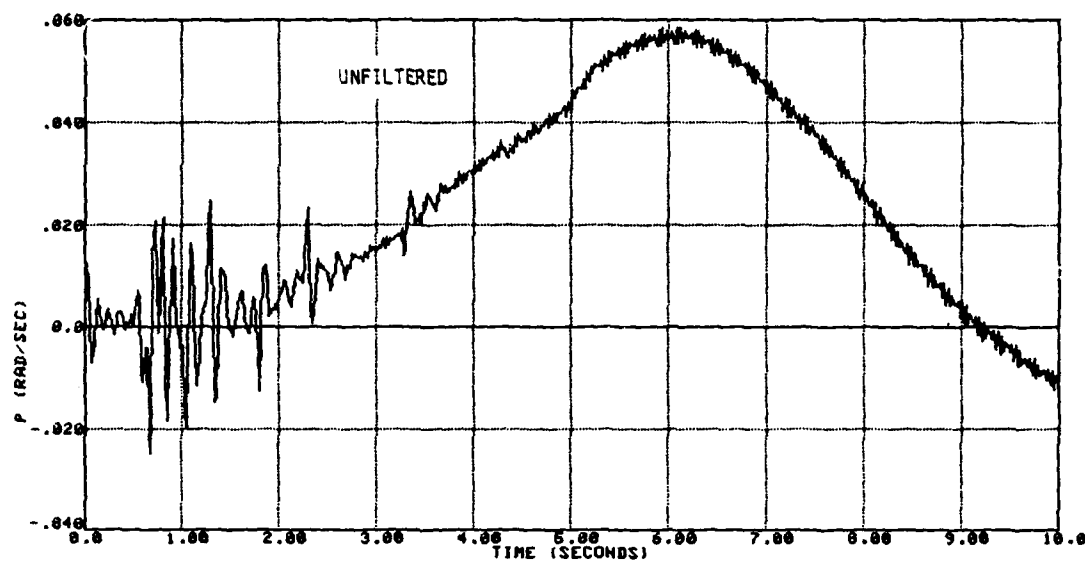


Figure 3.12 Effect of Fourth-Order Butterworth Filter ($\omega_B = 2\Omega$) on Roll Rate (Hover, Collective Input)

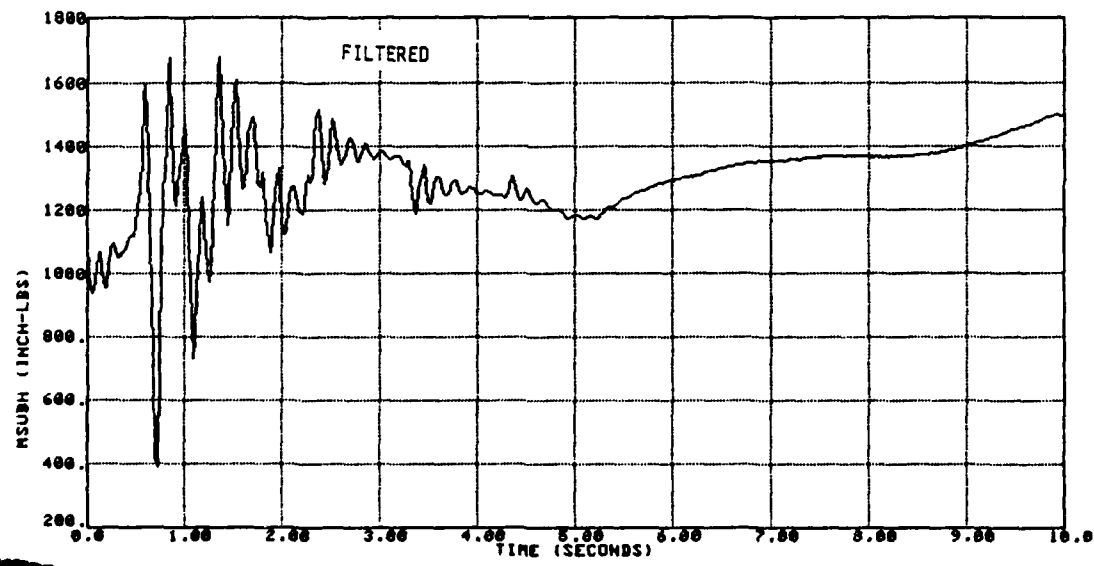
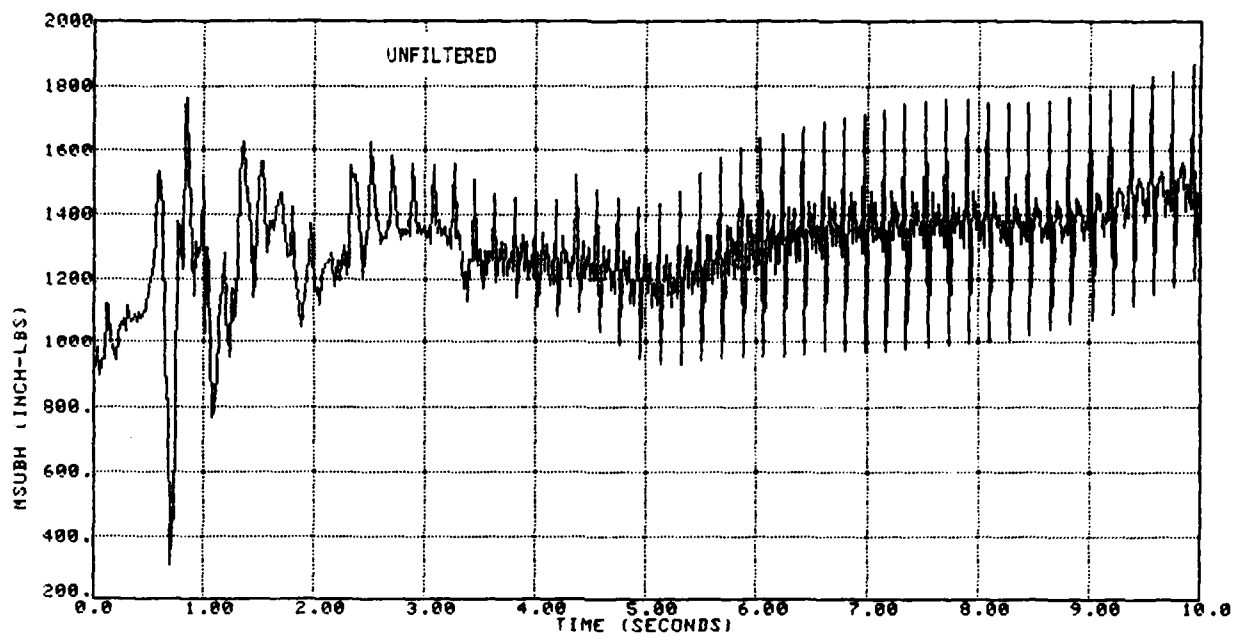


Figure 3.13 Effect of Fourth-Order Butterworth Filter ($\omega_B = 2\Omega$) on Pitch Hub Moment (Hover, Collective Input)

IV. IDENTIFICATION OF REDUCED-ORDER MODEL

4.1 OVERVIEW

This section describes a methodology for extracting reduced-order dynamic models of the X-wing configuration from REXOR simulation data. The data processing methodology is based on an adaptatin of system identification techniques which have been used to process flight test data [4]. Even though the described model extraction technique is demonstrated with the Lockheed X-wing configuration, it is intended to be applicable to any modeling task that requires the extraction of reduced-order models from complex simulations.

The scope of this chapter includes a discussion of system identification as it applies to the extraction of reduced-order models, a discussion of the X-wing modeling approach, and a presentation of X-wing reduced-order modeling results.

4.2 SYSTEM IDENTIFICATION OVERVIEW

System identification is a data processing technique which has been used to estimate the parameters of a math model from time histories of the dynamic response of that system. System identification, also called "parameter identification," has been used for a variety of different applications (see Table 4.1). Because of this diverse base of applications, several methods of approach for identifying moel structures and parameter values have been developed. The "best" identification algorithm/method is the one which is best suited to the particular requirements of each application.

The optimal subset regression (OSR) technique is well suited for the task of extracting reduced-order models from the REXOR simulation generated time histories. This choice is based on

Table 4.1
Role of Parameter Identification for Aircraft
Design, Test, and Evaluation

REDUCED-ORDER MODEL EXTRACTION FROM COMPLEX SYSTEM MATH MODEL
(e.g., ROTOR SIMULATION SUCH AS REXOR)

- ADEQUATE FIDELITY MODEL FOR REAL-TIME SIMULATION
- STATE MODELS FOR CONTROL SYSTEM DESIGN

FLIGHT TEST PLANNING

- INSTRUMENTATION AND DATA ACQUISITION SYSTEM REQUIREMENTS
- FLIGHT TEST CARD PREPARATION (INITIAL CONDITIONS AND PILOT INPUTS)
- DATA PROCESSING SOFTWARE DEVELOPMENT AND VALIDATION

FLIGHT TEST INSTRUMENTATION CALIBRATION (DYNAMIC)

AERODYNAMIC MODEL DOCUMENTATION FROM FLIGHT TEST MEASUREMENTS

- DATA FORMAT COMPATIBLE WITH USER REQUIREMENTS
- PREFLIGHT PREDICTION/FLIGHT OBSERVATION CORRELATION
- SIMULATION MATH MODEL VALIDATION

STATE MODEL EXTRACTION FROM FLIGHT TEST MEASUREMENTS

- APPLICATIONS: AIRFRAME, CONTROL SYSTEM, PROPULSION SYSTEM, ROTOR SYSTEM, STRUCTURAL MODES
- CONTROL SYSTEM PERFORMANCE ANALYSIS AND VALIDATION
- HANDLING QUALITY PARAMETERS FROM IDENTIFIED STATE MODELS

three considerations. First, OSR formulates the identification of parameters as an equation error problem. With the equation error technique, the parameters are the coefficients of the independent variables that, when combined in a linear equation, form the dependent variable (i.e., $\dot{P} = K_0 + K_1 p + K_2 Q + K_3 A_1 B + \dots$). Thus, OSR can be used to define the most significant model parameters (i.e. the model structure) for each degree of freedom. The aspect of obtaining the statistically most significant model structure is discussed in more detail later. The second reason for selecting the OSR algorithm is that it is computationally a very efficient program to use. The third consideration in the selection of OSR pertains to the source of the time history data which is used to identify the reduced-order model. For this study, the data were generated from the REXOR simulation of the X-wing configuration. Theoretically, if the simulation is set up properly, the resulting measurement time histories should be free of instrumentation errors and noise. The OSR algorithm works best with uncorrupted measurements. As an aside, when dealing with flight test measurements, which are often corrupted, a more sophisticated identification algorithm, such as the maximum likelihood approach, must be used.

The computational steps which are followed by the OSR algorithm are described as follows.

OSR is an algorithm which adds and deletes variables to a particular model in an iterative manner. The algorithm uses statistical hypothesis testing techniques based on the Fisher F ratio (e.g. F-tests). Formally, this ratio measures the difference in fit error with the current model relative to the error due to noise and model uncertainties. An "equation" F-ratio measures the entire model fit relative to error and a "parameter" F-ratio measures the incremental improvement in fit due to addition or deletion of a parameter in the model. Starting with a list of possible variables, the algorithm enters the first variable with the highest partial correlation to the

observations (i.e. the dependent variable). The contribution of this variable to reducing the fit error is made, and a new variable is entered. Subsequent tests add and delete variables to improve the "fit." This procedure is repeated until no variables are entered (or removed) from the model.

The model structure selected from the OSR results is based on a consideration of two statistical figures of merit and a comparison of candidate model structures with preflight predictions. This comparison also provides a means to validate the selected model structure. The two statistical figures of merit are the multitude correlation coefficient (R^2) and the equation F ratio. For a perfect fit, $R^2 = 1$. Generally, $R^2 \rightarrow 1$ as additional terms are added to the model. The equation F ratio relates fit goodness to fit error weighted by the degrees of freedom of the model. The desired model is one that has a good fit ($R^2 \rightarrow 1$) with the equation F ratio maximized.

One of the issues addressed at the outset of this study was the feasibility of using system identification to define the unaugmented math model parameters of an aircraft employing a high-gain feedback control system. The question arises from the fact that high-gain feedback loops prevent excitation of the unaugmented aircraft dynamics. Previous studies have shown that the unaugmented dynamics can be identified from the augmented dynamics, because the modes suppressed by the control system are reflected in the control system output (i.e. the control commands) time histories.

Thus, the math model for the unaugmented vehicle is obtained from measurements of the airplane's response and the control inputs. For the X-wing configuration, the control inputs are the hub moments, collective and cyclic blowing, and tail rotor collective.

4.3 X-WING MODELING APPROACH

Potential applications for a reduced-order model include an assessment of handling qualities, synthesis of flight control system control laws, and analysis of dynamic coupling between the rotor/flight control/propulsion systems. Linear models with good physical insight are desireable.

The desired modeling approach is based both on the intended usage of the reduced-order model and the X-wing configurational details.

A key feature of the X-wing configuration is its very rigid rotor system. Because of the rotor blade's structural stiffness, most maneuvers produce only small amounts of blade deflection. Thus, the X-wing's rotor system is not used for thrust vectoring through blade flapping. In addition, the first flapping degree of freedom occurs at a frequency greater than the principal rotor frequency.

Because of its extreme rigidity, the rotor exerts strong precessional moments on the aircraft as the result of commanded angular rates. Coupling moments are generated by aircraft rotations orthogonal to the rotor rotation. An established roll rate produces a pitch acceleration, and an established pitch rate generates a roll acceleration. These coupling moments are thus primarily dependent on rotor moment of inertia and RPM. Additional coupling effects due to rotor blade aerodynamics arise from nonuniformities in inflow, downwash, and blade loading. These variables are a function of rotor RPM, collective and cyclic blowing, and aircraft airspeed and angle of attack. Fuselage aerodynamic characteristics are dependent on rotor RPM, collective and cyclic blowing levels, aircraft angle of attack, sideslip and airspeed, aircraft rotational rates and tail rotor collective.

A linear state model representation is the most appropriate form for the reduced-order model. The state model formulation is

ideally suited for control system synthesis, coupled system analysis, and vehicle handling quality analysis problems. The state model formulation is based on constant coefficient equations that define the time rate of change of the state variables as a function of current values of the state and control variables. In addition, the state and control variables can be combined algebraically to form output variables. The equations below illustrate the state model formulation:

$$\dot{x} = Fx + Gu$$

$$y = Hx + Du$$

where F , G , H , D are constant coefficient system matrices, x is the state vector (e.g., axial velocity, body pitch rate, rotor collective flapping position), u is the control vector (e.g. collective blowing, cyclic blowing, etc.), and y is the output vector (e.g. rotor hub pitch torque). As a side comment at this point in the discussion, the identification of the elements that comprise the system matrices (F , G , H , D) from the REXOR simulation data is the technical objective of the study documented in this report. Continuing with the state model formulation discussion, the model form shown above can be constructed from a number of subsystem state models. This concept is illustrated in Figure 4.1, which shows the make-up of a coupled system state model that includes the body, stability augmentation system, rotor, drive train, engine and fuel controller degrees of freedom. The scope of this study pertains to only the airframe and rotor degrees of freedom. The REXOR simulation was run at constant rotor RPM; thus, decoupling the rotor from the engine and transmission.

The X-wing fuselage plus rotor state model can be define in one of two possible forms: viz, full-order state model and a quasi-static representation. For the full-order formulation, the

A/P	SAS	ROTOR #1	ROTOR #2	DRIVE TRAIN	ENG. #1	ENG. #2	FUEL CONTROL #1	FUEL CONTROL #2
RIGID BODY DOF	SAS COMMANDS	ROTOR / FUSELAGE	ROTOR / FUSELAGE		NOZZLE THRUST			
SAS INPUTS	SAS DYNAMICS	SAS INPUTS	SAS INPUTS					
FUSELAGE/ ROTOR	SAS COMMANDS	ROTOR #1 DOF	ROTOR #2 DOF	#1 ROTOR RPM	#2 ROTOR RPM			
FUSELAGE/ ROTOR	SAS COMMANDS	AERO LOAD AND LAG DAMPER	AERO LOAD AND LAG DAMPER	DRIVE TRAIN DOF	#1 ENG. TORQUE	#3 ENG. TORQUE		
					#1 ENG. NPT	ENG. #1 DOF	FUEL CONTROL COMMAND	
					#2 ENG. NPT	ENG. #2 DOF	FUEL CONTROL COMMANDS	
	FUEL CONTROL INPUTS				FUEL CONTROL INPUTS		FUEL CONTROL #2 DOF	

Figure 4.1 Total Coupled System Model Structure

rotor degrees of freedom are modeled explicitly (see Figure 4.2). For the illustrated example, the rotor degrees of freedom are described by the tip path plane displacements and velocities. For the quasi-steady formulation, the rotor states are implicitly modeled by fuselage states. The procedure followed in reducing a full-order state model to a quasi-static approximation is shown in Figure 4.3.

The quasi-static formulation was selected for the X-wing study due to the high stiffness of the rotor blades. Because of this stiffness, the flapping modes are well separated from the fuselage degrees of freedom. From a flight control engineer's point of view, the X-wing rotor behaves like a high bandwidth control actuator.

Specific modeling features for the quasi-steady X-wing model are described as follows:

- (1) The state and control variables are referenced to their initial values (i.e. $\dot{X} = \dot{X}_{Z_0} + F\Delta x + G\Delta u$). This was done since the REXOR simulation was not always initialized to zero.
- (2) Unsteady aerodynamic contributions for the moment equations were modeled in terms of $\Delta \dot{u}$, $\Delta \dot{v}$, $\Delta \dot{w}$ derivatives.
- (3) The angular acceleration equations model the rotor by a hub moment plus a moment resulting from the transfer of the hub force to the center of gravity. The hub force terms are proportional to A_y for the \dot{P} equation, A_x and A_z for the \dot{Q} equation and A_y for the \dot{R} equation.
- (4) The inertial coupling between P and R due to $I_{xz} \neq 0$ is not modeled explicitly. The P equation does not include \dot{R} terms, and the R equation does not include \dot{P} terms.

The equations of motion used for the X-wing analysis are presented in Table 4.2. The equations are developed for a body axis system representation, modeled the kinematic relationship with perturbation motion and assume untrimmed, wings-level

STATE EQUATIONS

$$\dot{x} = Fx + Gu$$

$$y = Hx + Du$$

STATES

$$x^T = \underbrace{[U \ V \ W \ P \ Q \ R \ \phi \ \theta]}_{\text{RIGID FUSELAGE}} \ ; \ \underbrace{[\zeta_0, \ \zeta_{1c}, \ \zeta_{1s}, \ \dot{\zeta}_0, \ \dot{\zeta}_{1c}, \ \dot{\zeta}_{1s}]}_{\text{ROTOR LAG (TIP PATH PLANE)}} \ ; \ \underbrace{[\beta_0, \ \beta_{1c}, \ \beta_{1s}, \ \dot{\beta}_0, \ \dot{\beta}_{1c}, \ \dot{\beta}_{1s}]}_{\text{ROTOR FLAP (TIP PATH PLANE)}}$$

CONTROLS

$$u^T = [A_{IB}, \ B_{IB}, \ R_{P0}, \ \theta_{TR}, \ L_H, \ M_H]$$

MEASUREMENTS

$$y^T = [p, \ q, \ r, \ a_x, \ a_y, \ a_z, \ \Omega, \ L_H, \ M_H]$$

Figure 4.2 General Rotorcraft State Model

CONVENTIONAL QUASI-STATIC DERIVATIVES CAN BE OBTAINED FROM THE FUSELAGE/ROTOR MOTOR

$$\text{RIGID BODY DOF: } \dot{x}_1 = F_{11} x_1 + F_{12} x_2 + G_{1\underline{u}} \quad (1)$$

$$\text{ROTOR DOF: } \dot{x}_2 = F_{21} x_1 + F_{22} x_2 + G_{2\underline{u}} \quad (2)$$

$$\text{LET: } \dot{x}_2 = 0 \quad (3)$$

$$\dot{x}_2 = - F_{22}^{-1} F_{21} x_1 - F_{22}^{-1} G_{2\underline{u}} \quad (4)$$

SUBSTITUTE EQ. (4) INTO EQ. (1)

$$\begin{aligned} & \text{FUSELAGE AND INITIAL} \\ & \text{ROTOR CONTRIBUTION} \\ \dot{x}_1 &= (\underbrace{F_{11} - F_{12} F_{21}^{-1} F_{21}}_{\substack{\text{QUASI-STATIC STABILITY} \\ \text{DERIVATIVE MATRIX}}}) x_1 + \underbrace{(G_1 - F_{12} F_{21}^{-1} G_2) \underline{u}}_{\substack{\text{QUASI-STATIC CONTROL} \\ \text{DERIVATIVE MATRIX}}} \end{aligned} \quad (5)$$

Figure 4.3 Method for Reducing Rotor/Fuselage Modes to Conventional Rigid-Body, Quasi-Static Derivatives

Table 4.2
Equations of Motion Used for X-Wing Analysis

$$\dot{u} = \dot{u}_{IC} + R_0 \Delta v - Q_0 \Delta w - w_0 \Delta Q + v_0 \Delta R$$

$$- g \cos \theta_0 \Delta \theta + A_x$$

$$\dot{v} = \dot{v}_{IC} - R_0 \Delta u + P_0 \Delta w + w_0 \Delta P - u_0 \Delta R$$

$$+ g \cos \theta_0 \Delta \theta + A_y$$

$$\dot{w} = \dot{w}_{IC} + Q_0 \Delta u - P_0 \Delta v - v_0 \Delta P + u_0 \Delta Q$$

$$- g \sin \theta_0 \Delta \theta + A_z$$

$$\dot{P} = \dot{P}_{IC} + \frac{\Delta M_x}{I_x}$$

$$\dot{Q} = \dot{Q}_{IC} + \frac{\Delta M_y}{I_y}$$

$$\dot{R} = \dot{R}_{IC} + \frac{\Delta M_z}{I_z}$$

$$\dot{\phi} = P + (Q \sin \phi + R \cos \phi) \tan \theta$$

$$\dot{\theta} = Q \cos \phi - R \sin \phi$$

initial conditions. The applied accelerations (i.e. A_x , A_y , A_z , $\Delta M_x/I_x$, $\Delta M_y/I_y$, $\Delta M_z/I_z$) are described by the identified X-wing math model. The a priori model structure, which includes all possible terms for the model structure determination and parameter identification analysis, is presented in Table 4.3.

4.4 IDENTIFIED MODEL RESULTS

Table 4.4 presents a summary of the equation fit statistics (R^2 and F_{EQ}) for the identified models for each flight condition. These statistics are based on the model fit errors (i.e. the difference between the identified model and the equation value calculated from REXOR data) for all four test inputs for each flight test condition. R^2 , the square of the equation multiple correlation coefficient, approaches one for reducing fit error. F_{EQ} , the equation F ratio, is related to R^2 , and it places a penalty on the number of terms included in the model. The relationship between R^2 and F_{EQ} is given by

$$F_{EQ} = \frac{R^2}{1-R^2} (N - 1)$$

where N = number of data points modeled, and

M = number of parameters in the model.

The identified model results are presented in Tables 4.5 through 4.12. Each of the tables shows the regression results for one dependent variable for each of the two flight conditions. Graphs showing a comparison of the identified model and the original time history are shown in Figures 4.4 through 4.35. The figures show: the four maneuvers for the hover flight condition, an enlarged view of one maneuver for the hover flight condition, the four maneuvers for the 100-fps flight condition, and an enlarged view of one maneuver for the 100 fps flight condition. The model is shown as a solid line, and the original

Table 4.3
X-Wing A Priori Applied Acceleration Models

Axial Acceleration (A_X)

$$A_X = A_{XIC} + X_u \Delta u + X_u \Delta v + X_w \Delta w + X_p \Delta p + X_q \Delta q + X_r \Delta r \\ + X_{A_{1B}} \Delta A_{1B} + X_{B_{1B}} \Delta B_{1B} + X_{R_{PO}} \Delta R_{PO} + X_{\theta_{OTR}} \Delta \theta_{OTR}$$

Lateral Acceleration (A_Y)

$$A_Y = A_{YIC} + Y_u \Delta u + Y_u \Delta v + Y_w \Delta w + Y_p \Delta p + Y_q \Delta q + Y_r \Delta r \\ + Y_{A_{1B}} \Delta A_{1B} + Y_{B_{1B}} \Delta B_{1B} + Y_{R_{PO}} \Delta R_{PO} + Y_{\theta_{OTR}} \Delta \theta_{OTR}$$

Vertical Acceleration (A_Z)

$$A_Z = A_{ZIC} + Z_u \Delta u + Z_u \Delta v + Z_w \Delta w + Z_p \Delta p + Z_q \Delta q + Z_r \Delta r \\ + Z_{A_{1B}} \Delta A_{1B} + Z_{B_{1B}} \Delta B_{1B} + Z_{R_{PO}} \Delta R_{PO} + Z_{\theta_{OTR}} \Delta \theta_{OTR}$$

Roll Acceleration (\dot{P})

$$\frac{\Delta M_X}{I_X} = L_u \Delta u + L_v \Delta v + L_w \Delta w + L_p \Delta p + L_q \Delta q + L_r \Delta r \\ + L_{A_{1B}} \Delta A_{1B} + L_{B_{1B}} \Delta B_{1B} + L_{R_{PO}} \Delta R_{PO} + L_{\theta_{OTR}} \Delta \theta_{OTR} \\ + L_{LH} \Delta L_H + L_{MH} \Delta M_H + L_{\dot{u}} \Delta \dot{u} + L_{\dot{v}} \Delta \dot{v} + L_{\dot{w}} \Delta \dot{w} + L_{AY} A_Y$$

Pitch Acceleration (\dot{Q})

$$\frac{\Delta M_Y}{I_Y} = M_u \Delta u + M_v \Delta v + M_w \Delta w + M_p \Delta p + M_q \Delta q + M_r \Delta r \\ + M_{A_{1B}} \Delta A_{1B} + M_{B_{1B}} \Delta B_{1B} + M_{R_{PO}} \Delta R_{PO} + M_{\theta_{OTR}} \Delta \theta_{OTR} \\ + M_{LH} \Delta L_H + M_{MH} \Delta M_H + M_{\dot{u}} \Delta \dot{u} + M_{\dot{v}} \Delta \dot{v} + M_{\dot{w}} \Delta \dot{w} + M_{AZ} A_Z$$

Table 4.3 (Continued)

Yaw Acceleration (R)

$$\frac{\Delta M_Z}{I_Z} = N_u \Delta u + N_v \Delta v + N_w \Delta w + N_p \Delta p + N_q \Delta q + N_r \Delta r \\ + N_{A_{1B}} \Delta A_{1B} + N_{B_{1B}} \Delta B_{1B} + N_{R_{PO}} \Delta R_{PO} + N_{\theta_{OTR}} \Delta \theta_{OTR} \\ + N_{LH} \Delta L_H + N_{MH} \Delta M_H + N_u \dot{\Delta u} + N_v \dot{\Delta v} + N_w \dot{\Delta w} + N_{AY} A_Y$$

Rotor Hub Rolling Moment (L_H)

$$L_H = L_{HIC} + L_{H_u} \Delta u + L_{H_v} \Delta v + L_{H_w} \Delta w + L_{H_p} \Delta p + L_{H_q} \Delta q \\ + L_{H_r} \Delta r + L_{H_{A_{1B}}} \Delta A_{1B} + L_{H_{B_{1B}}} \Delta B_{1B} + L_{H_{R_{PO}}} \Delta R_{PO} \\ L_{H_{\theta_{OTR}}} \Delta \theta_{OTR} + L_{H_u} \dot{\Delta u} + L_{H_v} \dot{\Delta v} + L_{H_w} \dot{\Delta w} \\ M_H = M_{HIC} + M_{H_u} \Delta u + M_{H_v} \Delta v + M_{H_w} \Delta w + M_{H_p} \Delta p + M_{H_q} \Delta q \\ + M_{H_r} \Delta r + M_{H_{A_{1B}}} \Delta A_{1B} + M_{H_{B_{1B}}} \Delta B_{1B} + M_{H_{R_{PO}}} \Delta R_{PO} \\ M_{H_{\theta_{OTR}}} \Delta \theta_{OTR} + M_{H_u} \dot{\Delta u} + M_{H_v} \dot{\Delta v} + M_{H_w} \dot{\Delta w}$$

Table 4.4
Summary of Identified Model Equation Error Fit Statistics

EQUATION	HOVER		100 fps	
	R ²	F _{EQ}	R ²	F _{EQ}
A _x	.998	96,555	.905	1,840
A _y	.999	181,550	.973	6,326
A _z	.999	506,990	.999	541,410
P	.904	1,207	.951	2,686
Q	.919	1,451	.977	4,459
R	.996	31,106	.997	43,888
L _H	.994	22,666	.989	13,394
M _H	.997	50,886	.997	67,052

time history is shown as a series of circles. Not all points used were plotted, so some of the apparent mismatch during high-frequency transients is due to the plotting.

The data presented in Table 4.4 indicate that the identified reduced-order models reproduce the applied accelerations generated by REXOR for each of the four control inputs. The fit errors are very good (i.e. $R^2 \geq .99$) with the exception of \dot{P} and \dot{Q} at both flight conditions, and A_x and A_y at the 100-fps flight condition.

The time histories for A_x and A_y (see Figures 4.6 and 4.10) indicate that the modeling problem with these accelerations is primarily with the high-frequency portion of collective blowing input. The models did not account for load sharing between the main and tail systems, and it also did not include direct thrust terms.

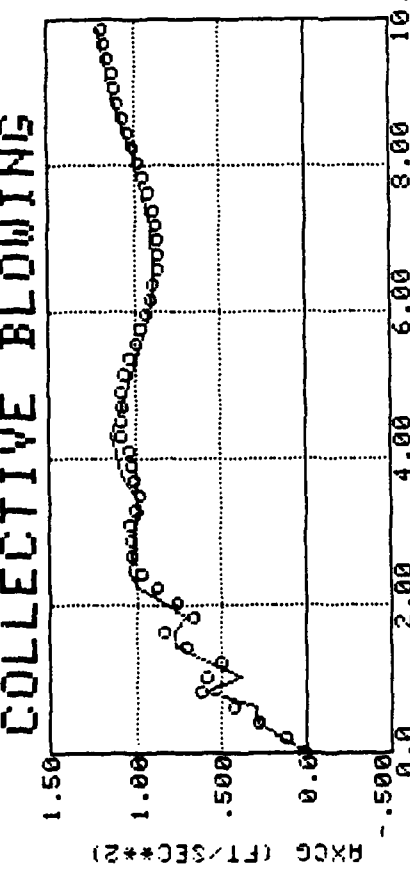
Examination of the regression statistics and graphical comparisons showed that a modeling discrepancy existed in the pitch and roll accelerations and, to a lesser extent, the pitch hub moment. The angular acceleration errors may be related to the discrepancy, previously noted, between the pitch and roll rates and accelerations from REXOR. Comparison of the model error for \dot{Q} at hover (Figure 4.21) with the original data for M_H at hover (Figure 4.33), both with the same input (longitudinal cyclic), shows a strong similarity. These comparisons indicate that the pitch acceleration (\dot{Q}) and the hub pitching moment from REXOR are not completely consistent with each other.

Table 4.5
Regression on A_X

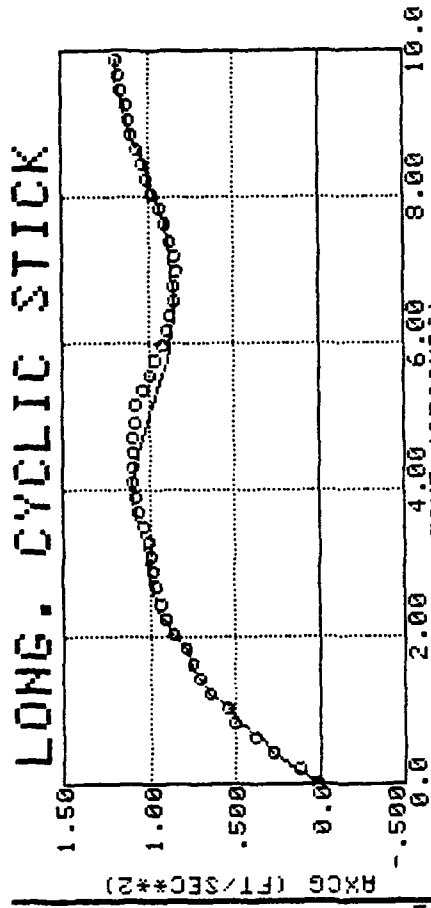
HOVER			100 FPS		
VARIATION EXPLAINED BY R^2 : 0.99778289			VARIATION EXPLAINED BY R^2 : 0.90509230		
EQUATION F-RATIO: 96555.			EQUATION F-RATIO: 1840.6		
VARIABLE	COEFFICIENT	PARAM. F-RATIO	VARIABLE	COEFFICIENT	PARAM. F-RATIO
Δu	0.0361688	1231.	Δu	-0.0226901	286.4
Δv	0.00374915	78.38	Δv	-0.00514939	105.7
Δw	0.127009	1359.	Δw	-0.0450900	119.3
Δp	-0.524142	12.55	Δp	-5.06478	3329.
Δq	-4.12427	1078.	Δq	2.05791	308.1
Δr	-0.0500819	32.37	Δr	0.142897	66.94
Δb_{1B}	2.35073	2324.	Δb_{1B}	1.57060	443.3
Δr_{p0}	0.504574	99.00	Δb_{1B}	0.625611	417.6
$\Delta \theta_{0TR}$	-1.19130	306.9	Δr_{p0}	0.180412	586.9

LINE CODE
1 IDENTIFIED MODEL
000000000 REXOR SIMULATION DATA

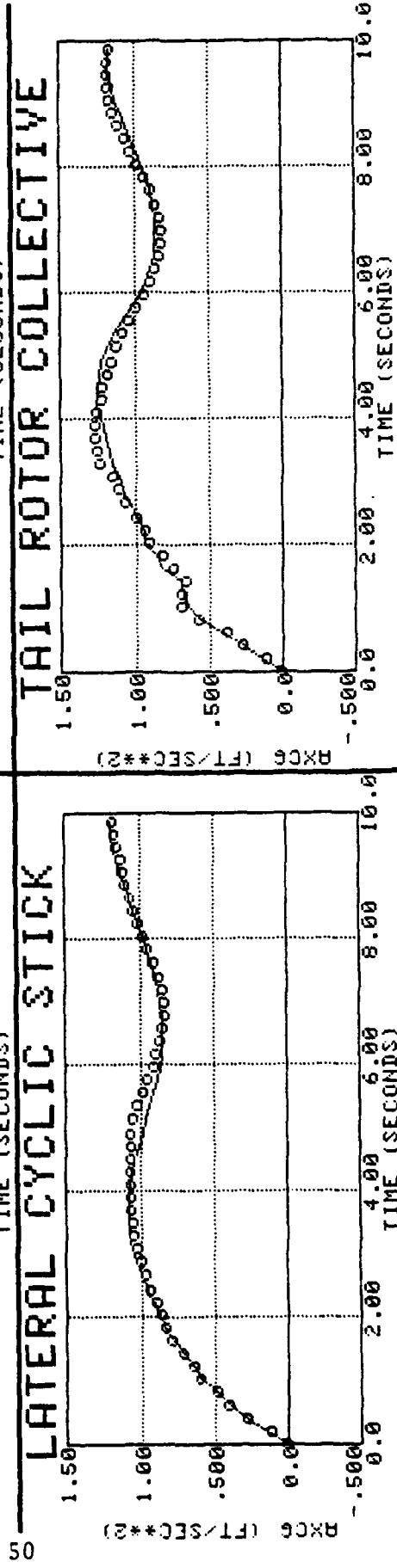
COLLECTIVE BLOWING



LONG. CYCLIC STICK



LATERAL CYCLIC STICK



TAIL ROTOR COLLECTIVE

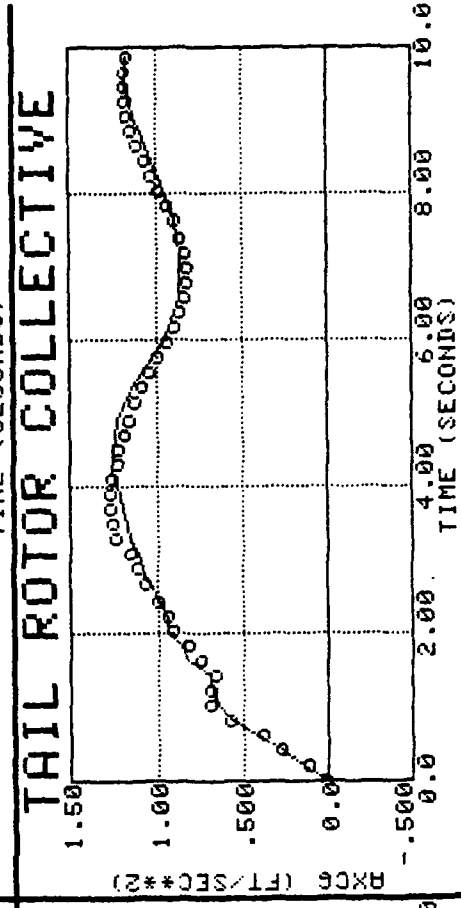


Figure 4.4 Forward Acceleration (Hover)

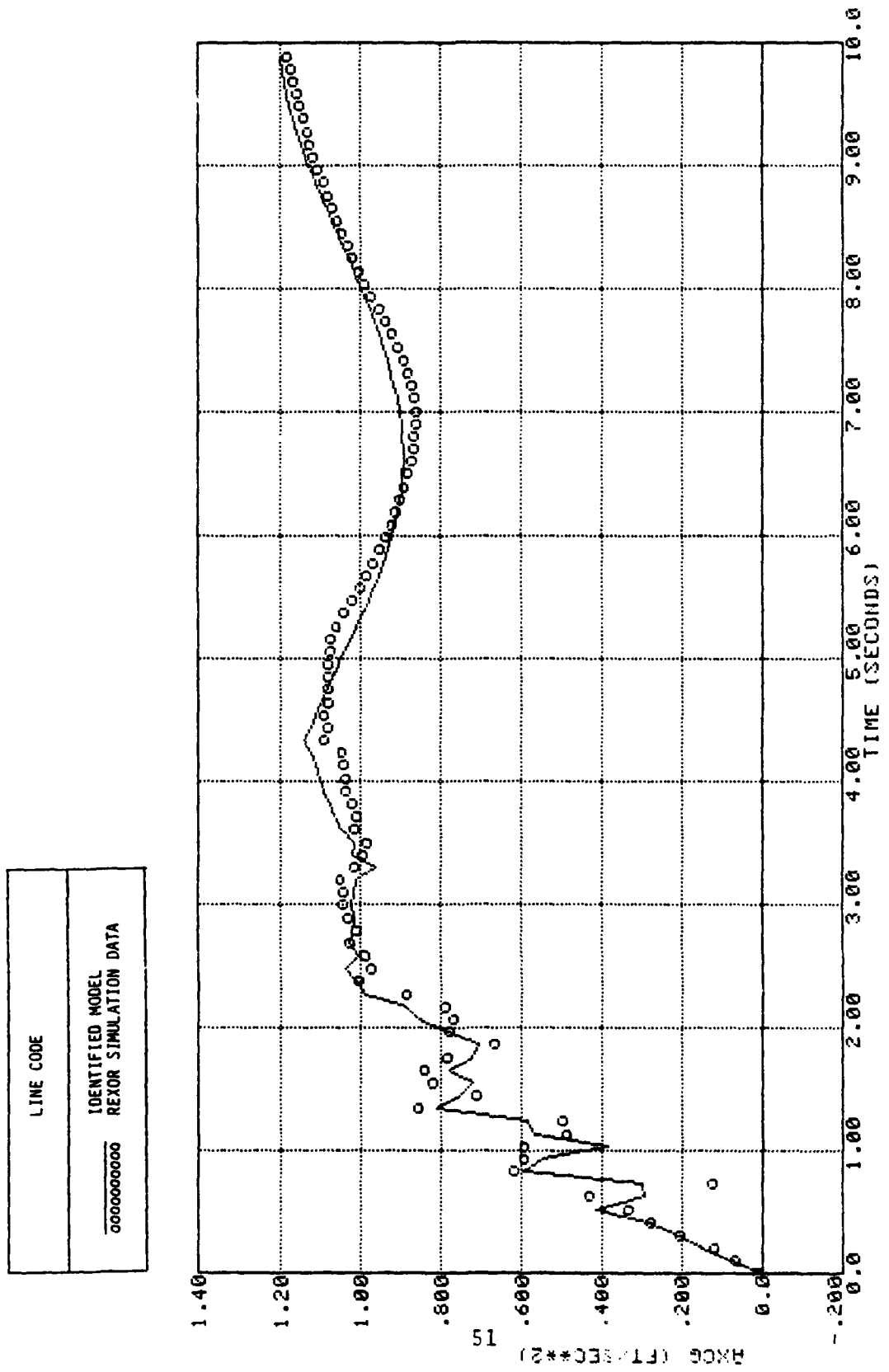
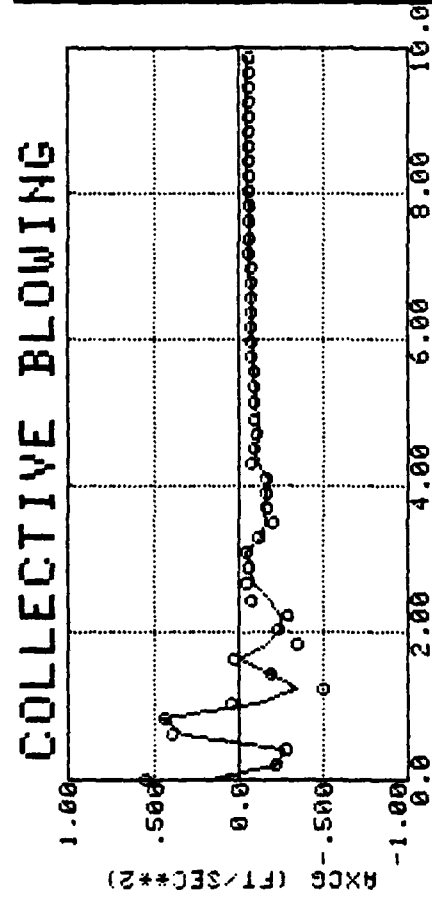


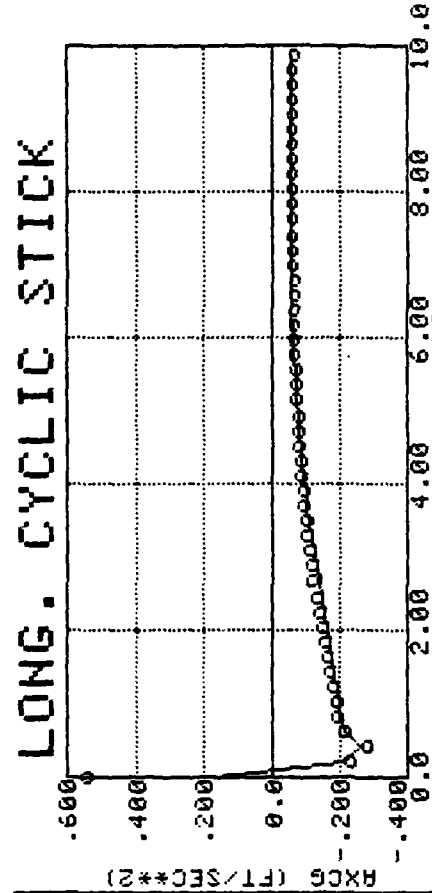
Figure 4.5 Forward Acceleration (Hover, Collective Input)

LINE CODE	IDENTIFIED MODEL REXOR SIMULATION DATA
-----------	---

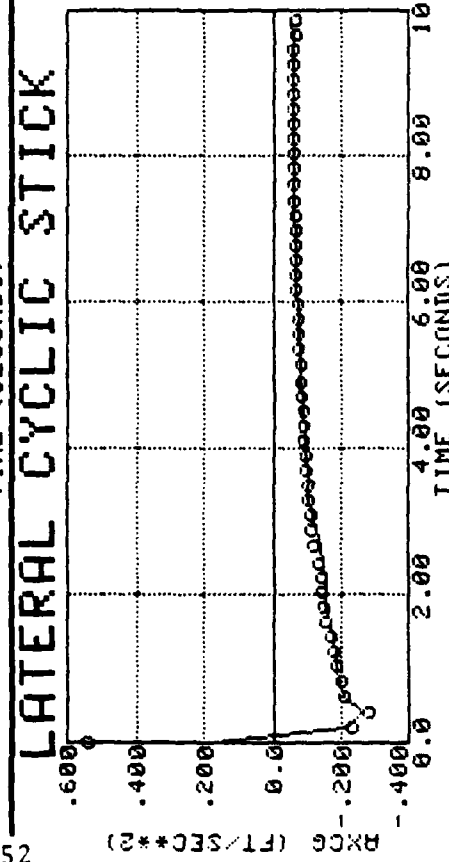
COLLECTIVE BLOWING



LONG . CYCLIC STICK



LATERAL CYCLIC STICK



TAIL ROTOR COLLECTIVE

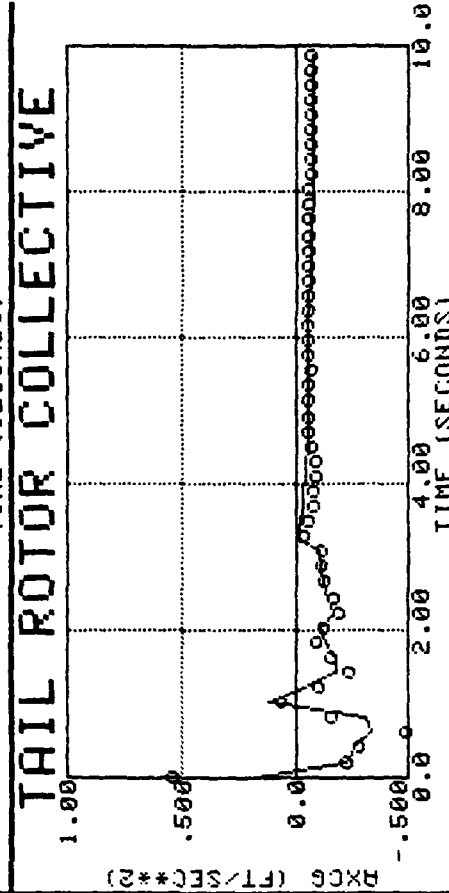
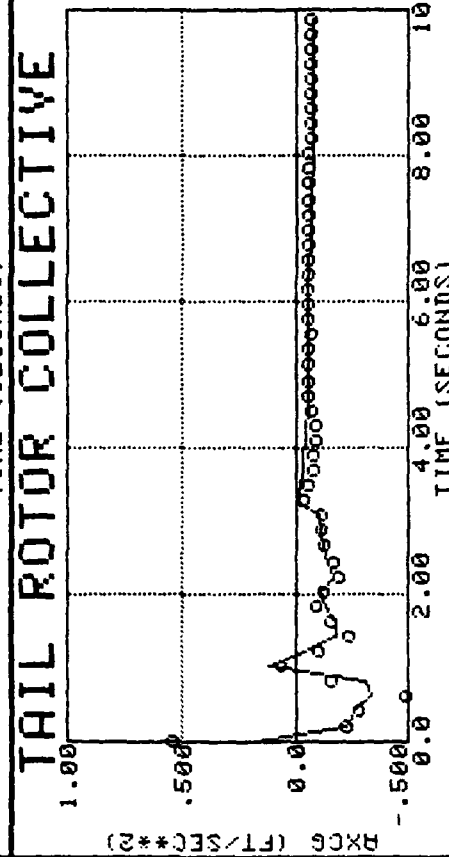


Figure 4.6 Forward Acceleration (100 fps)

LINE CODE	
0000000000	IDENTIFIED MODEL REXOR SIMULATION DATA

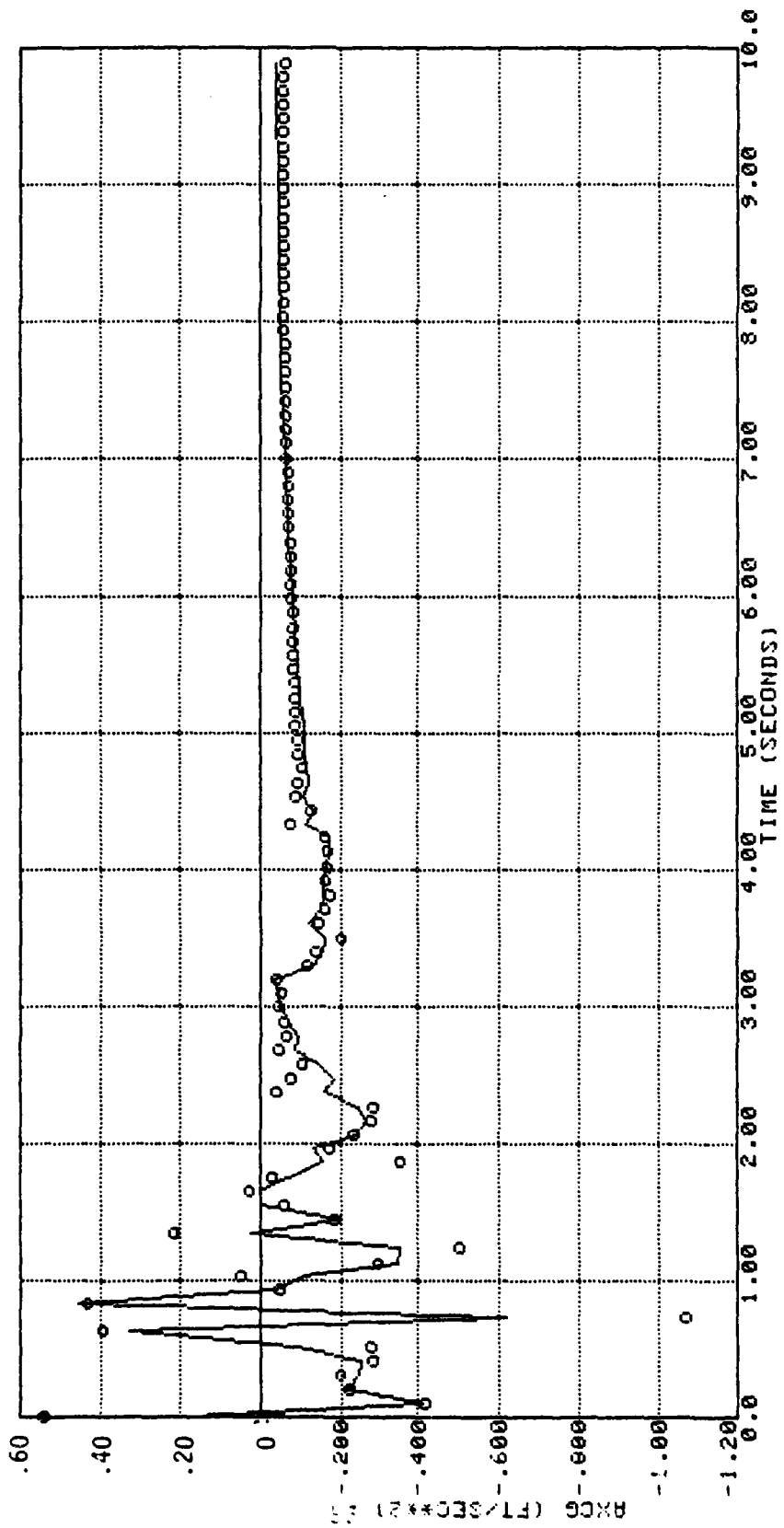


Figure 4.7 Forward Acceleration (100 fps, Collective Input)

Table 4.6
Regression on A_Y

HOVER			100 FPS		
VARIATION EXPLAINED BY R ² : 0.99893814			VARIATION EXPLAINED BY R ² : 0.97302657		
EQUATION F-RATIO: 181550.			EQUATION F-RATIO: 6326.0		
VARIABLE	COEFFICIENT	PARAM. F-RATIO	VARIABLE	COEFFICIENT	PARAM. F-RATIO
Δu	-0.0582492	620.8	Δu	0.0167003	21.08
Δv	0.00590237	15.96	Δv	-0.00887424	43.38
Δw	-0.174493	716.7	Δw	-0.0218713	3.943
Δp	10.1595	1393.	Δp	5.92479	606.1
Δq	-6.22686	252.4	Δq	-9.83833	739.5
Δr	0.507576	975.1	Δr	1.84915	1345.
ΔA_{1B}	1.38220	54.10	ΔA_{1B}	-1.86828	86.35
ΔB_{1B}	-1.54490	205.3	ΔB_{1B}	-0.813999	98.05
$\Delta \theta_{0TR}$	18.1581	14710.	ΔR_{p0}	-4.29429	589.7
CONST.	2.89626	105200.	$\Delta \theta_{0TR}$	17.8188	8957.
			CONST.	0.118500	32.34

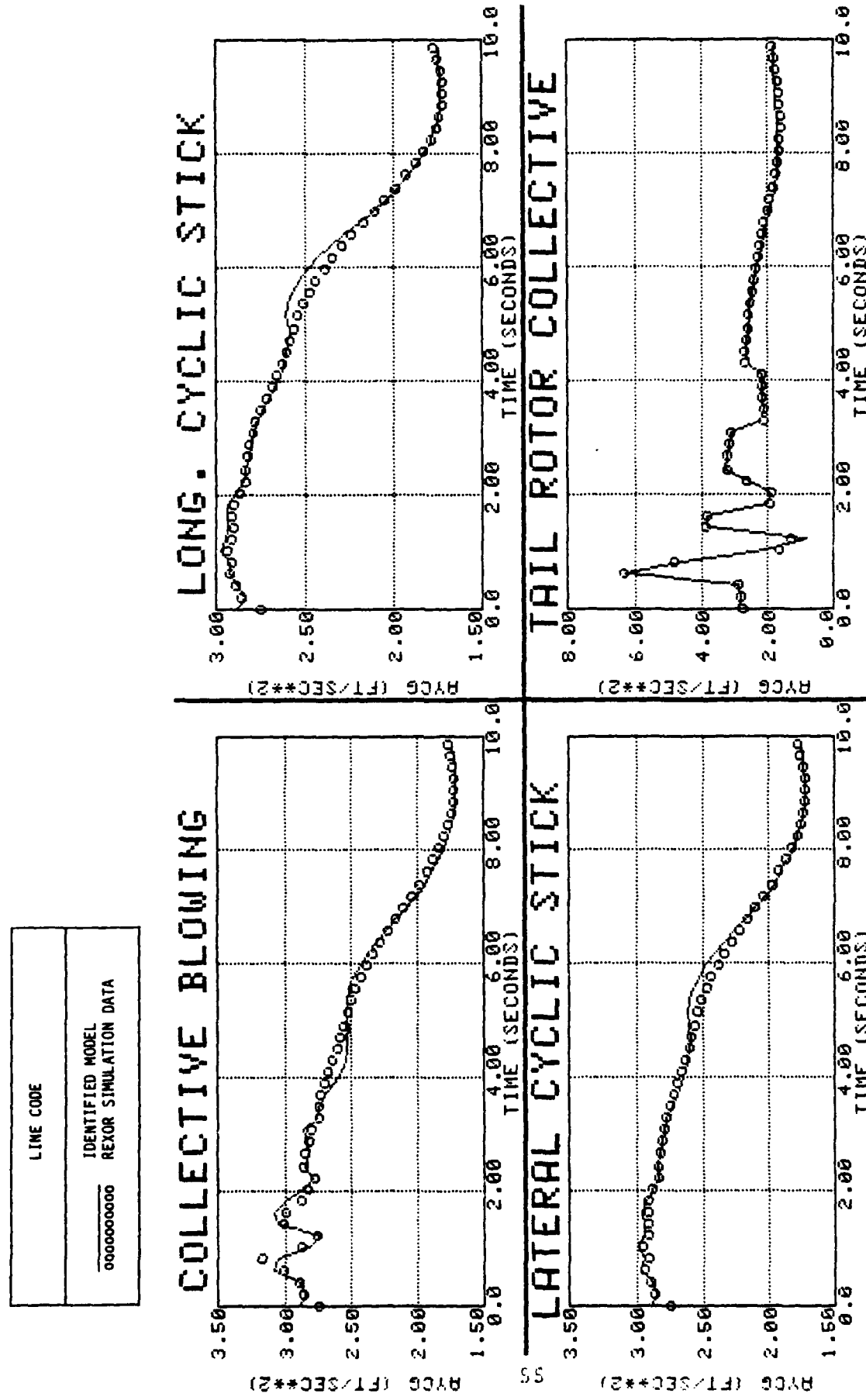


Figure 4.8 Lateral Acceleration (llover)

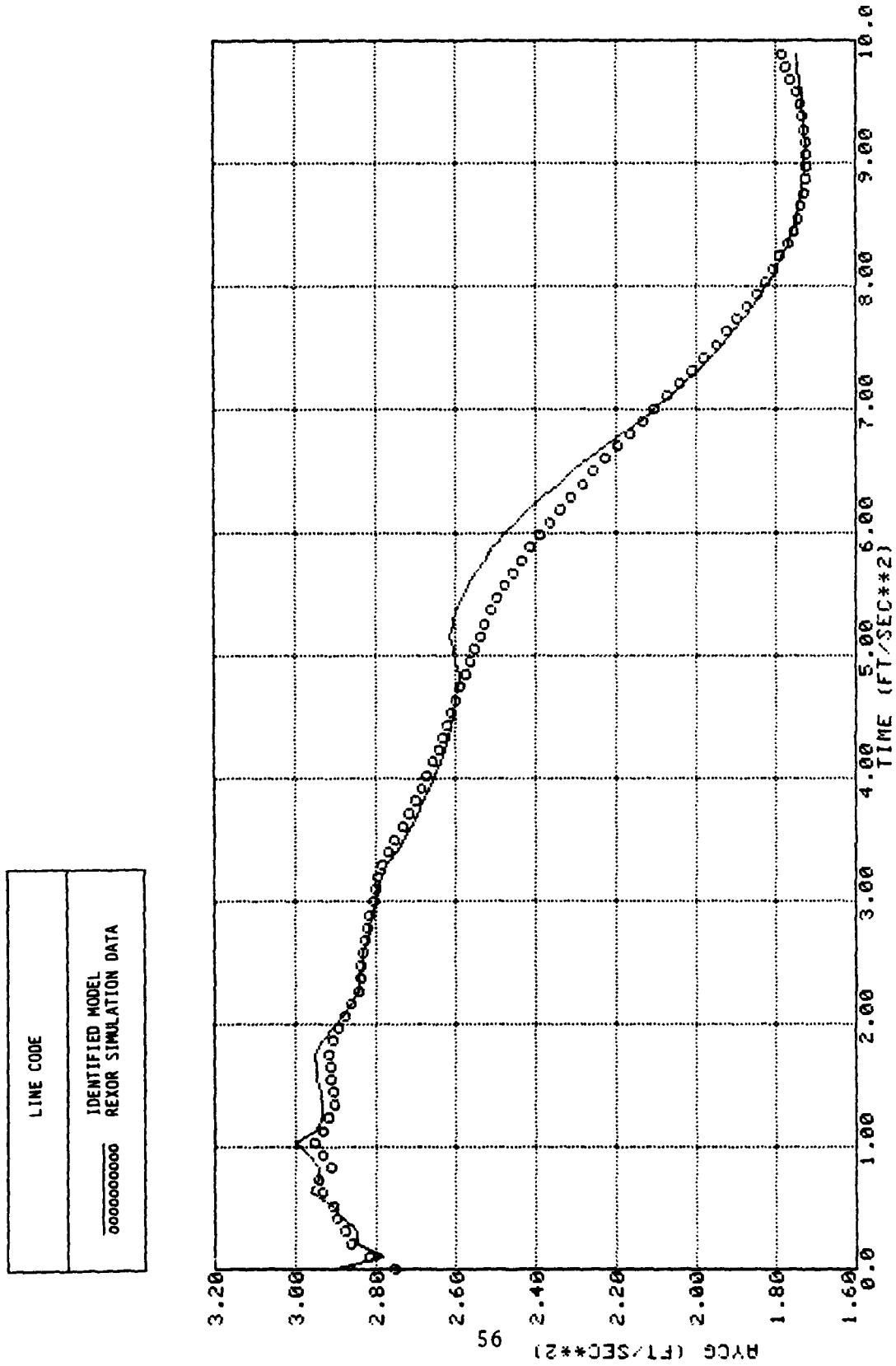


Figure 4.9 Lateral Acceleration (Hover, Collective Input)

LINE CODE	IDENTIFIED MODEL REXOR SIMULATION DATA
0000000000	

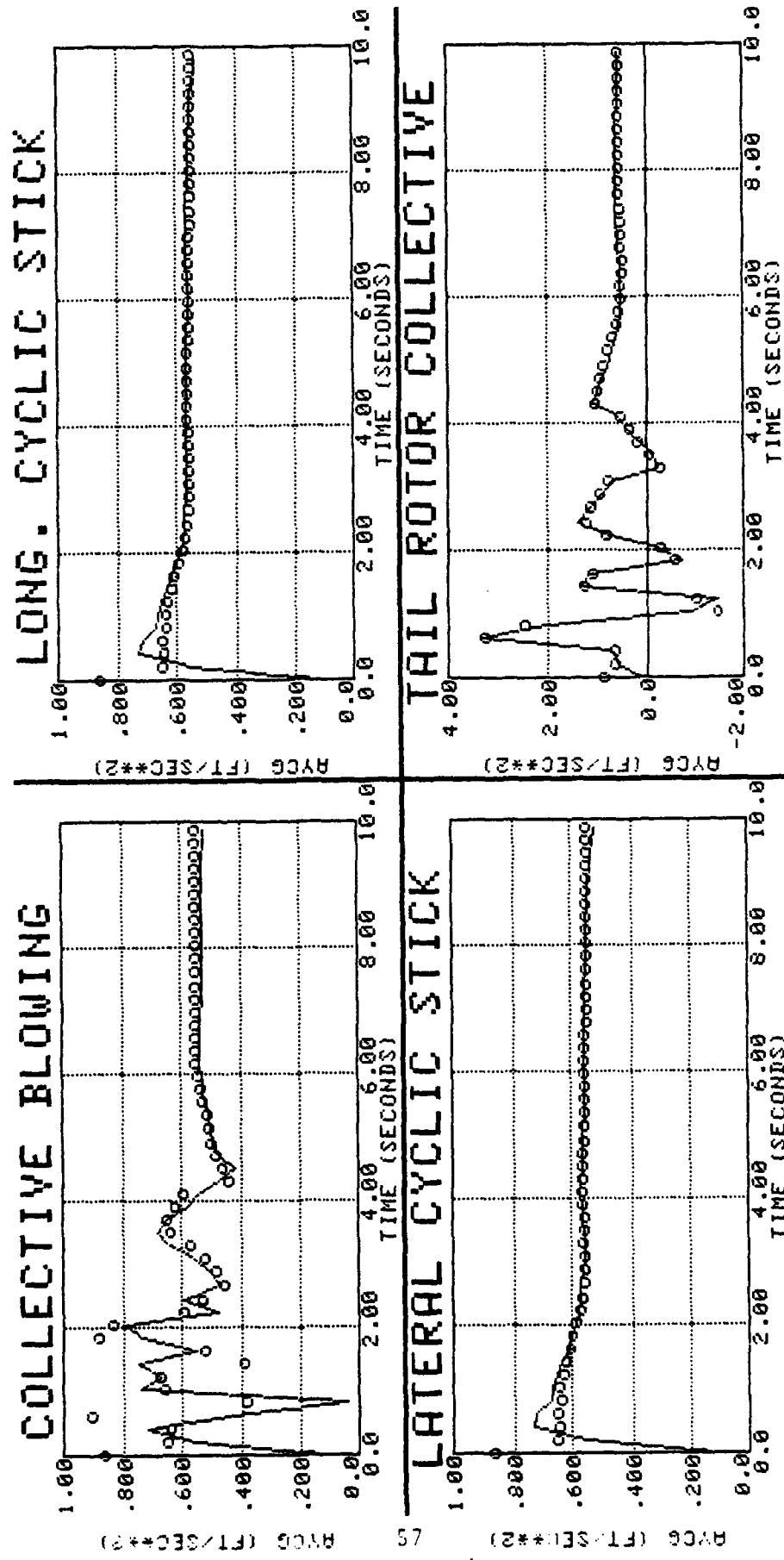


Figure 4.10 Lateral Acceleration (100 fps)

LINE CODE
0000000000 IDENTIFIED MODEL REXOR SIMULATION DATA

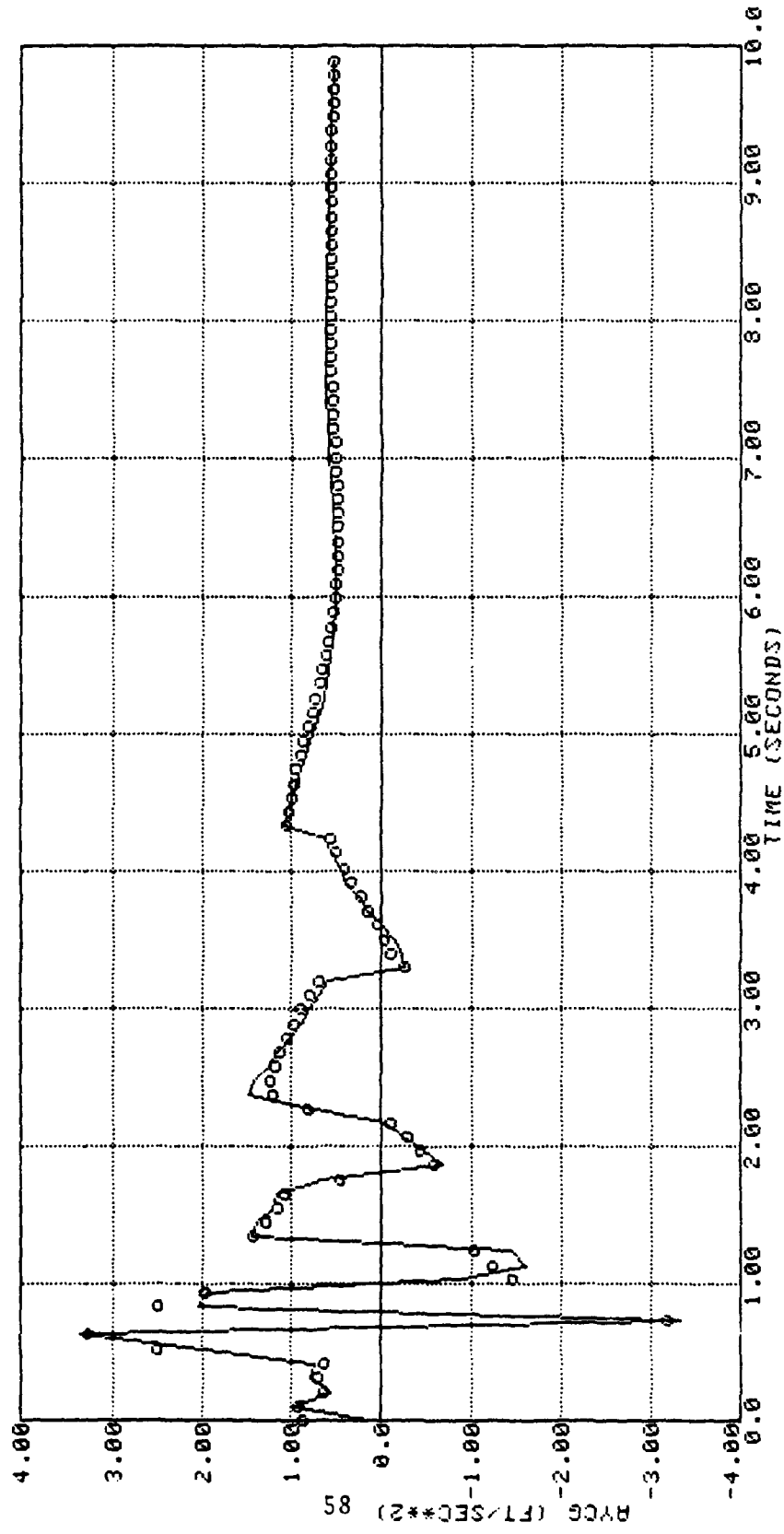


Figure 4.11 Lateral Acceleration (100 fps, Tail Rotor Collective)

Table 4.7
Regression on A_Z

HOVER		100 FPS	
VARIATION EXPLAINED BY R^2 : 0.99952382		VARIATION EXPLAINED BY R^2 : 0.99964362	
EQUATION F-RATIO: 506990.		EQUATION F-RATIO: 541410.	
VARIABLE	COEFFICIENT	PARAM. F-RATIO	VARIABLE
Δu	0.101499	441.2	Δu
Δv	-0.0300388	21.29	Δv
Δp	-16.2252	99.15	Δw
Δr	0.900824	57.87	Δp
Δa_{1B}	14.2282	268.2	Δq
Δb_{1B}	-2.91791	36.97	Δa_{1B}
Δr_{p0}	-54.6296	5126.	Δb_{1B}
CONST.	-32.3994	186800.	Δr_{p0}
			-39.2598
			$\Delta \theta_{OTR}$
			3.33134
			CONST. -32.129
			91090.

LINE CODE
IDENTIFIED MODEL REXOR SIMULATION DATA 000000000

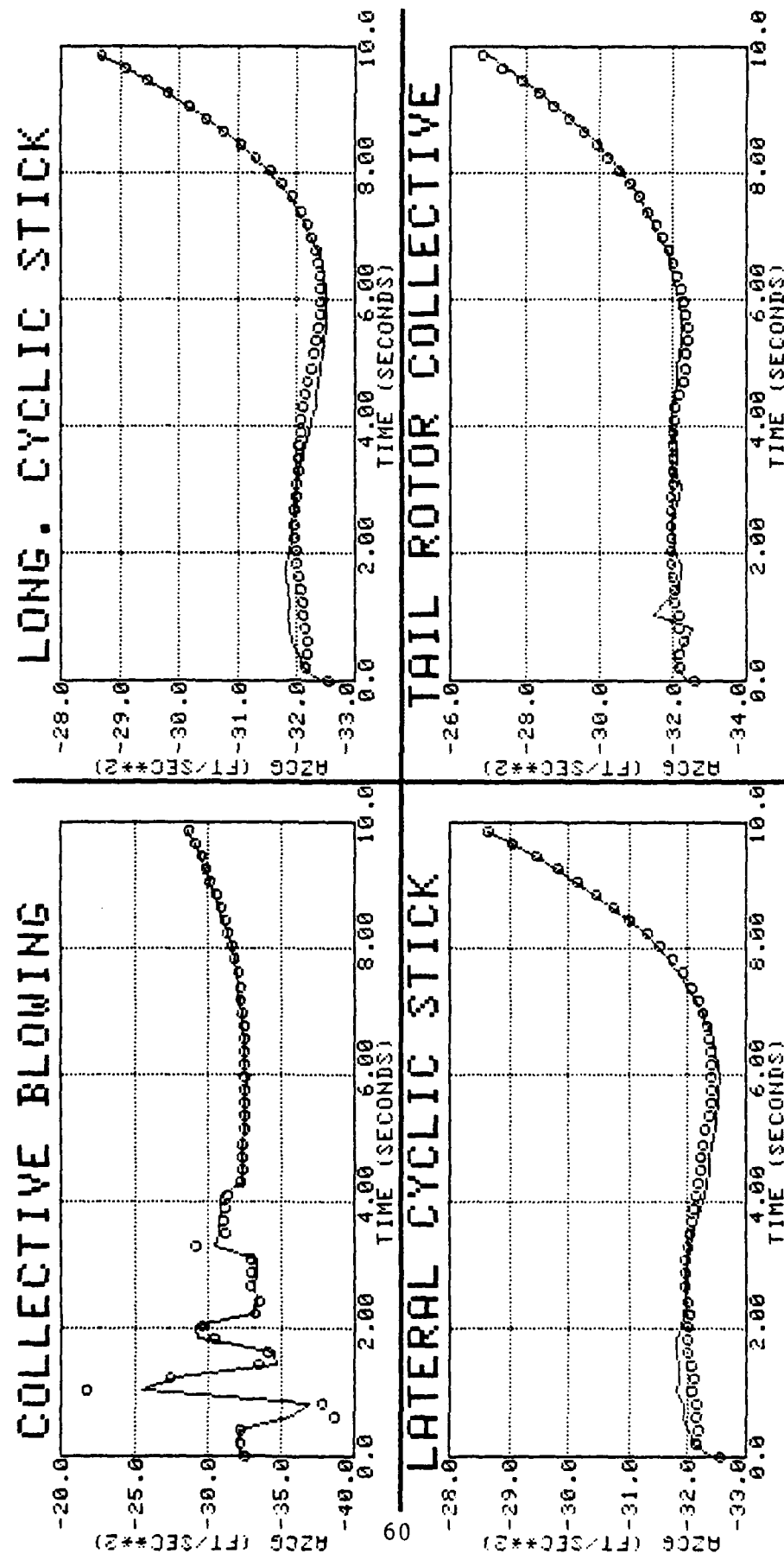


Figure 4.12 Normal Acceleration (Hover)

LINE CODE
IDENTIFIED MODEL
REXOR SIMULATION DATA
<u>0000000000</u>

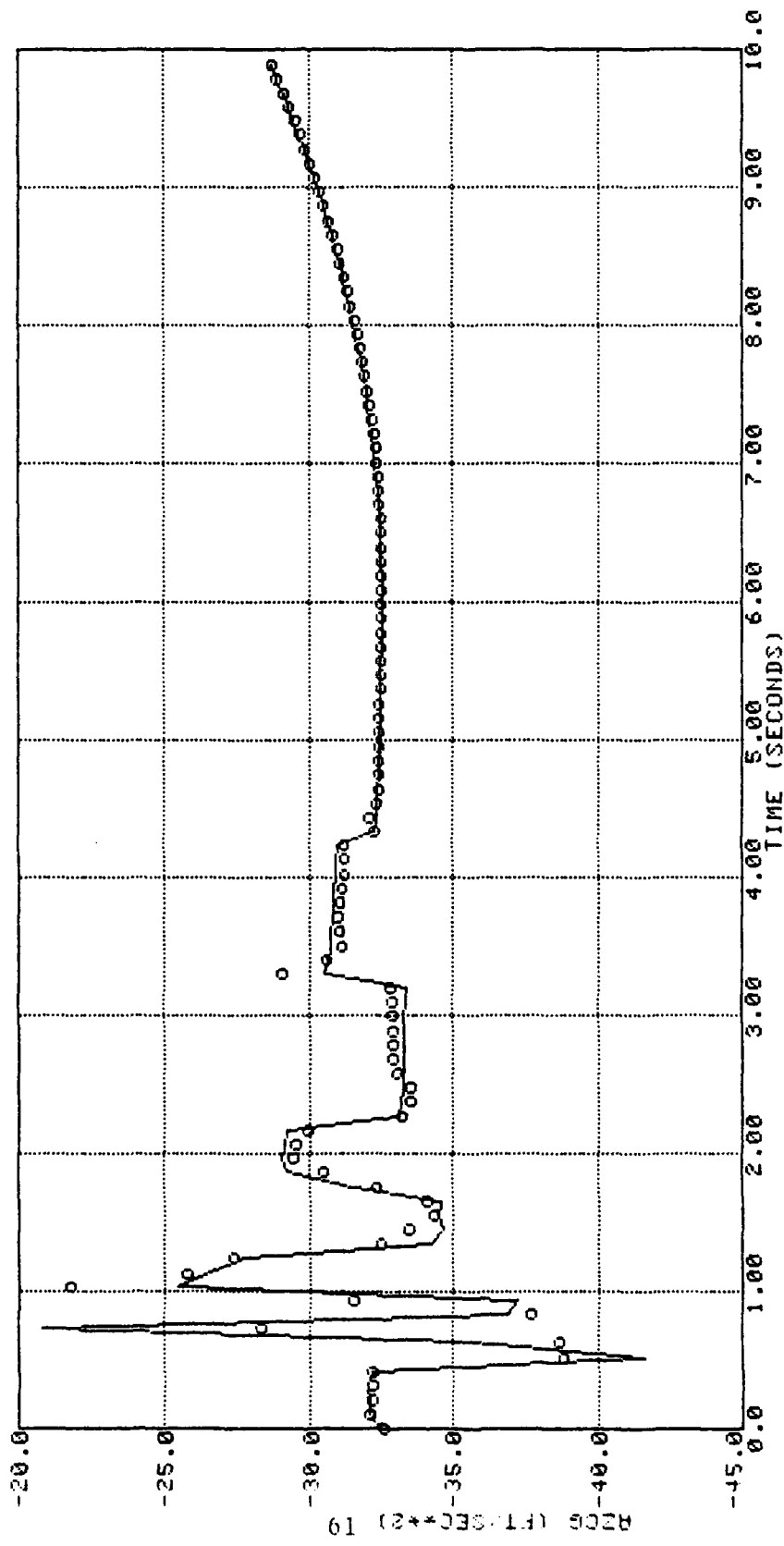
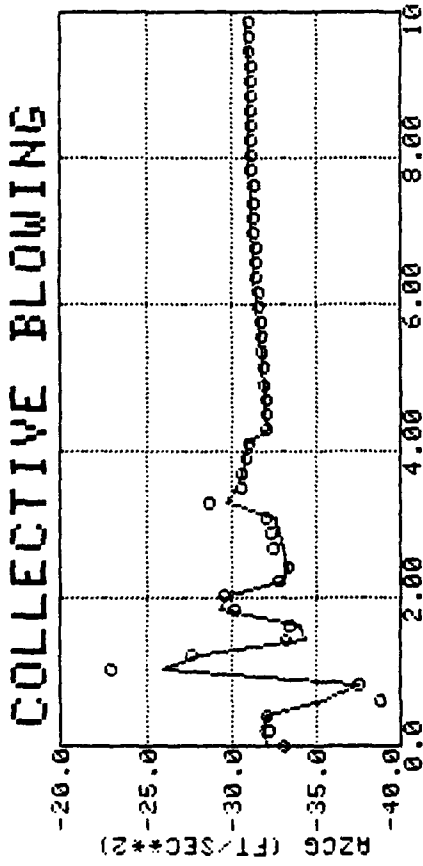


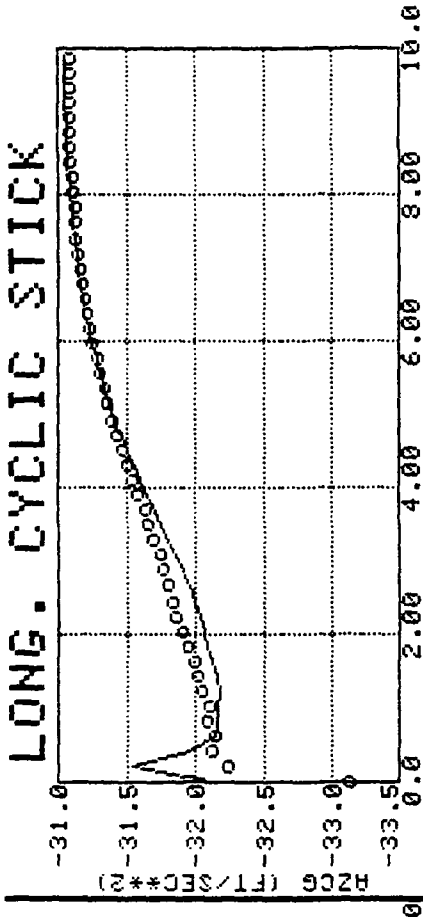
Figure 4.13 Normal Acceleration (Hover, Collective Input)

LINE CODE	
	IDENTIFIED MODEL
000000000	REXOR SIMULATION DATA

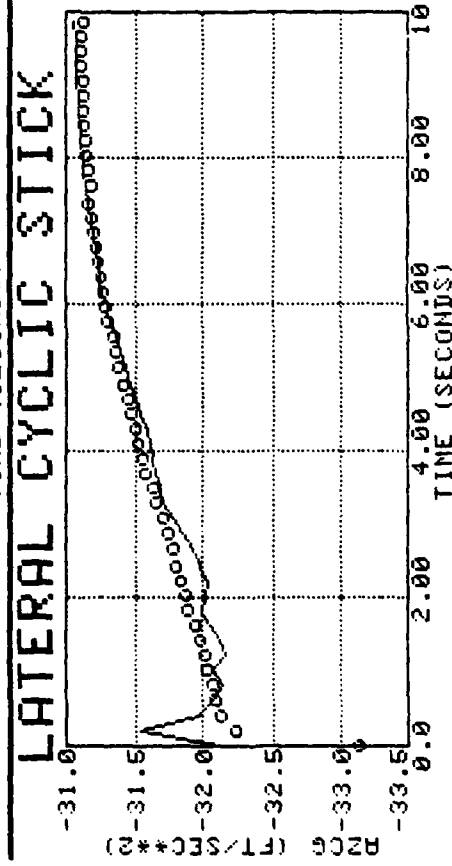
COLLECTIVE BLOWING



LONG. CYCLIC STICK



LATERAL CYCLIC STICK



TAIL ROTOR COLLECTIVE

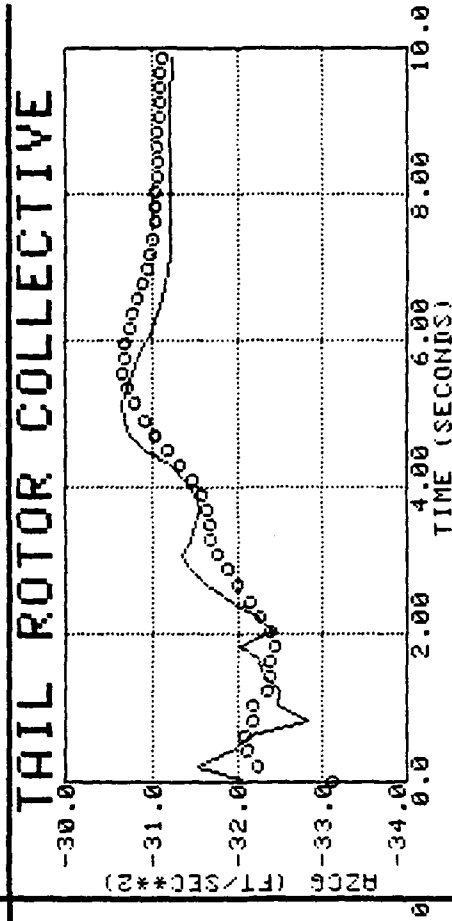


Figure 4.14 Normal Acceleration (100 fps)

LINE CODE
IDENTIFIED MODEL REXOR SIMULATION DATA
0000000000

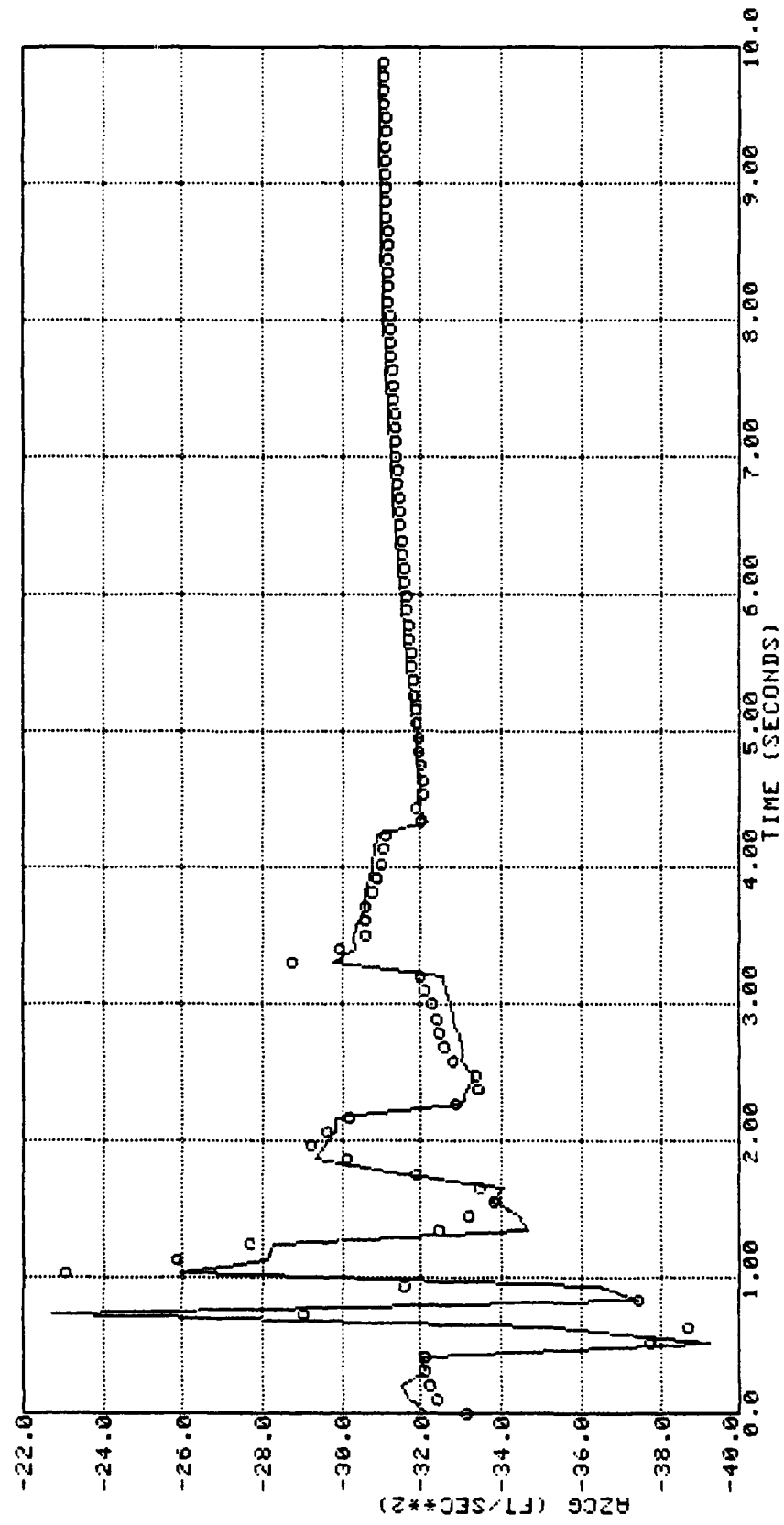


Figure 4.15 Normal Acceleration (100 fps, Collective Input)

Table 4.8
Regression on \dot{P}

HOVER			100 FPS		
VARIATION EXPLAINED BY R^2 : 0.90392160			VARIATION EXPLAINED BY R^2 : 0.95128113		
VARIABLE	COEFFICIENT	PARAM. F-RATIO	VARIABLE	COEFFICIENT	PARAM. F-RATIO
Δu	0.0207611	64.75	Δu	-0.0611522	225.7
Δv	0.0102289	103.3	Δv	0.0301222	331.9
Δw	0.0206216	7.077	Δw	-0.0948021	60.42
Δp	8.97866	660.2	Δp	-11.0907	1310.
Δq	47.0976	10290.	Δq	70.1132	5325.
Δr	-1.88311	4523.	Δa_{18}	4.21199	334.0
Δb_{18}	1.41577	115.0	Δb_{18}	1.66284	314.2
Δr_{p0}	0.381965	15.59	Δr_{p0}	-5.75918	24.07
$\Delta \theta_{OTR}$	7.35574	367.3	$\Delta \theta_{OTR}$	-1.08932	9.330
Δl_H	0.00424158	14560.	Δl_H	0.00454312	14220.
Δm_H	-0.000251747	107.7	Δm_H	-0.000182272	90.
$\Delta \dot{u}$	0.0115351	29.94	$\Delta \dot{w}$	-0.068116	121.2
$\Delta \dot{v}$	-0.00755679	73.71	A_y	1.90513	5794.
A_y	1.10465	2112.	CONST.	-1.30088	1914.
CONST.	-2.19794	1096.			

LINE CODE
IDENTIFIED MODEL
REXOR SIMULATION DATA
<u>0000000000</u>

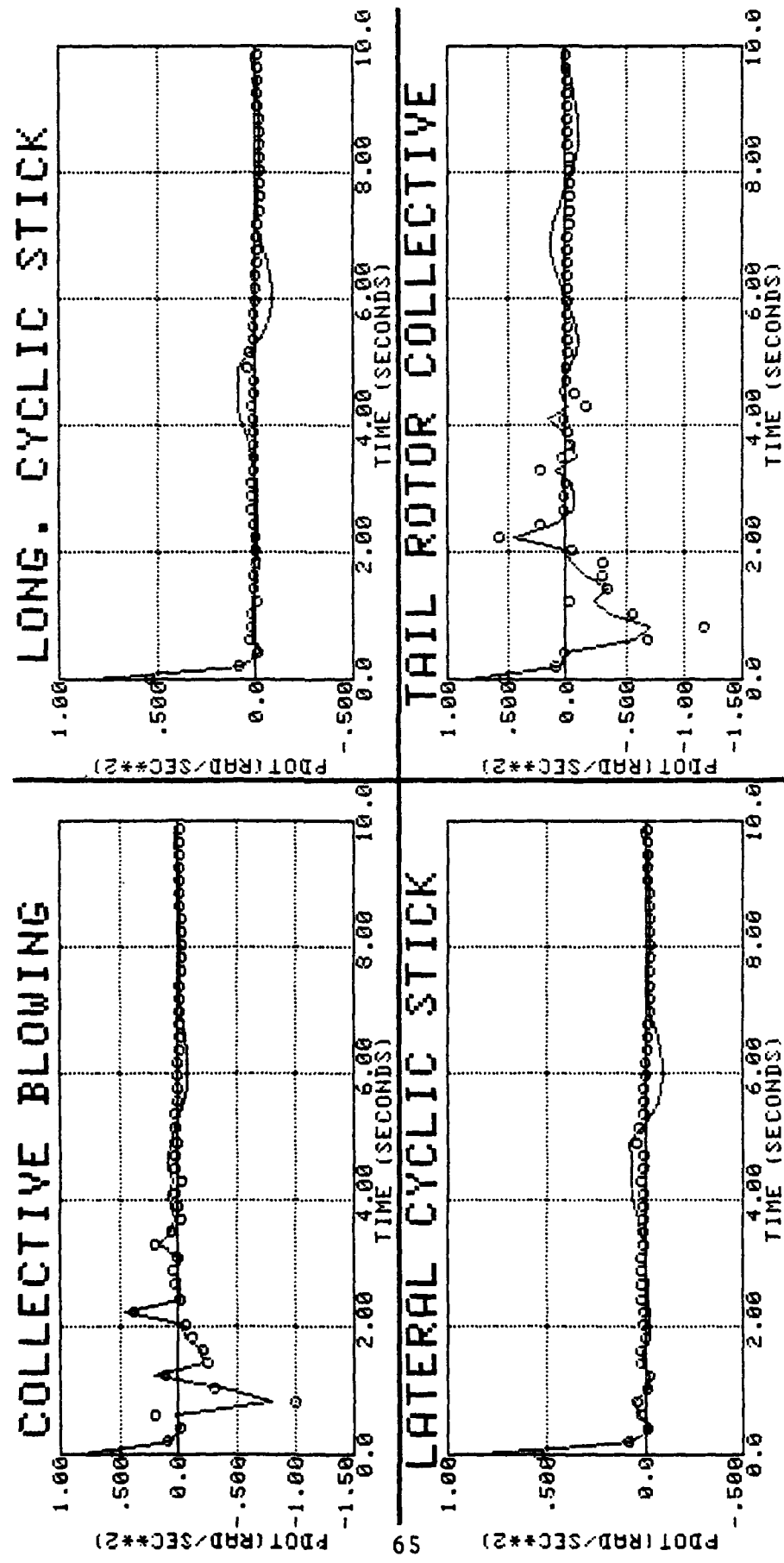


Figure 4.16 Roll Acceleration (Hover)

LINE CODE	
IDENTIFIED MODEL	
REXOR SIMULATION DATA	
<hr/>	
0000000000	

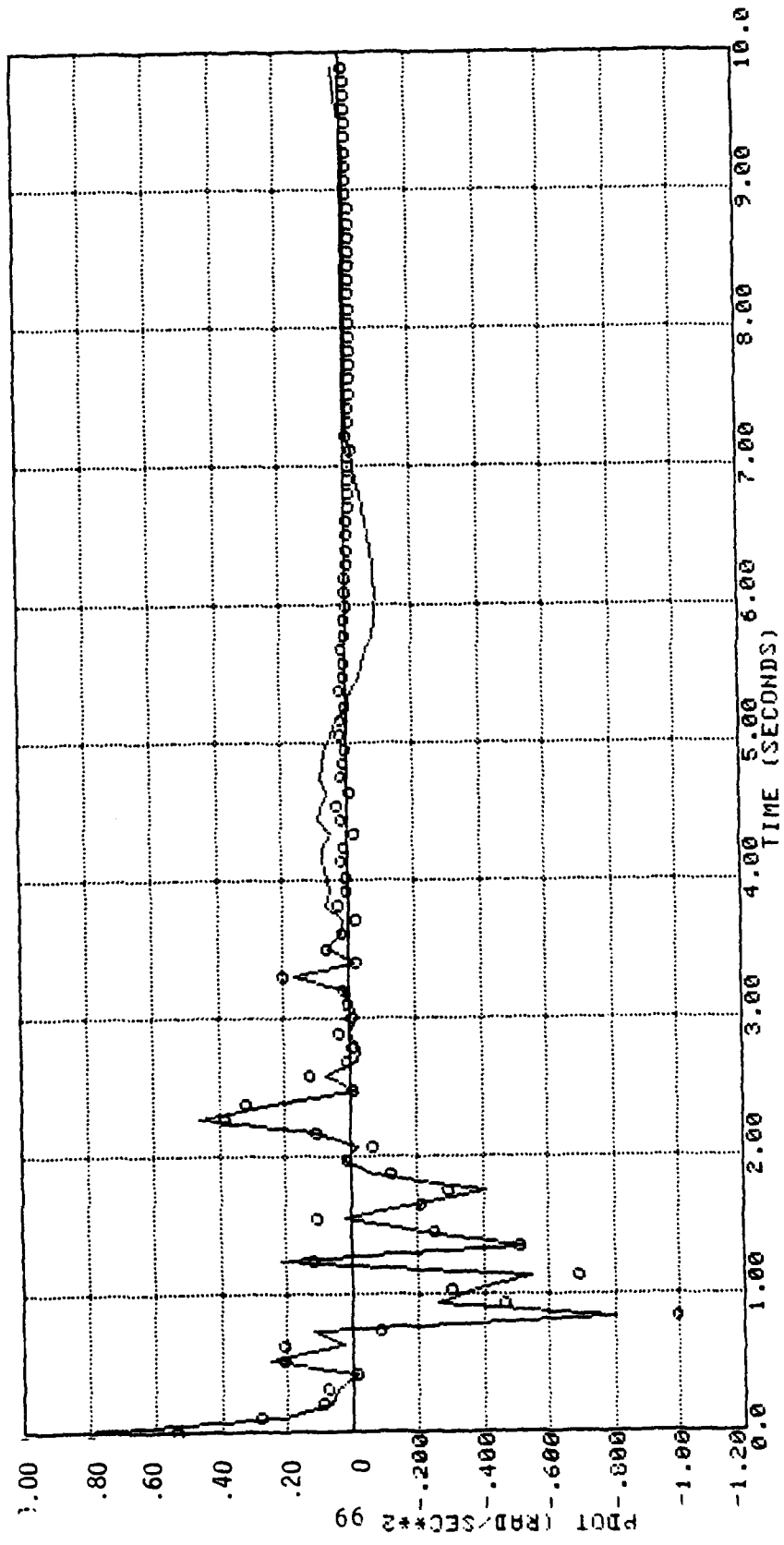


Figure 4.17 Roll Acceleration (Hover, Collective Input)

LINE CODE	
000000000	IDENTIFIED MODEL REXOR SIMULATION DATA

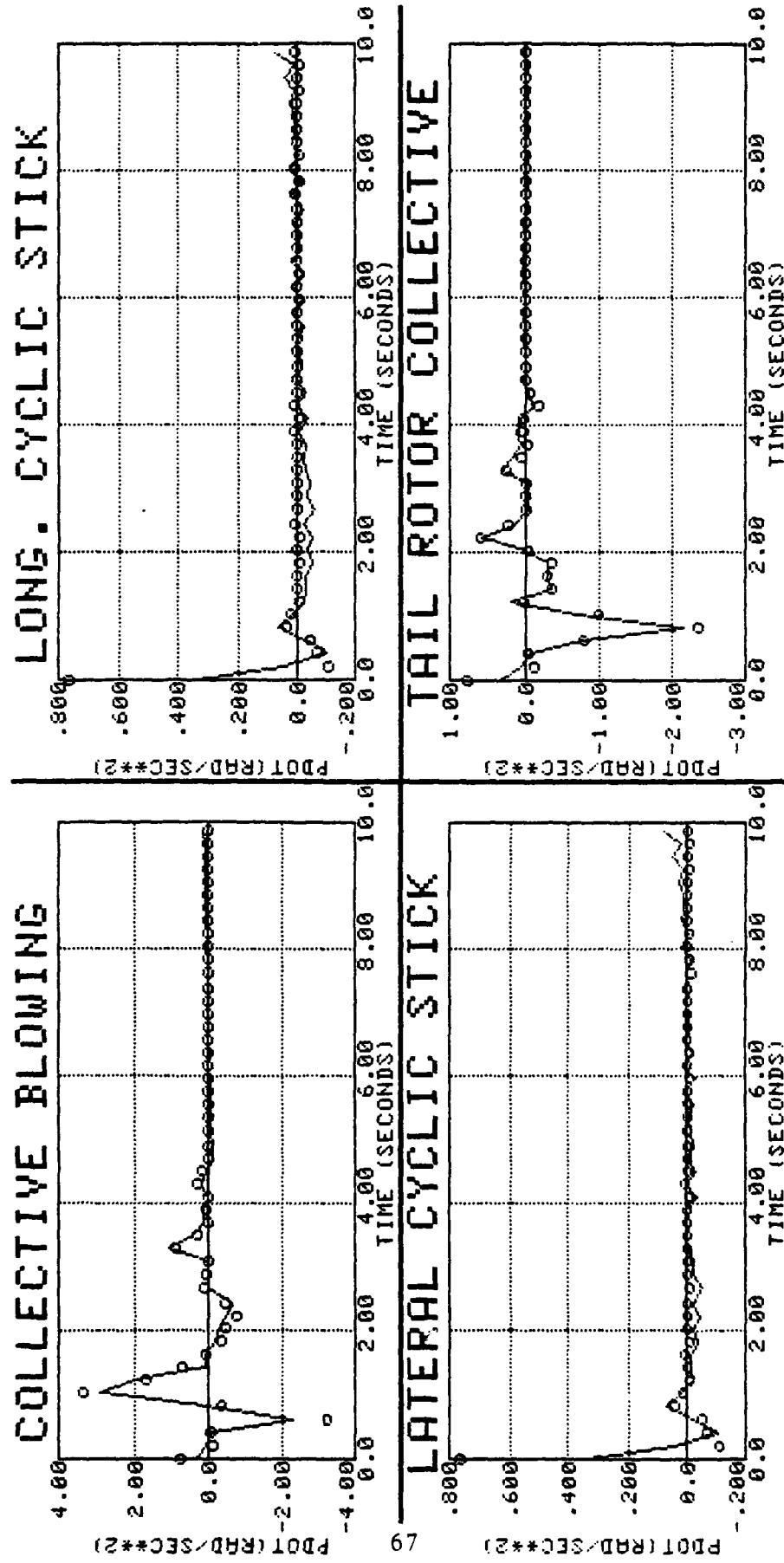


Figure 4.18 Roll Acceleration (100 fps)

LINE CODE	
	IDENTIFIED MODEL
000000000	REXOR SIMULATION DATA

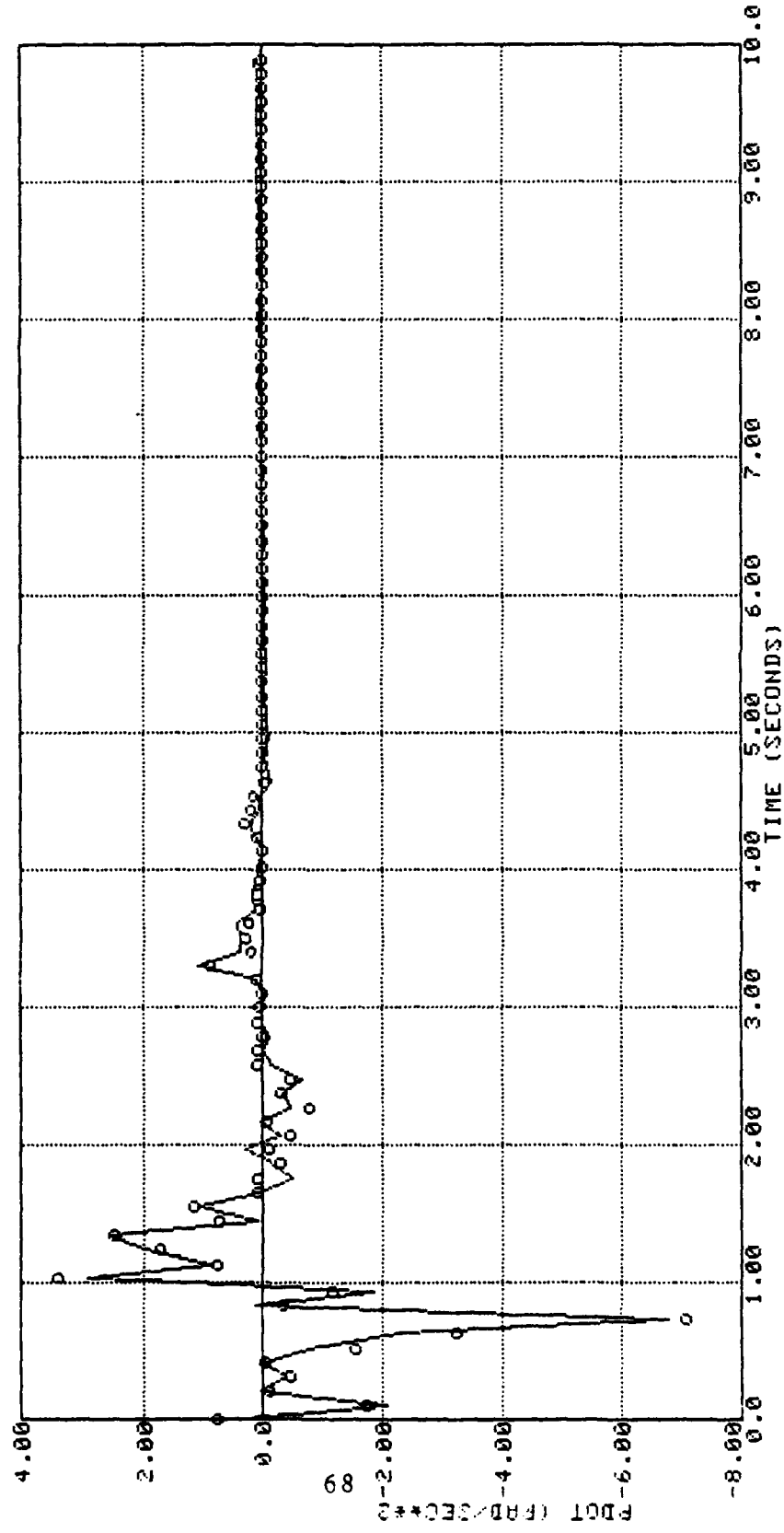


Figure 4.19 Roll Acceleration (100 fps, Collective Input)

Table 4.9
Regression on \dot{Q}

HOVER			100 FPS		
VARIATION EXPLAINED BY R^2 : 0.91874158			VARIATION EXPLAINED BY R^2 : 0.97661561		
VARIABLE	COEFFICIENT	PARAM. F-RATIO	VARIABLE	COEFFICIENT	PARAM. F-RATIO
Δw	0.0375316	1093.	Δu	0.0375001	178.6
Δp	-12.6538	5434.	Δv	0.0146625	159.3
Δq	5.26030	716.1	Δw	0.0543127	81.78
Δr	-0.287918	388.1	Δp	-14.1868	3622.
ΔA_{1B}	-2.42522	1971.	Δq	-14.2434	26.49
ΔB_{1B}	-4.66679	3069.	Δr	14.3501	244.5
ΔR_{p0}	-1.14406	124.0	ΔA_{1B}	-0.560806	11.04
$\Delta \theta_{OTR}$	1.53243	127.1	ΔB_{1B}	-0.933818	377.8
ΔL_H	-0.000144149	65.89	ΔR_{p0}	-5.26926	699.6
ΔM_H	0.00103564	5466.	$\Delta \theta_{OTR}$	2.00070	96.78
$\Delta \dot{u}$	0.0294313	527.1	ΔL_H	0.000372978	507.4
$\Delta \dot{v}$	-0.0151663	868.3	ΔM_H	0.000873825	4357.
$\Delta \dot{w}$	0.0245589	267.6	$\Delta \dot{u}$	0.0224886	22.02
A_x	1.29859	3415.	$\Delta \dot{v}$	0.147567	237.7
CONST.	-0.0302397	25.81	$\Delta \dot{w}$	0.179023	41.80
			A_x	1.41308	980.5
			A_z	-0.124869	19.94
			CONST.	-2.89699	9.815

LINE CODE	
0000000000	IDENTIFIED MODEL REXOR SIMULATION DATA

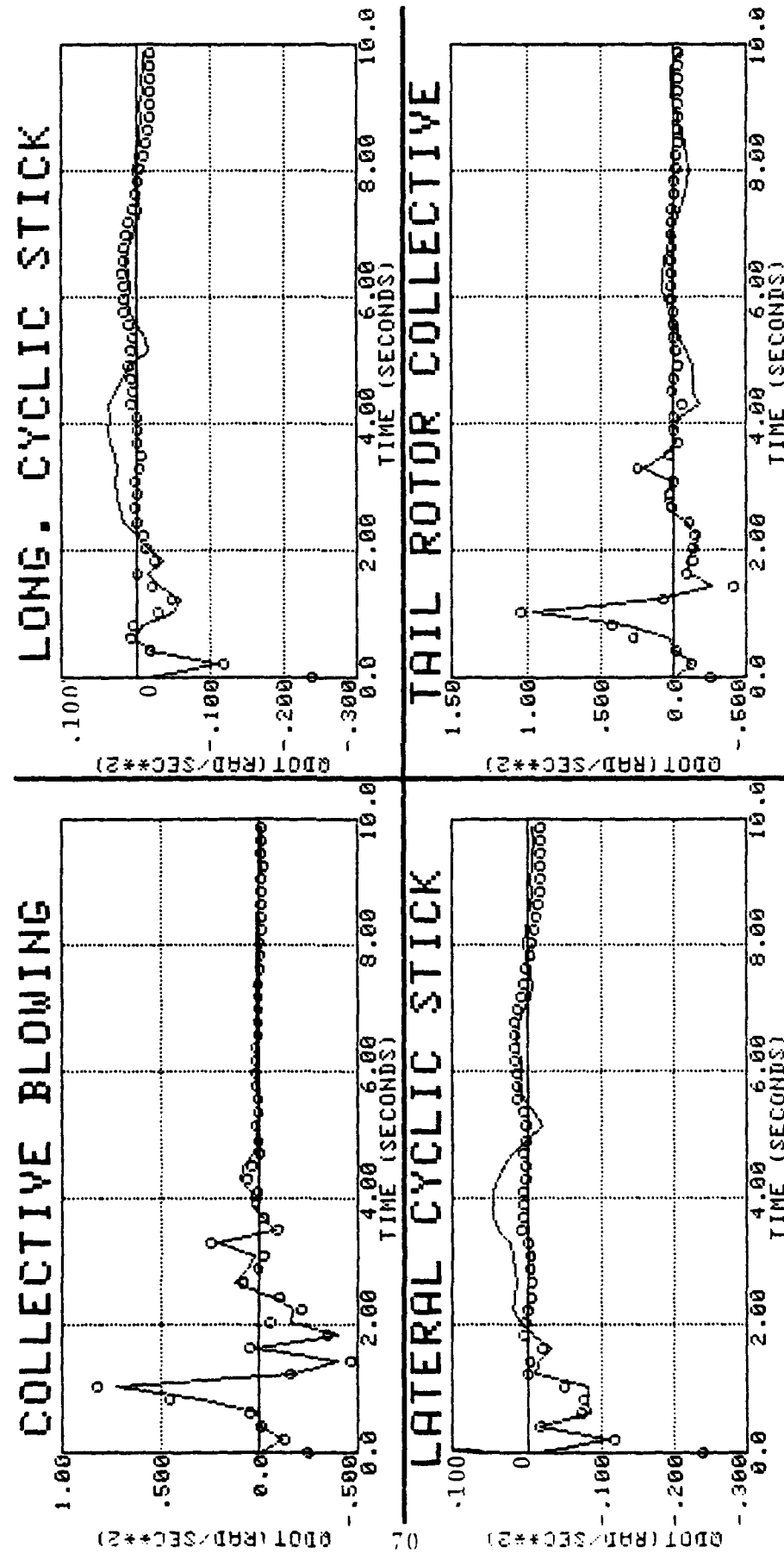


Figure 4.20 Pitch Acceleration (Hover)

LINE CODE
IDENTIFIED MODEL
REXOR SIMULATION DATA

0000000000

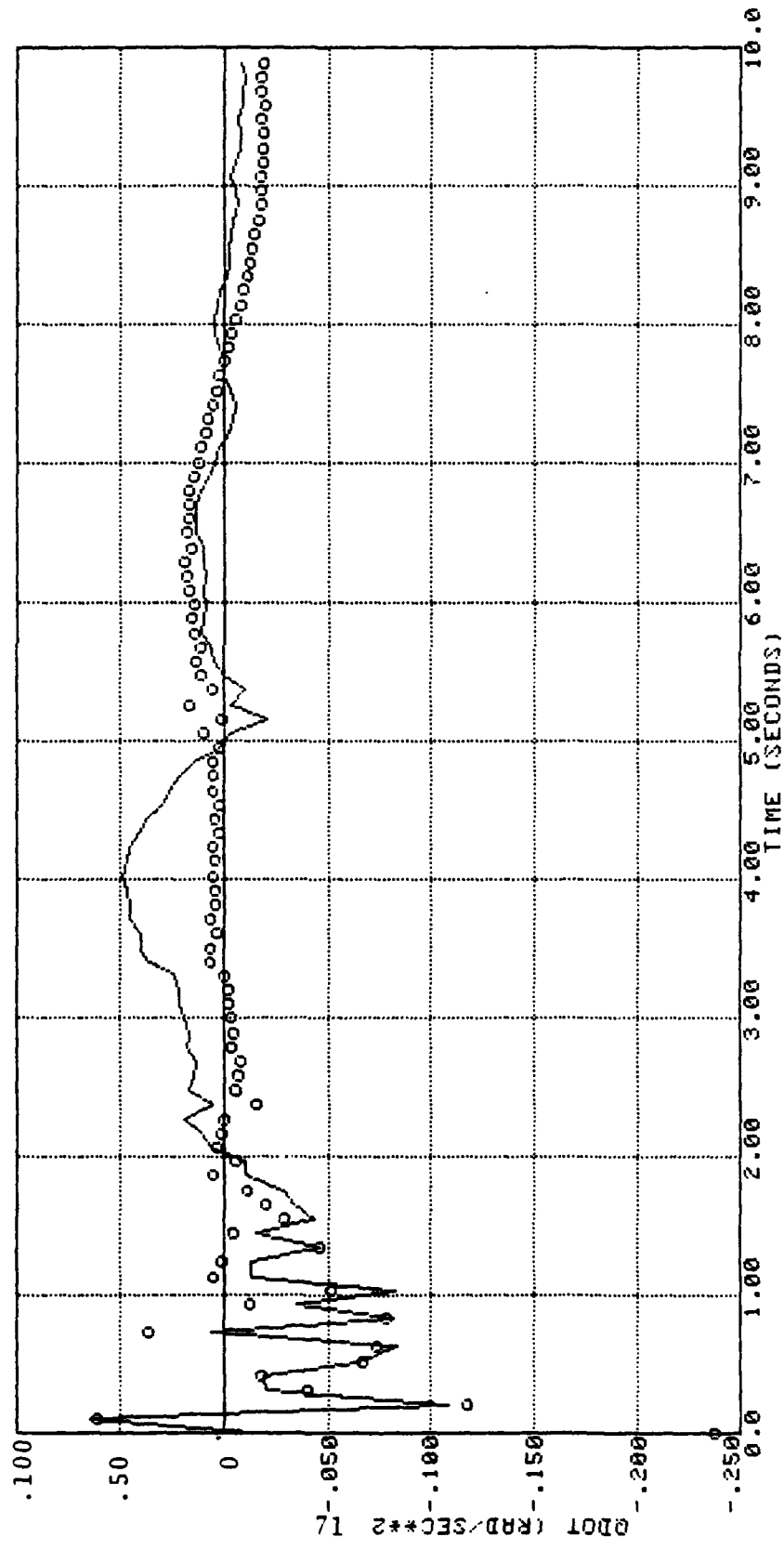


Figure 4.21 Pitch Acceleration (Hover, Longitudinal Cyclic)

LINE CODE	IDENTIFIED MODEL REXOR SIMULATION DATA
0000000000	

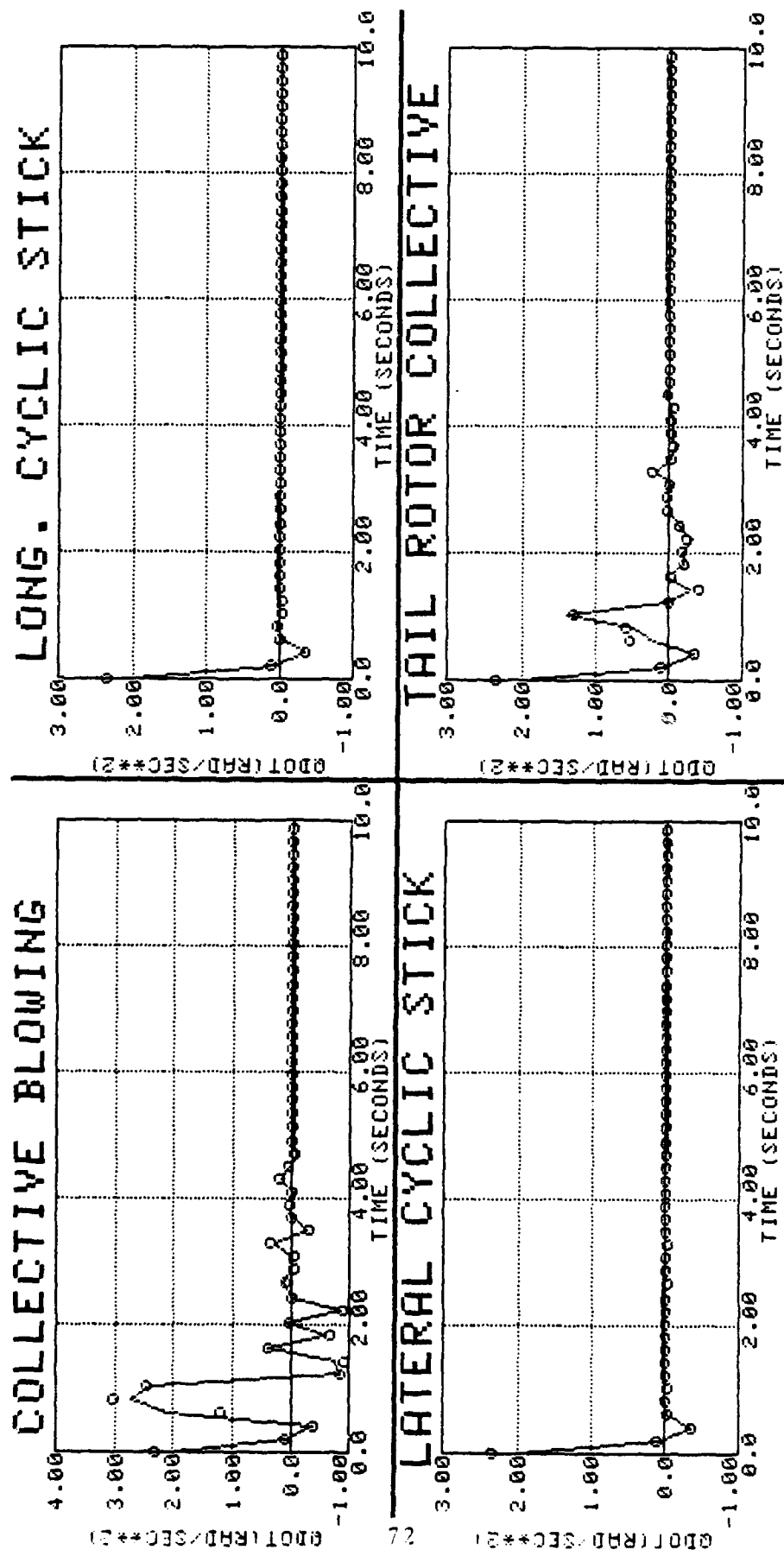


Figure 4.22 Pitch Acceleration (100 fps)

LINE CODE
IDENTIFIED MODEL REXOR SIMULATION DATA

000000000

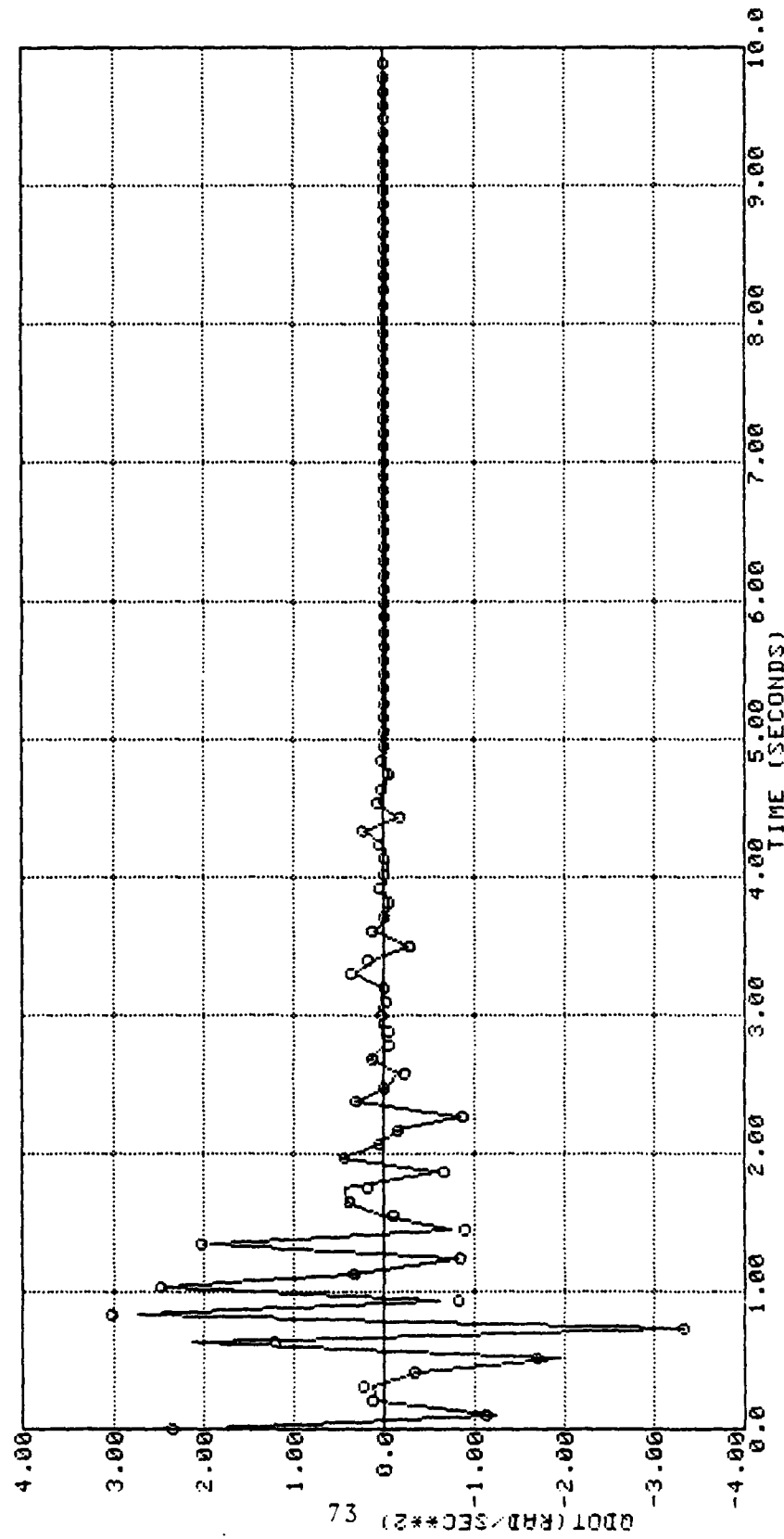


Figure 4.23 Pitch Acceleration (100 fsp, Collective Input)

Table 4.10
Regression on R

HOVER			100 FPS		
VARIATION EXPLAINED BY R^2 : 0.99614894			VARIATION EXPLAINED BY R^2 : 0.99708450		
VARIABLE	COEFFICIENT	PARAM. F-RATIO	VARIABLE	COEFFICIENT	PARAM. F-RATIO
Δu	-0.00344913	10.1	Δu	0.00858504	97.34
Δw	0.0220235	54.83	Δv	-0.0132009	1890.
Δp	-1.59912	159.9	Δw	-0.0530431	476.3
Δq	-9.30556	3232.	Δp	2.05455	1273.
Δr	0.544170	2249.	Δq	-12.0759	4156.
ΔA_{1B}	3.74247	5521.	Δr	1.51370	15.37
ΔB_{1B}	-1.37695	1412.	ΔA_{1B}	-0.201839	11.46
ΔR_{PO}	3.97052	4284.	ΔB_{1B}	-0.166797	80.39
$\Delta \theta_{OTR}$	-2.49114	274.0	ΔR_{PO}	-0.673275	90.53
ΔL_H	-0.000863718	4588.	ΔL_H	-0.000792314	11570.
ΔM_H	0.000168149	373.6	ΔM_H	0.0000232729	39.57
$\Delta \dot{u}$	0.00697193	68.90	$\Delta \dot{v}$	0.0166052	17.60
$\Delta \dot{v}$	0.00975561	781.5	$\Delta \dot{w}$	0.00948151	63.59
$\Delta \dot{w}$	-0.0156250	294.5	A_Y	-1.52544	83330.
A_Y	-1.35129	20380.	CONST.	1.03957	25040.
CONST.	3.77182	20700.			

LINE CODE	
IDENTIFIED MODEL	
0000000000	REXOR SIMULATION DATA

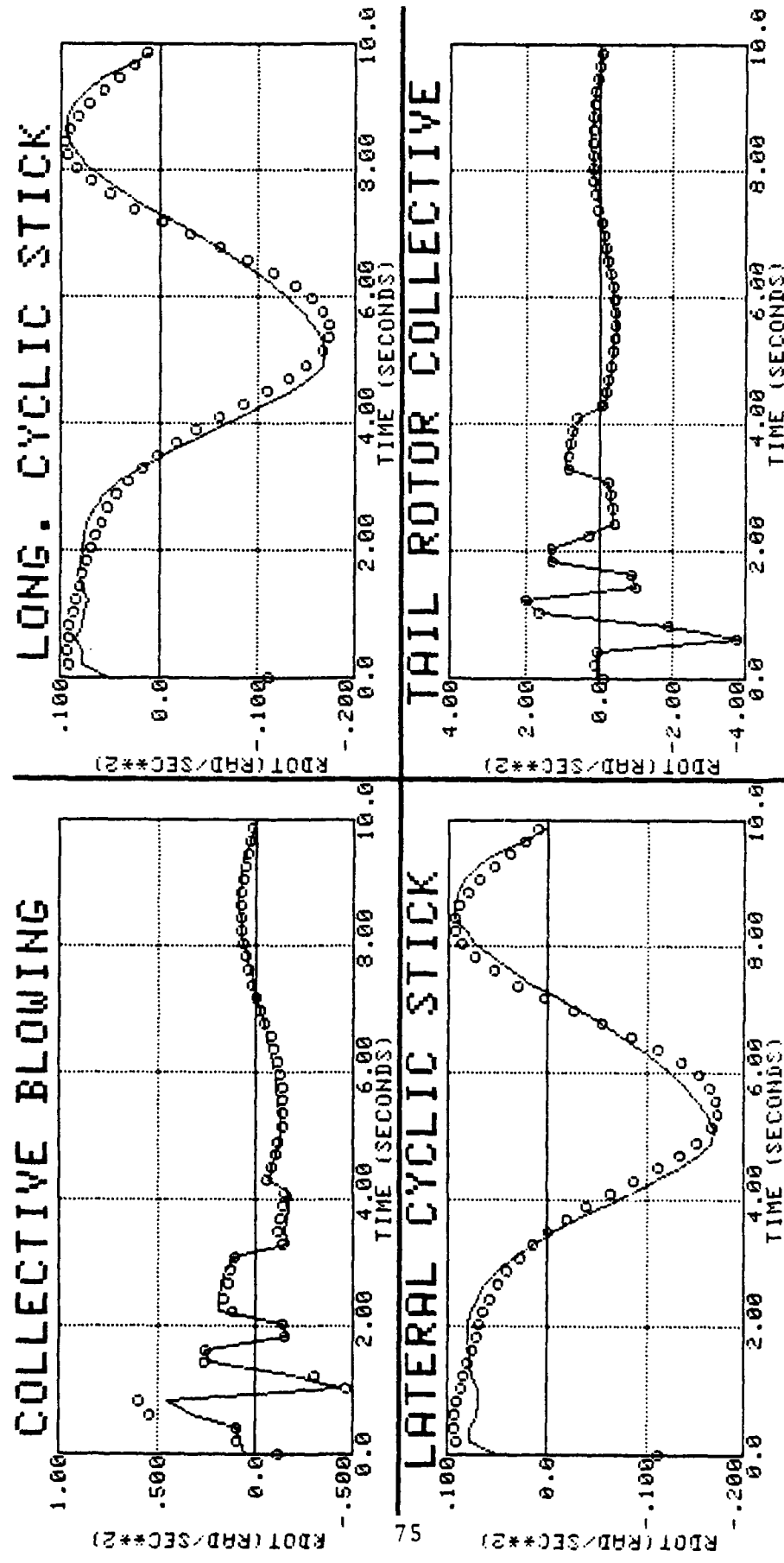


Figure 4.24 Yaw Acceleration (llover)

LINE CODE
IDENTIFIED MODEL REXOR SIMULATION DATA

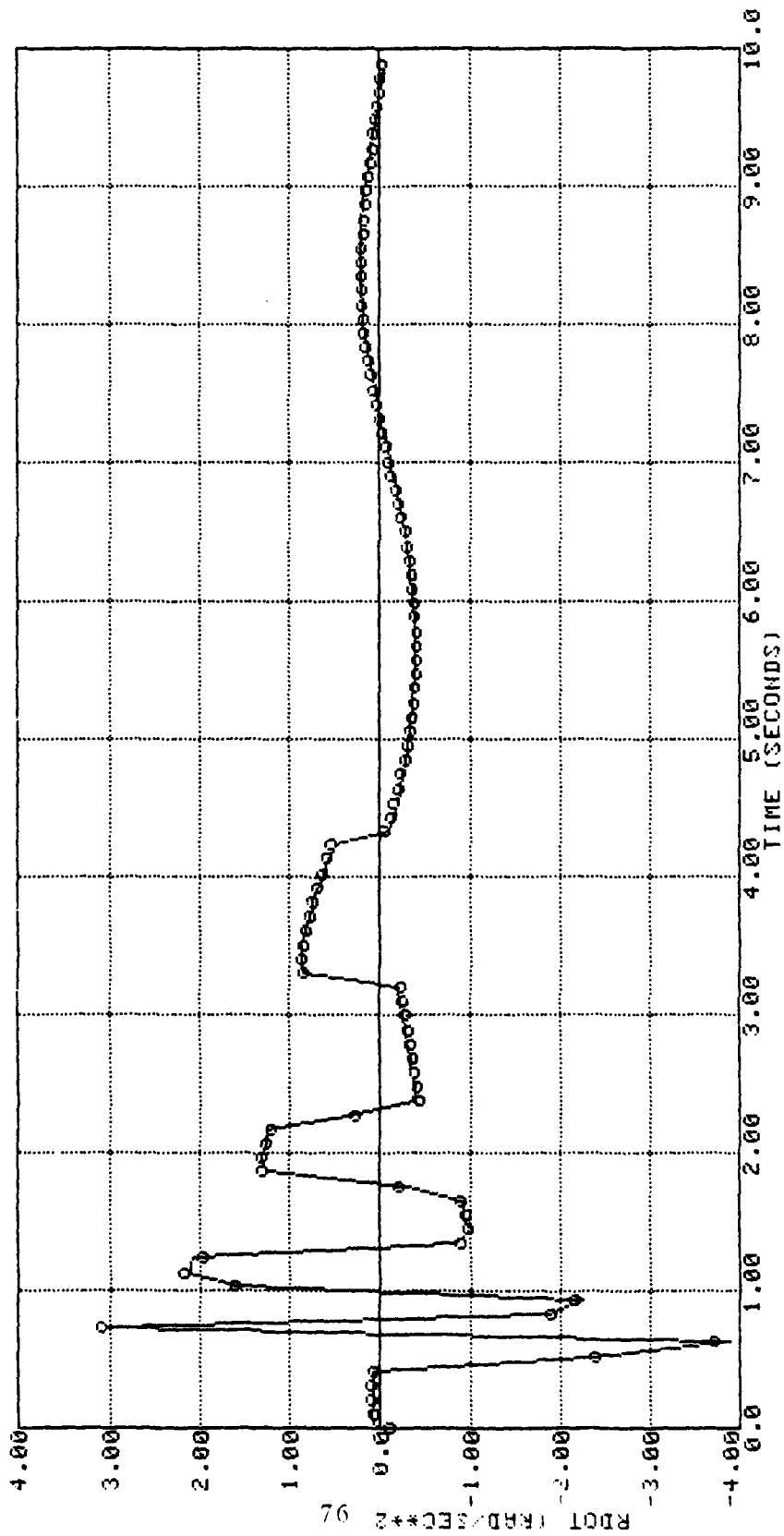
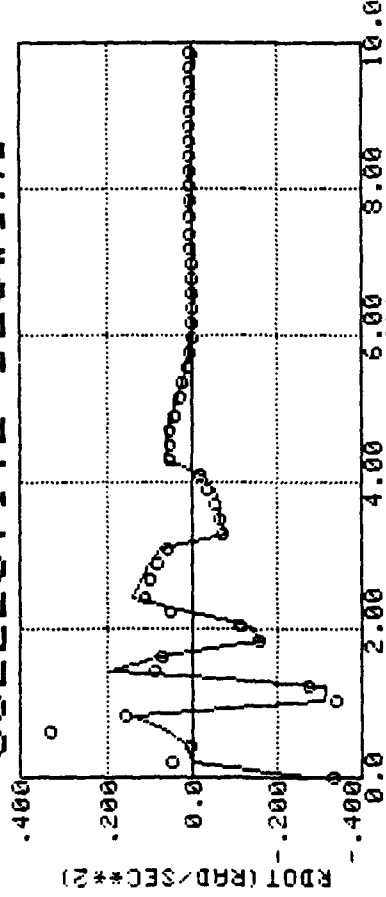


Figure 4.25 Yaw Acceleration (Hover, Tail Rotor Collective)

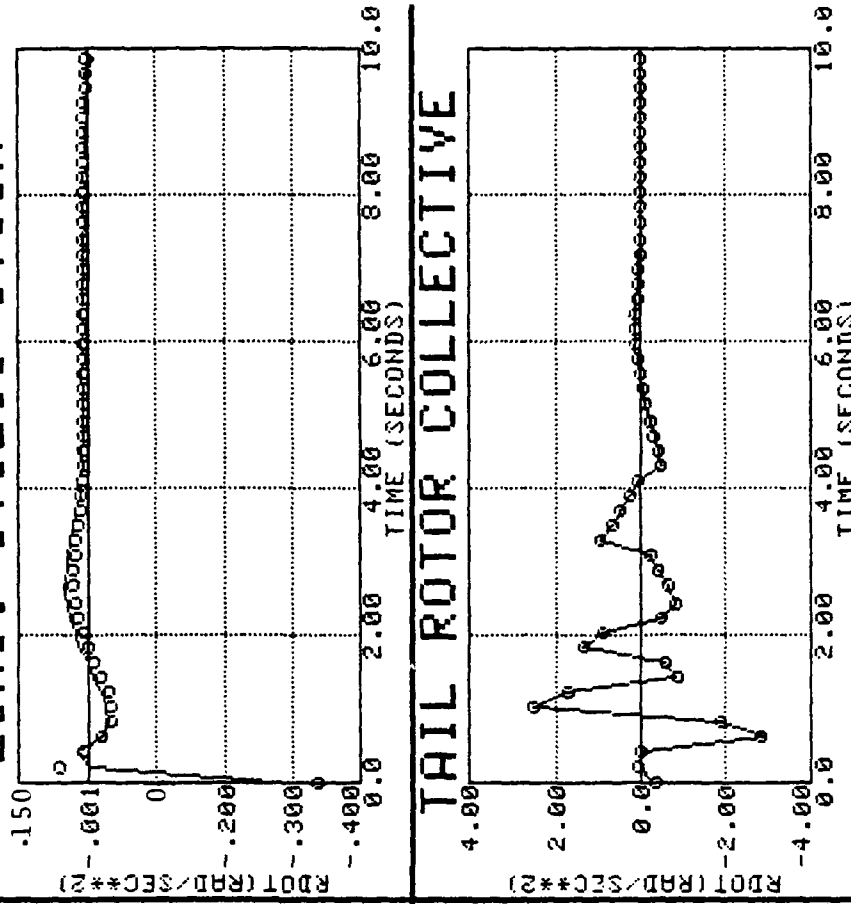
LINE CODE
IDENTIFIED MODEL REXOR SIMULATION DATA

0000000000

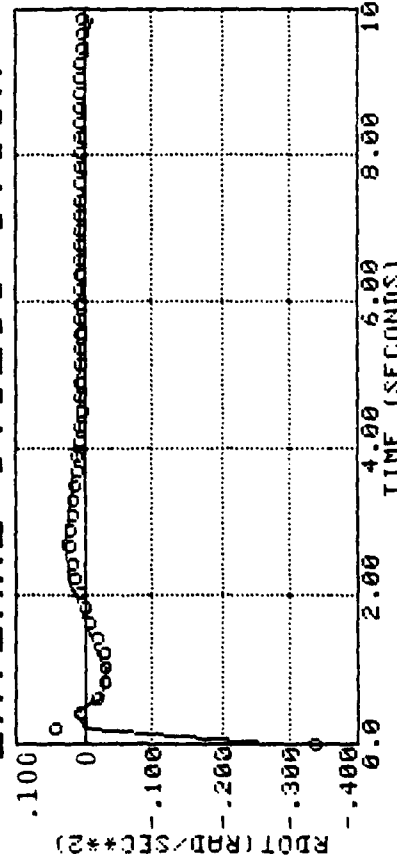
COLLECTIVE BLOWING



LONG. CYCLIC STICK



LATERAL CYCLIC STICK



TAIL ROTOR COLLECTIVE

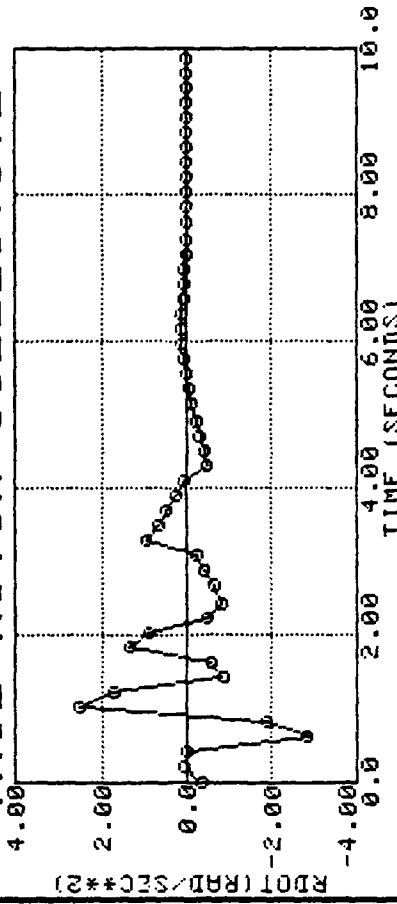


Figure 4.26 Yaw Acceleration (100 fps)

LINE CODE
<u>IDENTIFIED MODEL</u> <u>REXOR SIMULATION DATA</u>

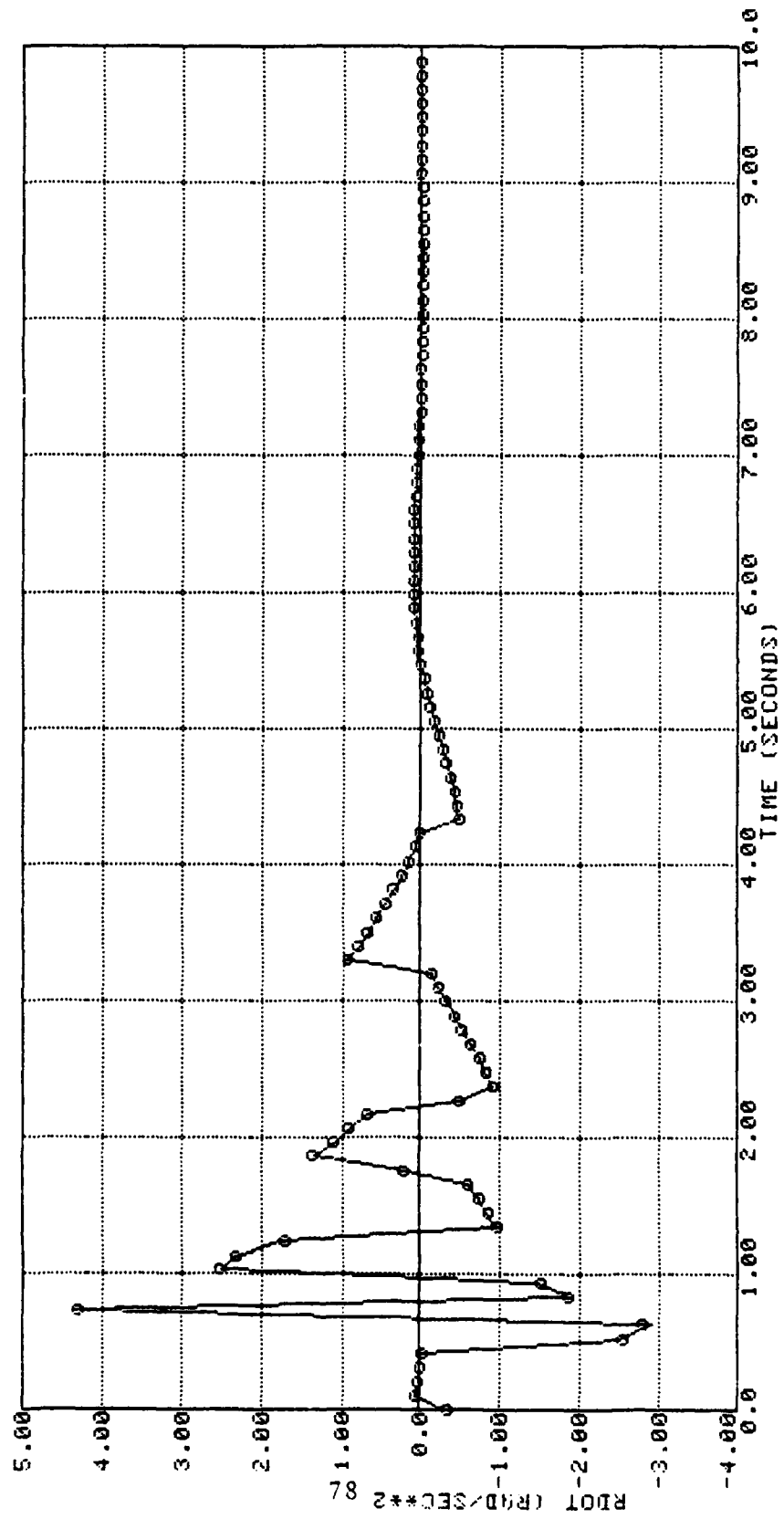


Figure 4.27 Yaw Acceleration (100 fps, Tail Rotor Collective)

Table 4.11
Regression on L_H

HOVER			100 FPS		
VARIATION EXPLAINED BY R^2 : 0.99350286			VARIATION EXPLAINED BY R^2 : 0.98905438		
EQUATION F-RATIO: 22666.			EQUATION F-RATIO: 13394.		
VARIABLE	COEFFICIENT	PARAM. F-RATIO	VARIABLE	COEFFICIENT	PARAM. F-RATIO
Δu	6.26771	15.20	Δu	8.89394	11.87
Δv	-24.9992	800.7	Δv	-20.8489	493.3
Δw	-11.6902	7.785	Δw	40.5570	60.81
Δp	-1262.32	41.95	Δp	-350.810	3.248
Δq	-5160.66	448.2	Δq	-16525.1	1774.
Δr	563.580	2777.	ΔA_{1B}	226.245	26.56
ΔA_{1B}	3112.06	699.7	ΔR_{p0}	4675.30	563.8
$\Delta \theta_{1B}$	997.119	229.7	$\Delta \theta_{OTR}$	5229.86	254.8
ΔR_{p0}	586.745	126.8	Δu	45.5093	61.29
$\Delta \theta_{OTR}$	2200.32	87.50	Δv	-5.48350	145.4
$\Delta \dot{u}$	-14.3104	125.3	$\Delta \dot{w}$	89.3007	885.0
A_y	-417.352	1203.	A_y	-599.450	1397.
CONST.	260.987	55.03	CONST.	-722.783	2404.

LINE CODE	
oooooooooooo	IDENTIFIED MODEL REXOR SIMULATION DATA

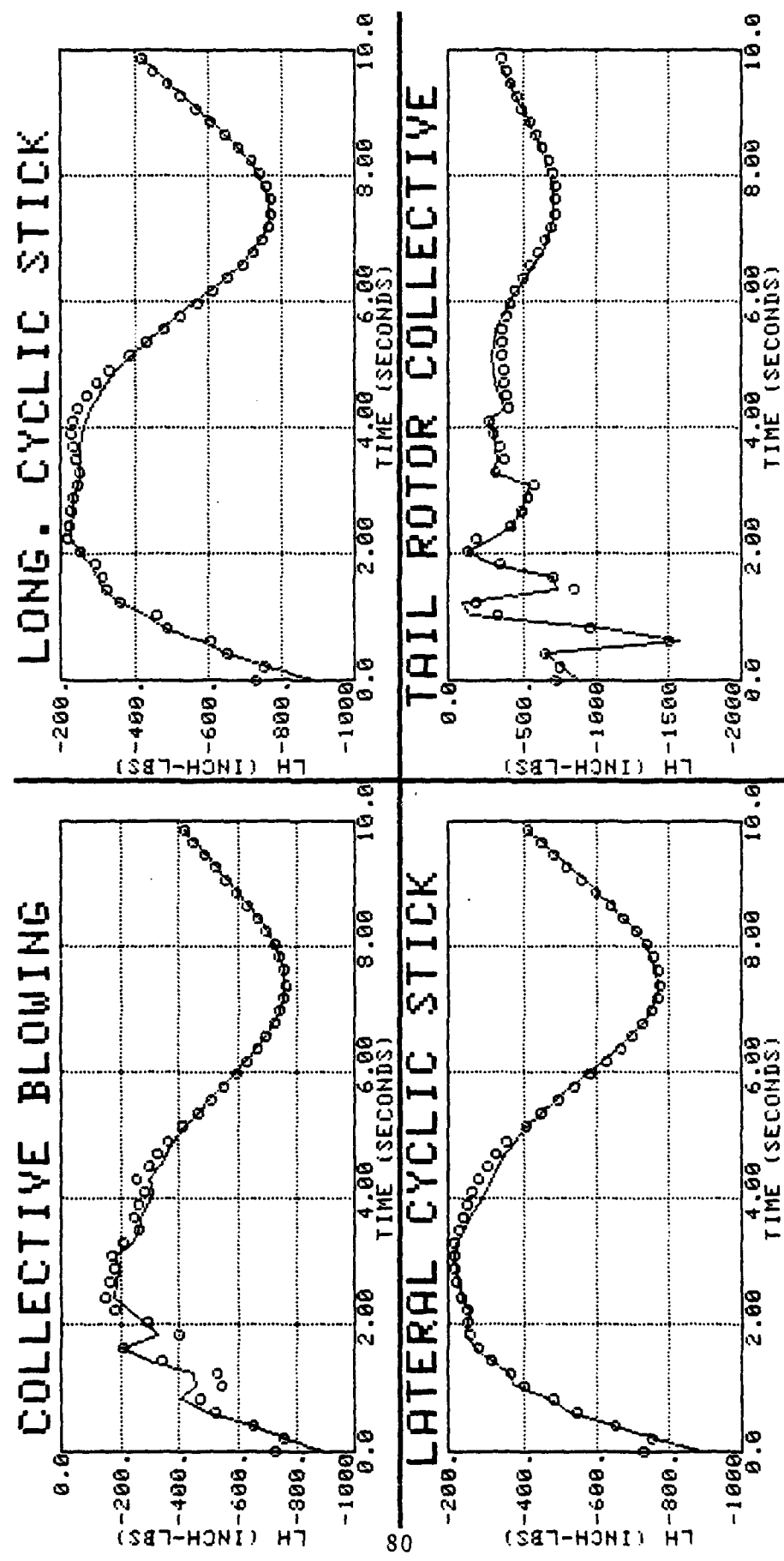


Figure 4.28 Roll Hub Moment (Hover)

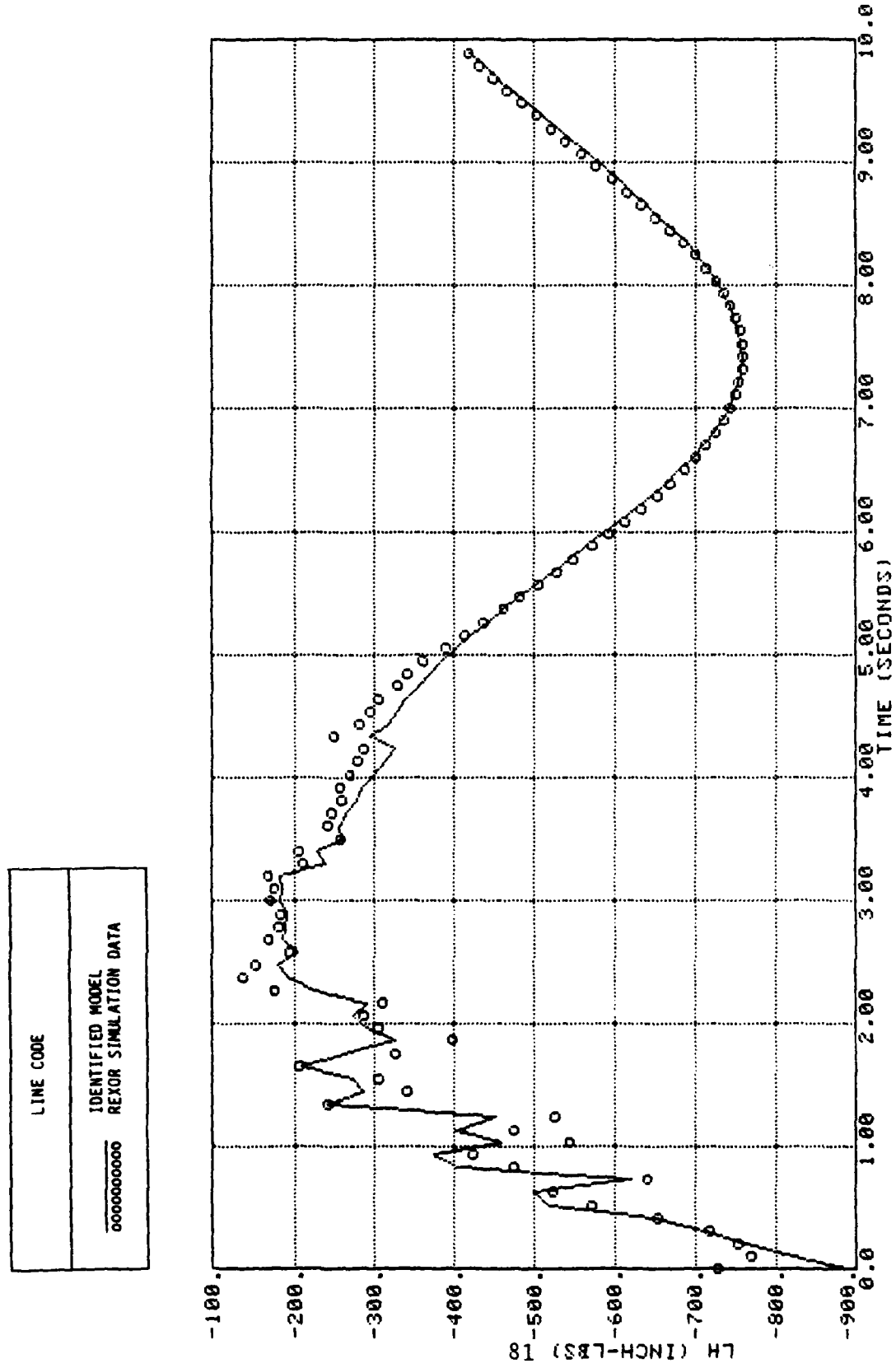


Figure 4.29 Roll Hub Moment (Hover, Collective Input)

LINE CODE	IDENTIFIED MODEL
0000000000	REXOR SIMULATION DATA

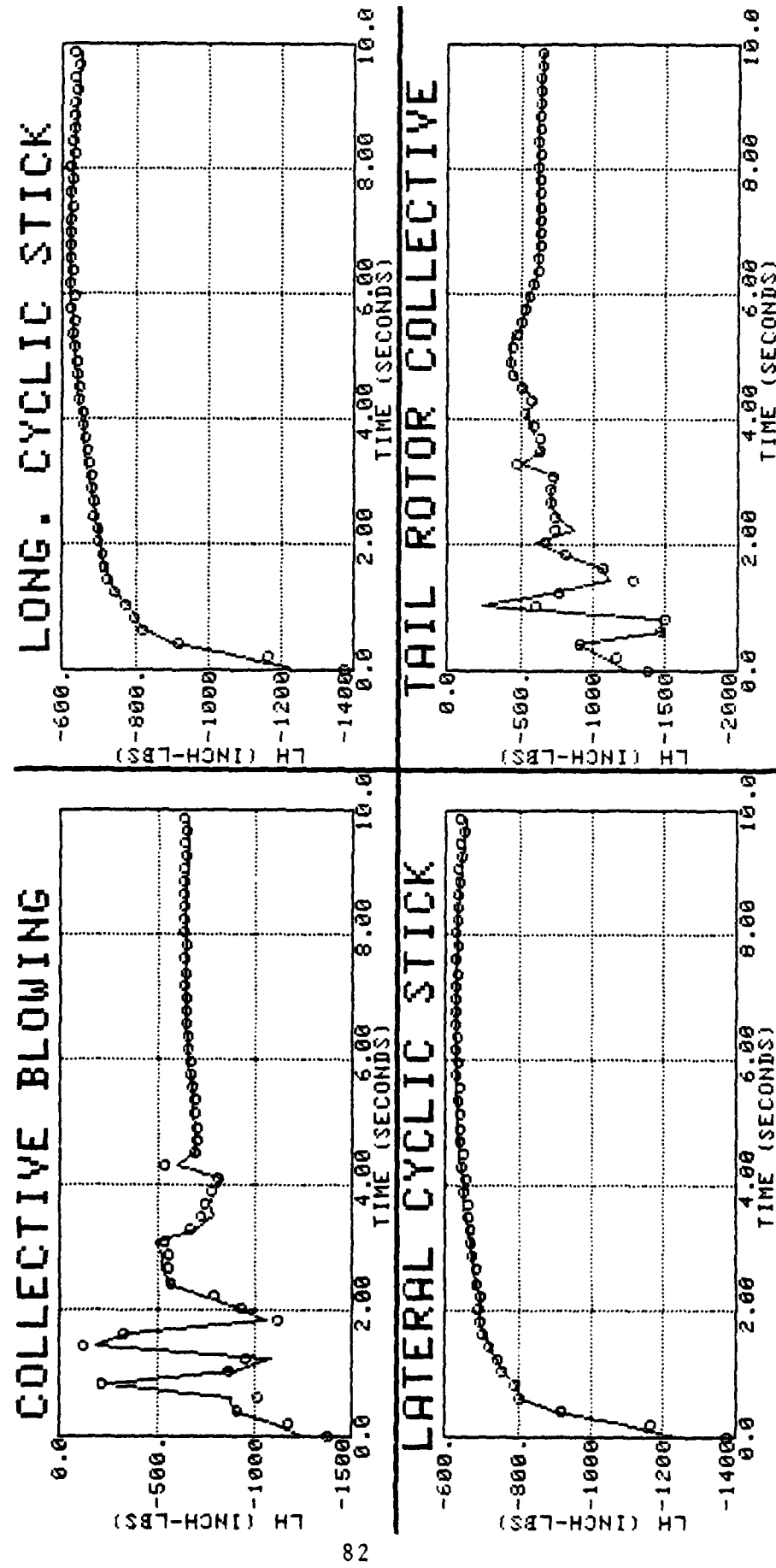


Figure 4.30 Roll Hub Moment (100 fps)

LINE CODE
IDENTIFIED MODEL
REXOR SIMULATION DATA

0000000000

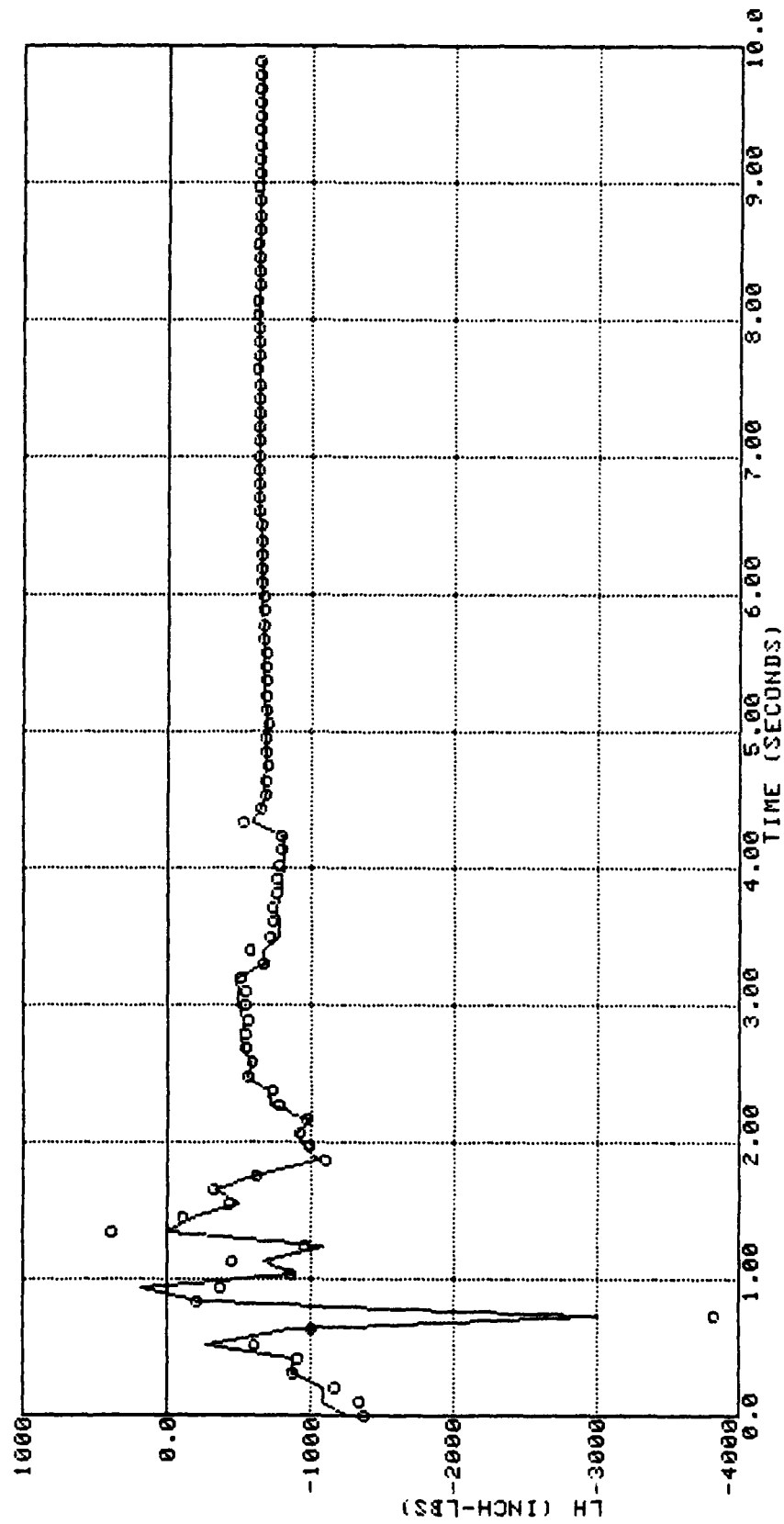


Figure 4.31 Roll Hub Moment (100 fps, Collective Input)

Table 4.12
Regression on M_H

HOVER			100 FPS		
VARIATION EXPLAINED BY R^2 : 0.99748439			VARIATION EXPLAINED BY R^2 : 0.99712998		
VARIABLE	COEFFICIENT	PARAM. F-RATIO	VARIABLE	COEFFICIENT	PARAM. F-RATIO
Δu	24.9415	40.95	Δu	37.4316	99.46
Δv	-36.5539	558.6	Δv	-14.4361	147.6
Δw	-23.6087	9.556	Δp	-7307.50	470.6
Δp	-3263.56	186.3	Δq	5160.67	82.55
Δq	4914.21	148.1	ΔB_{1B}	-52.6170	13.31
Δr	-78.2995	22.30	ΔR_{p0}	-3103.93	176.2
ΔA_{1B}	4368.84	251.8	$\Delta \theta_{OTR}$	2592.14	245.8
ΔB_{1B}	1425.29	108.3	$\Delta \dot{w}$	-29.6058	52.11
ΔR_{p0}	1924.18	157.4	A_x	245.398	46.03
$\Delta \theta_{OTR}$	1255.79	82.09	CONST.	2088.23	9162.
$\Delta \dot{u}$	9.51980	21.90			
$\Delta \dot{w}$	108.436	84.95			
A_x	2594.15	2426.			
A_z	-112.266	46.03			
CONST.	-2726.96	49.35			

LINE CODE	IDENTIFIED MODEL REXOR SIMULATION DATA
000000000	

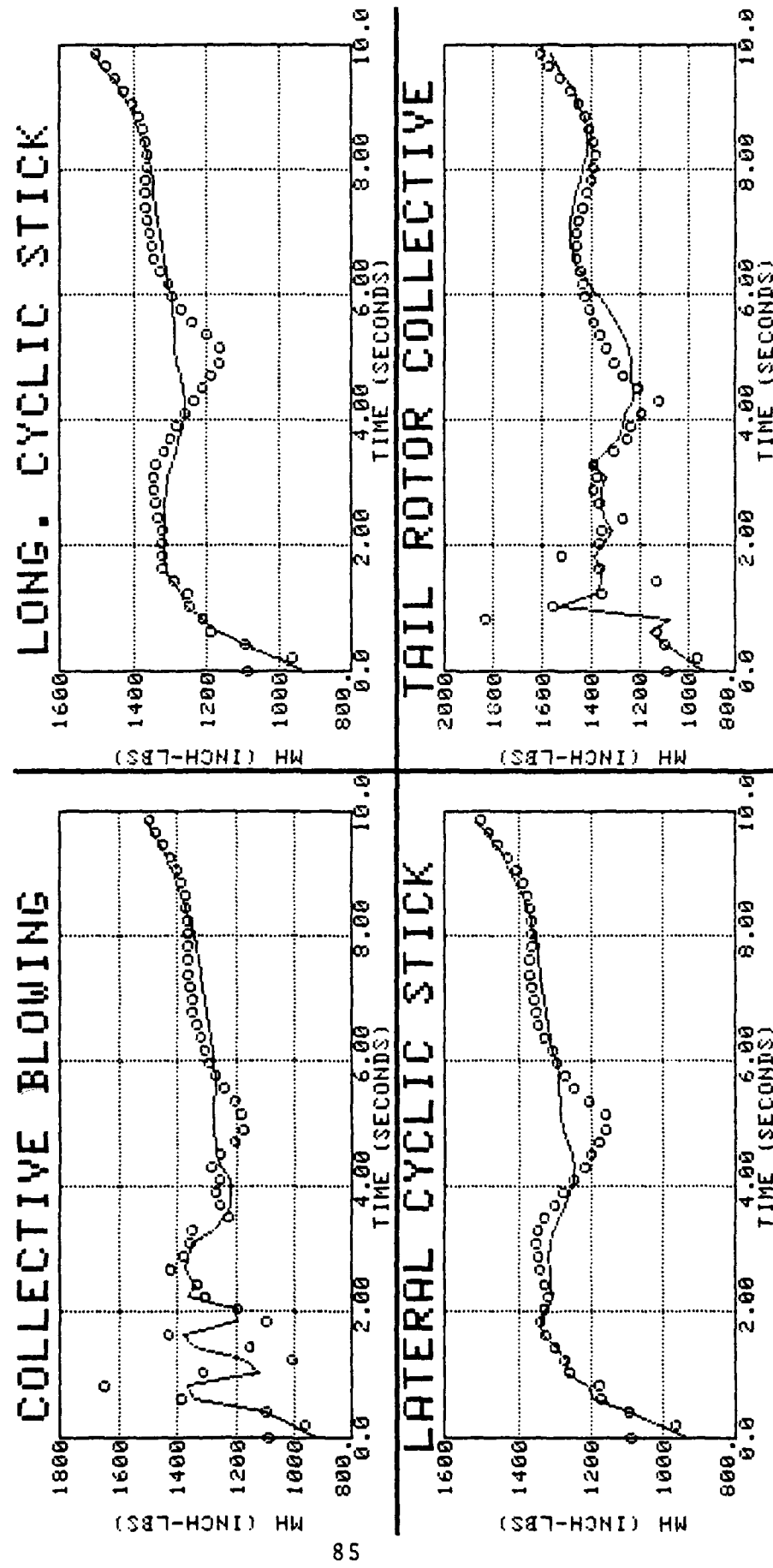


Figure 4.32 Pitch Hub Moment (Hover)

LINE CODE	IDENTIFIED MODEL REXOR SIMULATION DATA
0000000000	

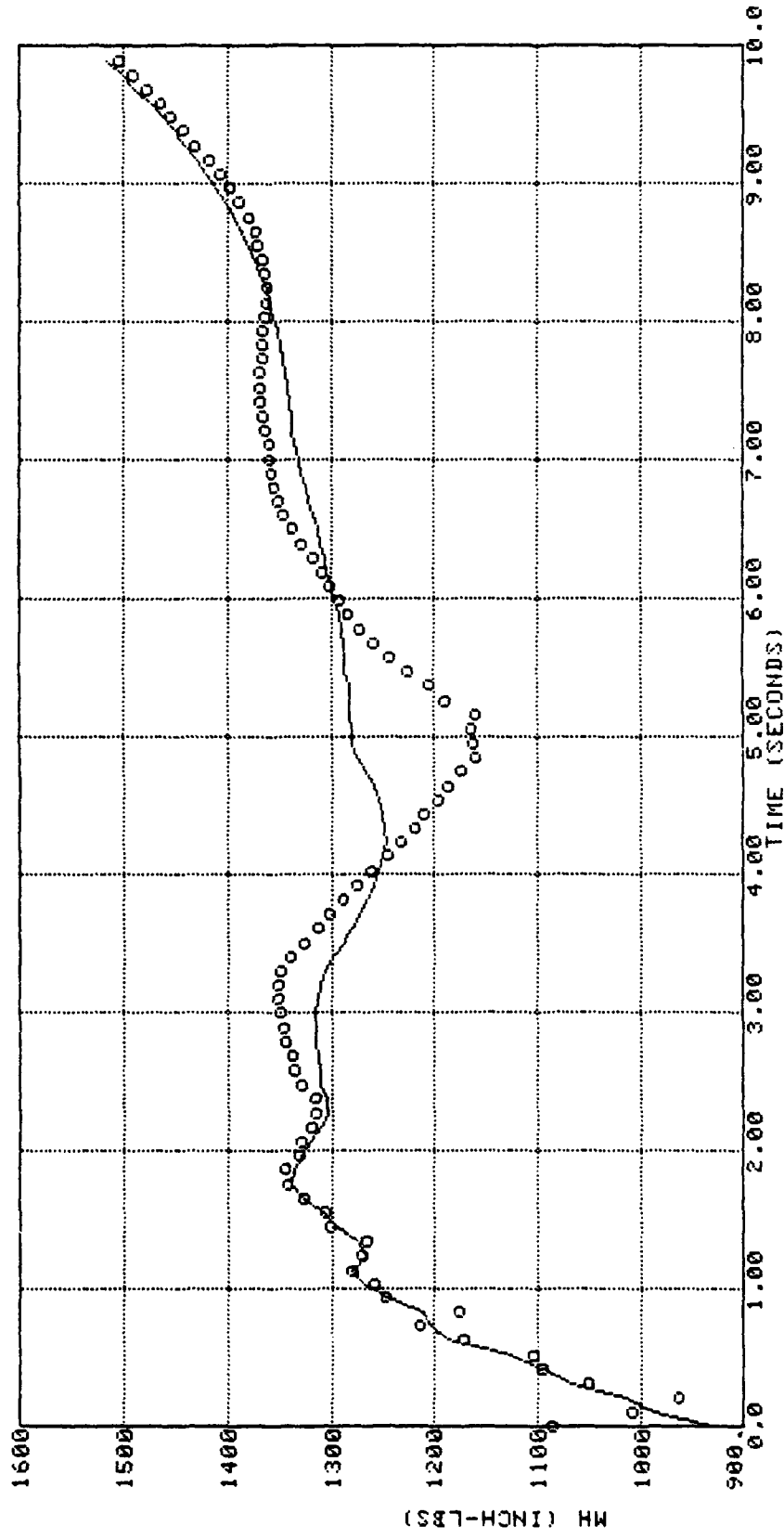


Figure 4.33 Pitch Hub Moment (Hover, Longitudinal Cyclic Input)

LINE CODE
IDENTIFIED MODEL
<u>0000000000</u>
REXOR SIMULATION DATA

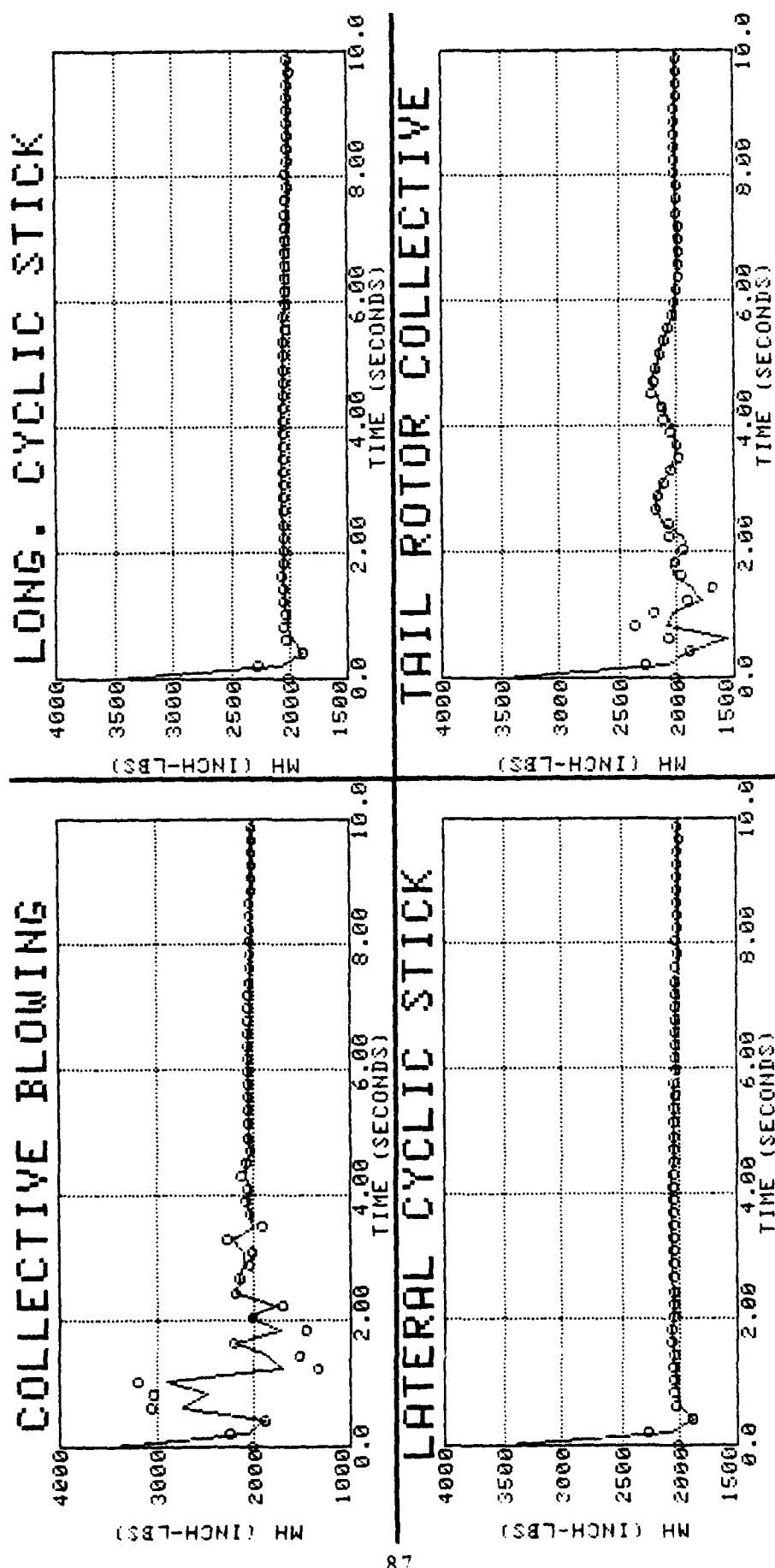


Figure 4.34 Pitch Hub Moment (100 fps)

AD-A113 760

SYSTEMS CONTROL INC (VT) PALO ALTO CA
DEVELOPMENT OF A LOW-ORDER MODEL OF AN X-WING AIRCRAFT BY SYSTEMS ETC(U)
FEB 82 J H VINCENT, J W BUNNELL

F/6 1/3

N00014-79-C-0578

RL

UNCLASSIFIED

2 of 2
AC 3760



END
DATE
FILED
5-82
DTIC

LINE CODE	IDENTIFIED MODEL REXOR SIMULATION DATA
0000000000	

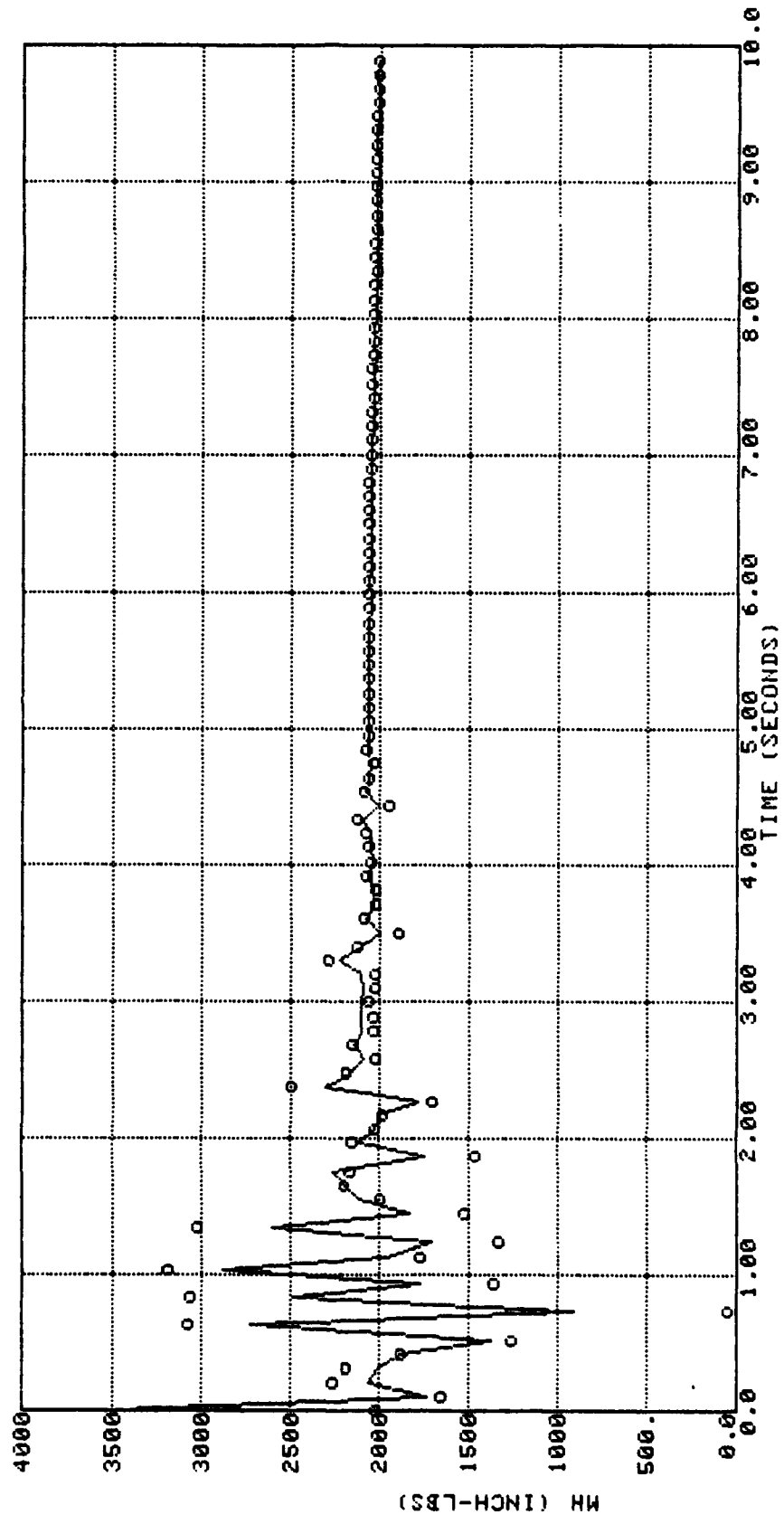


Figure 4.35 Pitch Hub Moment (100 fps, Collective Input)

V. CONCLUSIONS AND RECOMMENDATIONS

5.1 CONCLUSIONS

In general, the identified models of the X-wing configuration show good correlation with the original data. Further, the identified models are all simple and of much lower order than those used in the REXOR simulation. This indicates that it is indeed feasible to use system identification techniques as a method of developing a low-order math model for a rotorcraft from a simulation math model that represents the rotor by its individual blades in a rotating frame of reference.

The discrepancies seen in the identified results seem to be related to the discrepancies noted in the data produced by the REXOR program (see Sections 3.3 and 3.4 of this report), although time did not permit a thorough analysis of these discrepancies. This should serve as a caveat in the use of the identified model, as well as the REXOR X-wing simulation as implemented at NASA-Ames.

5.2 RECOMMENDATIONS

In order to fully treat the validity of the identified model, a stand-alone simulation using this model should be compared to the filtered REXOR time histories. In addition, the REXOR model itself should be verified, and the causative factors in the noted data inconsistencies should be determined and corrected. This was not done due to time constraints and the fact that no documentation exists for the X-wing version of the REXOR.

In general, it can be recommended that system identification be used as a tool for developing low-order models of rotorcraft in general. This may be done from simulation data or from flight tests.

REFERENCES

1. Williams, R.O., Leitner, R.T., and Rogers, E.O., "X-Wing: A New Concept in Rotary Wing VTOL," presented at the American Helicopter Society Symposium in Rotor Technology, August 1976.
2. Kesling, P.H., et al., "Final Report: X-Wing Vehicle Design Study and Composite Blade Design," Lockheed Report SP-4601, June 1977.
3. Anderson, W.D., Connor, F., Kretsinger, P., and Reaser, J.S., "REXOR Rotorcraft Simulation Model," U.S. Army Air Mobility Research and Development Laboratory Report, USAAMRDL-TR-76-28 (Vols. I, II, III), July 1978.
4. Hall, W.E., Bohn, J.G., and Vincent, J.H., "Development of Advanced Techniques for Rotorcraft State Estimation and Parameter Identification," Final Report, NASA Contractor Report 159297, August 1980.

DISTRIBUTION

NO. OF COPIES

Office of Naval Research 800 N. Quincy Street Arlington, VA 22217 Code 260 Code 432	1 2
Commander David Taylor Naval Ship Research & Development Center Bethesda, MD 20084 Code 1619 (E. Rodgers)	1
Defense Advanced Research Projects Agency 1400 Wilson Blvd. Arlington, VA 22209 Code AVTO (Mr. R.O. Williams)	1
Defense Documentation Center Cameron Station Alexandria, VA	12
NASA-Lewis Research Center Moffett Field, CA 94035 Attn: Jim Sellers Attn: Jack Zeller	1 1
NASA-Ames Research Center Bldg. 247-1 Moffett Field, CA 94035 Attn: Bill Warmbrodt	1
NASA-Ames Research Center Bldg. 247-3 Moffett Field, CA 94035 Attn: John Jinkerson	1
Research and Technical Group Strike Aircraft Test Directorate Naval Air Test Center Patuxent River, MD 20670 Attn: Mack Mutchler	1
Naval Air Development Center Code 6012 Warminster, PA 18974 Attn: Charlie Abrams	1